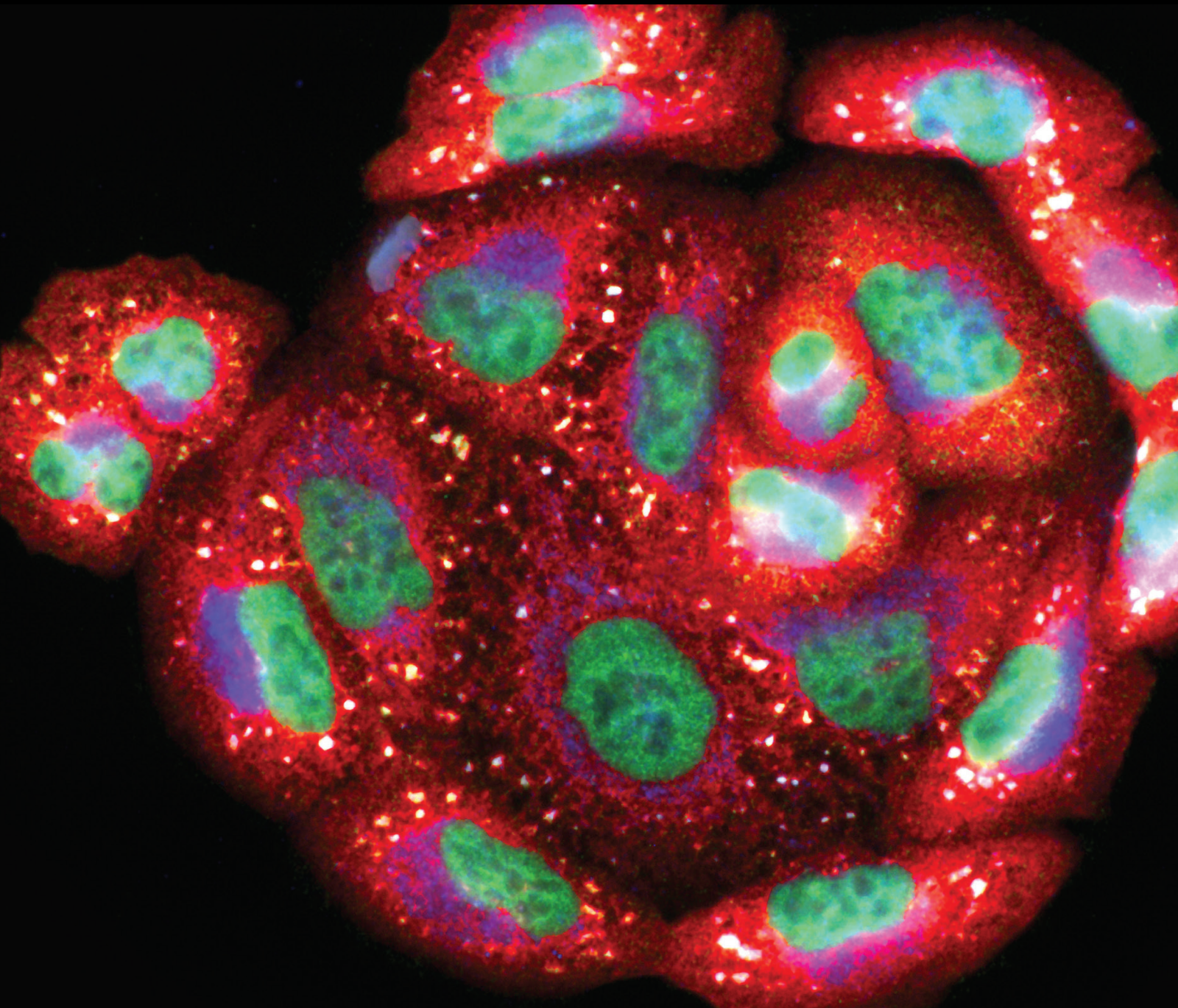


How Oxidative Stress Affects Multiple Blood Disorders

Lead Guest Editor: Liren Qian

Guest Editors: Ciprian Tomuleasa and Antonio Macciò





How Oxidative Stress Affects Multiple Blood Disorders

Oxidative Medicine and Cellular Longevity

How Oxidative Stress Affects Multiple Blood Disorders

Lead Guest Editor: Liren Qian

Guest Editors: Ciprian Tomuleasa and Antonio Macciò



Copyright © 2021 Hindawi Limited. All rights reserved.

This is a special issue published in "Oxidative Medicine and Cellular Longevity" All articles are open access articles distributed under the Creative Commons Attribution License, which permits unrestricted use, distribution, and reproduction in any medium, provided the original work is properly cited.

Chief Editor

Jeannette Vasquez-Vivar, USA

Associate Editors

Amjad Islam Aqib, Pakistan
Angel Catalá , Argentina
Cinzia Domenicotti , Italy
Janusz Gebicki , Australia
Aldrin V. Gomes , USA
Vladimir Jakovljevic , Serbia
Thomas Kietzmann , Finland
Juan C. Mayo , Spain
Ryuichi Morishita , Japan
Claudia Penna , Italy
Sachchida Nand Rai , India
Paola Rizzo , Italy
Mithun Sinha , USA
Daniele Vergara , Italy
Victor M. Victor , Spain

Academic Editors

Ammar AL-Farga , Saudi Arabia
Mohd Adnan , Saudi Arabia
Ivanov Alexander , Russia
Fabio Altieri , Italy
Daniel Dias Rufino Arcanjo , Brazil
Peter Backx, Canada
Amira Badr , Egypt
Damian Bailey, United Kingdom
Rengasamy Balakrishnan , Republic of Korea
Jiaolin Bao, China
Ji C. Bihl , USA
Hareram Birla, India
Abdelhakim Bouyahya, Morocco
Ralf Braun , Austria
Laura Bravo , Spain
Matt Brody , USA
Amadou Camara , USA
Marcio Carochio , Portugal
Peter Celec , Slovakia
Giselle Cerchiaro , Brazil
Arpita Chatterjee , USA
Shao-Yu Chen , USA
Yujie Chen, China
Deepak Chhangani , USA
Ferdinando Chiaradonna , Italy

Zhao Zhong Chong, USA
Fabio Ciccarone, Italy
Alin Ciobica , Romania
Ana Cipak Gasparovic , Croatia
Giuseppe Cirillo , Italy
Maria R. Ciriolo , Italy
Massimo Collino , Italy
Manuela Corte-Real , Portugal
Manuela Curcio, Italy
Domenico D'Arca , Italy
Francesca Danesi , Italy
Claudio De Lucia , USA
Damião De Sousa , Brazil
Enrico Desideri, Italy
Francesca Diomede , Italy
Raul Dominguez-Perles, Spain
Joël R. Drevet , France
Grégory Durand , France
Alessandra Durazzo , Italy
Javier Egea , Spain
Pablo A. Evelson , Argentina
Mohd Farhan, USA
Ioannis G. Fatouros , Greece
Gianna Ferretti , Italy
Swaran J. S. Flora , India
Maurizio Forte , Italy
Teresa I. Fortoul, Mexico
Anna Fracassi , USA
Rodrigo Franco , USA
Juan Gambini , Spain
Gerardo García-Rivas , Mexico
Husam Ghanim, USA
Jayeeta Ghose , USA
Rajeshwary Ghosh , USA
Lucia Gimeno-Mallench, Spain
Anna M. Giudetti , Italy
Daniela Giustarini , Italy
José Rodrigo Godoy, USA
Saeid Golbidi , Canada
Guohua Gong , China
Tilman Grune, Germany
Solomon Habtemariam , United Kingdom
Eva-Maria Hanschmann , Germany
Md Saquib Hasnain , India
Md Hassan , India

Tim Hofer , Norway
John D. Horowitz, Australia
Silvana Hrelia , Italy
Dragan Hrnčić, Serbia
Zebo Huang , China
Zhao Huang , China
Tariq Hussain , Pakistan
Stephan Immenschuh , Germany
Norsharina Ismail, Malaysia
Franco J. L. , Brazil
Sedat Kacar , USA
Andleeb Khan , Saudi Arabia
Kum Kum Khanna, Australia
Neelam Khaper , Canada
Ramoji Kosuru , USA
Demetrios Kouretas , Greece
Andrey V. Kozlov , Austria
Chan-Yen Kuo, Taiwan
Gaocai Li , China
Guoping Li , USA
Jin-Long Li , China
Qiangqiang Li , China
Xin-Feng Li , China
Jialiang Liang , China
Adam Lightfoot, United Kingdom
Christopher Horst Lillig , Germany
Paloma B. Liton , USA
Ana Lloret , Spain
Lorenzo Loffredo , Italy
Camilo López-Alarcón , Chile
Daniel Lopez-Malo , Spain
Massimo Lucarini , Italy
Hai-Chun Ma, China
Nageswara Madamanchi , USA
Kenneth Maiese , USA
Marco Malaguti , Italy
Steven McAnulty, USA
Antonio Desmond McCarthy , Argentina
Sonia Medina-Escudero , Spain
Pedro Mena , Italy
V́ctor M. Mendoza-Núñez , Mexico
Lidija Milkovic , Croatia
Alexandra Miller, USA
Sara Missaglia , Italy

Premysl Mladenka , Czech Republic
Sandra Moreno , Italy
Trevor A. Mori , Australia
Fabiana Morroni , Italy
Ange Mouithys-Mickalad, Belgium
Iordanis Mourouzis , Greece
Ryoji Nagai , Japan
Amit Kumar Nayak , India
Abderrahim Nemmar , United Arab Emirates
Xing Niu , China
Cristina Nocella, Italy
Susana Novella , Spain
Hassan Obied , Australia
Pál Pacher, USA
Pasquale Pagliaro , Italy
Dilipkumar Pal , India
Valentina Pallottini , Italy
Swapnil Pandey , USA
Mayur Parmar , USA
Vassilis Paschalis , Greece
Keshav Raj Paudel, Australia
Ilaria Peluso , Italy
Tiziana Persichini , Italy
Shazib Pervaiz , Singapore
Abdul Rehman Phull, Republic of Korea
Vincent Pialoux , France
Alessandro Poggi , Italy
Zsolt Radak , Hungary
Dario C. Ramirez , Argentina
Erika Ramos-Tovar , Mexico
Sid D. Ray , USA
Muneeb Rehman , Saudi Arabia
Hamid Reza Rezvani , France
Alessandra Ricelli, Italy
Francisco J. Romero , Spain
Joan Roselló-Catafau, Spain
Subhadeep Roy , India
Josep V. Rubert , The Netherlands
Sumbal Saba , Brazil
Kunihiro Sakuma, Japan
Gabriele Saretzki , United Kingdom
Luciano Saso , Italy
Nadja Schroder , Brazil

Anwen Shao , China
Iman Sherif, Egypt
Salah A Sheweita, Saudi Arabia
Xiaolei Shi, China
Manjari Singh, India
Giulia Sita , Italy
Ramachandran Srinivasan , India
Adrian Sturza , Romania
Kuo-hui Su , United Kingdom
Eisa Tahmasbpour Marzouni , Iran
Hailiang Tang, China
Carla Tatone , Italy
Shane Thomas , Australia
Carlo Gabriele Tocchetti , Italy
Angela Trovato Salinaro, Italy
Rosa Tundis , Italy
Kai Wang , China
Min-qi Wang , China
Natalie Ward , Australia
Grzegorz Wegrzyn, Poland
Philip Wenzel , Germany
Guangzhen Wu , China
Jianbo Xiao , Spain
Qiongming Xu , China
Liang-Jun Yan , USA
Guillermo Zalba , Spain
Jia Zhang , China
Junmin Zhang , China
Junli Zhao , USA
Chen-he Zhou , China
Yong Zhou , China
Mario Zoratti , Italy

Contents

Deficiency of Antioxidative Paraoxonase 2 (Pon2) Leads to Increased Number of Phenotypic LT-HSCs and Disturbed Erythropoiesis

Lisa Spiecker , Ines Witte , Julia Mehlig , Viral Shah , Markus Meyerhöfer, Patricia S. Haehnel , Victoria Petermann , Andrea Schüler, Piyush More , Nina Cabezas-Wallscheid , Sven Horke , Andrea Pautz , Andreas Daiber , Daniel Sasca , Thomas Kindler , and Hartmut Kleinert 
Research Article (18 pages), Article ID 3917028, Volume 2021 (2021)

Preparation, Biosafety, and Cytotoxicity Studies of a Newly Tumor-Microenvironment-Responsive Biodegradable Mesoporous Silica Nanosystem Based on Multimodal and Synergistic Treatment

Zelai He, Huijun Zhang, Hongwei Li, Yanyan Wang, Jing Qian, Xixi Cai, Li Sun, and Jingwen Huang 
Research Article (14 pages), Article ID 7152173, Volume 2020 (2020)

Polydatin Attenuates 14.1 MeV Neutron-Induced Injuries via Regulating the Apoptosis and Antioxidative Pathways and Improving the Hematopoiesis of Mice

Jiaming Guo , Tingting Liu, Long Ma, Wei Hao, Hongli Yan, Taosheng Li, Yanyong Yang , Jianming Cai , Fu Gao , Zhao Xu , and Hu Liu 
Research Article (16 pages), Article ID 8905860, Volume 2020 (2020)

Hematopoietic Stem Cells and Mesenchymal Stromal Cells in Acute Radiation Syndrome

Liren Qian  and Jian Cen
Review Article (10 pages), Article ID 8340756, Volume 2020 (2020)

Research Article

Deficiency of Antioxidative Paraoxonase 2 (Pon2) Leads to Increased Number of Phenotypic LT-HSCs and Disturbed Erythropoiesis

Lisa Spiecker ¹, Ines Witte ¹, Julia Mehlig ¹, Viral Shah ^{2,3}, Markus Meyerhöfer,^{2,3}
Patricia S. Haehnel ^{2,3}, Victoria Petermann ¹, Andrea Schüler,² Piyush More ¹,
Nina Cabezas-Wallscheid ⁴, Sven Horke ¹, Andrea Pautz ¹, Andreas Daiber ⁵,
Daniel Sasca ^{2,3}, Thomas Kindler ^{2,3} and Hartmut Kleinert ¹

¹Department of Pharmacology, Johannes Gutenberg University Medical Center, Mainz, Germany

²Department of Hematology, Medical Oncology and Pneumology, University Medical Center, Mainz, Germany

³University Cancer Center of Mainz, Germany

⁴Max Planck Institute of Immunobiology and Epigenetics, 79108 Freiburg, Germany

⁵Department of Cardiology, Cardiology I, Johannes Gutenberg University Medical Center Mainz, Germany

Correspondence should be addressed to Daniel Sasca; daniel.sasca@unimedizin-mainz.de,
Thomas Kindler; thomas.kindler@unimedizin-mainz.de, and Hartmut Kleinert; kleinert@uni-mainz.de

Received 29 June 2020; Revised 26 April 2021; Accepted 27 May 2021; Published 25 June 2021

Academic Editor: Liren Qian

Copyright © 2021 Lisa Spiecker et al. This is an open access article distributed under the Creative Commons Attribution License, which permits unrestricted use, distribution, and reproduction in any medium, provided the original work is properly cited. The publication of this article was funded by Max Planck.

Background. Long-term hematopoietic stem cells (LT-HSCs) reside in bone marrow niches with tightly controlled reactive oxygen species (ROS) levels. ROS increase results into LT-HSC differentiation and stem cell exhaustion. Paraoxonase 2 (PON2) has been shown to be important for ROS control. **Objectives.** We investigate the effects of inactivation of the *PON2* gene on hematopoietic cell differentiation and activity. **Methods and Results.** In young mice with inactivated *Pon2* gene (*Pon2*^{-/-}, <3 months), we observed an increase of LT-HSCs and a reduced frequency of progenitor cells. In competitive transplantations, young *Pon2*^{-/-} BM outcompeted WT BM at early time points. ROS levels were significantly increased in *Pon2*^{-/-} whole BM, but not in *Pon2*^{-/-} LT-HSCs. In more differentiated stages of hematopoiesis, *Pon2* deficiency led to a misbalanced erythropoiesis both in physiologic and stress conditions. In older mice (>9 months), *Pon2* depletion caused an increase in LT-HSCs as well as increased levels of granulocyte/macrophage progenitors (GMPs) and myeloid skewing, indicating a premature aging phenotype. No significant changes in ROS levels in old *Pon2*^{-/-} LT- and short-term (ST-) HSCs were observed, but a significant reduction of spontaneous apoptotic cell death was measured. RNA-seq analysis in *Pon2*^{-/-} LT-HSCs identified overrepresentation of genes involved in the C-X-C chemokine receptor type 4 (Cxcr4) signaling, suggesting compensatory mechanisms to overcome ROS-mediated accelerated aging in hematopoietic progenitor cells. **Conclusions.** In summary, our current data indicate that PON2 is involved in the regulation of HSC functions.

1. Introduction

Aerobic metabolism is inevitably linked to the production of reactive oxygen species (ROS) such as superoxide, hydrogen peroxide, and hydroxyl radicals, which may have harmful effects on normal cellular function [1]. A tight balance

between generation and detoxification of ROS has been shown to modulate cell physiology and development through redox signaling (low concentrations of ROS acting as signal molecules in physiologic processes) [2] and oxidative stress (high concentration of ROS exceeding the detoxification ability of cells). Oxidative stress results in destruction of proteins,

DNA, and membrane lipids [3] and has been described to be involved in carcinogenesis [4], cardiovascular diseases [5], and aging [6].

The family of paraoxonase (PON) enzymes consists of three proteins PON1, PON2, and PON3 that differ in their enzymatic activity, localization, and regulation [7]. PON2 is a ubiquitously expressed protein located exclusively intracellularly [8]. PON2 exerts antioxidative and anti-inflammatory functions and displays important effects in diseases dominated by oxidative stress [9]. PON2 modulates mitochondrial function and reduces the release of superoxide from the inner mitochondrial membrane [10]. PON2 also displays a protective effect against lipid peroxidation [11] and intracellular ROS formation [12]. Our group showed recently that dysregulated redox regulation in mice with inactivated *Pon2* gene (*Pon2*^{-/-}) causes endothelial dysfunction, vascular inflammation, and tissue factor-dependent hypercoagulability [13]. As a result of its antioxidative activity, antiapoptotic functions of PON2 have also been described both in mitochondria-related [14] and ER stress-related [12] apoptosis.

Hematopoiesis describes the hierarchically coordinated production of all blood cells with hematopoietic stem cells (HSCs) sitting at the apex. HSCs are characterized by their lifelong self-renewal ability and their capability to differentiate into all lineage committed progenitor cells [1]. To maintain hematopoiesis, the tight balance between differentiation and self-renewal in HSCs must be strictly regulated [15]. Defects in this balance lead to hematopoietic insufficiency and/or to the development of hematopoietic malignancies. In adult organisms, most HSCs are located in the bone marrow (BM). Different cell types, soluble factors, and anatomical structures collaborate to maintain HSC function. This delicate environment is referred as “niche” [16]. The BM niche and in particular the endosteal niche are characterized by a low oxygen concentration. A more restricted access to oxygen is likely to result in lower ROS levels. Analyses have shown that ROS are important to regulate the balance between self-renewal and differentiation of stem cells. Low levels of ROS are important to maintain the multipotency of these cells, whereas higher ROS levels would commit them to a restricted lineage [17, 18]. The low oxygen tension in the niche supports the ability of HSCs to self-renew and to stay quiescent. Self-renewing HSCs use anaerobic glycolysis as the main energy source to adapt to hypoxic conditions and meet the relative low energy needs of HSC [19]. However, the mitochondrial oxidative phosphorylation program is used if HSCs start to proliferate and differentiate [20]. Therefore, the primitive multipotent quiescent long-term (LT-) HSC is located in the endosteal niche [21]. In addition, ROS levels are tightly regulated by intrinsic mechanisms, e.g., regulation via the transcription factors FoxO1-3 [22].

The ability of stem cells to regenerate cells or tissues declines with age [23]. Compared to young animals, HSCs from aged animals display defined differences such as functional changes in homing and differentiation [24], enhanced ROS production, inflammation, and apoptosis [25, 26]. In older organisms, hematopoiesis displays a preferential generation of myeloid cells on the expense of lymphoid cells. This so-called myeloid skewing and the related immunosenes-

cence seem to result from the clonal expansion of myeloid-committed hematopoietic stem and progenitor cells (HSPCs) and the reduction of lymphoid-committed HSPCs [24, 26].

The process of erythroid commitment and differentiation—termed as “erythropoiesis”—represents another crucial “checkpoint” of ROS-dependent regulation [27]. Erythropoiesis results in the production of red blood cells (RBCs) [28] from megakaryocyte/erythrocyte precursor cells (MEPs) [28]. Erythroid precursors are exposed to some of the highest ROS levels; however, similar to LT-HSCs, they also possess a large number of defense mechanisms against ROS and other insults [29]. The importance of ROS in erythroid maturation is supported for instance by the abnormalities of hematologic parameters in genetic diseases that lead to deficiency of mechanisms involved in antioxidation defence/reduction [30–32].

As mentioned above, HSC are mostly quiescent, show low metabolic activity with dependence on anaerobic glycolysis, and are prone to stimulation and damage by oxidative stress. PON2 is an antioxidant and antiapoptotic enzyme. Besides its important effects in the cardiovascular system, the antioxidative/antiapoptotic effects of PON2 seem to be exploited by different tumor cell types to enhance growth and resistance to chemotherapy [33]. Although PON2 expression has been correlated with the pathology of different forms of leukemia [33], the role of PON2 in hematopoiesis has not been analyzed. Therefore, the current study was performed to analyze the general involvement of PON2 in hematopoiesis.

2. Materials and Methods

2.1. Materials. All cell culture grade plastic materials were obtained from Greiner Bio-One, Frickenhausen, Germany, or SARSTEDT, Nümbrecht, Germany. All chemicals (as not otherwise stated), fetal calf serum, IgG from rat serum, RPMI 1640, Dulbecco's phosphate-buffered saline (PBS), Proteinase K, and Taq Polymerase were from Sigma, Deisenhofen, Germany. CM-H₂DCF-DA was obtained from Molecular Probes/Thermo Fisher Scientific, Dreieich, Germany. L-012 (8-amino-5-chloro-7-phenyl-pyrido [3,4-d]pyridazine-1,4(2H,3H)dione) was obtained from Wako Chemicals, Richmond, U.S.A. The penicillin/streptomycin solution (100x; 10.000 U/ml penicillin, 10.000 µg/ml streptomycin), Dulbecco's modified Eagle medium (DMEM), and GlutaMax™ were obtained from Gibco/Thermo Fisher Scientific, Dreieich, Germany. The High-Capacity cDNA Reverse Transcription Kit and the Arcturus® PicoPure® RNA Isolation Kit were purchased from Applied Biosystems, Darmstadt, Germany. The peqGOLD Total RNA Kit, peqGOLD TriFast™, and the dNTP-Mix were purchased from Peqlab, Darmstadt, Germany. The PrecisionPLUS 2x qPCR Master-Mix with SYBR green was obtained from Primer Design, Chandler's Ford, United Kingdom. The Anti-Rat/Hamster Ig, κ/Negative Control (FBS*) Compensation Particles Set, BD Cytotfix/Cytoperm™ Fixation/Permeabilization Kit, BD™ CompBeads, PE Annexin V Apoptosis Detection Kit I, anti-Ki-67 antibody, and Perm/Wash buffer were obtained from BD Biosciences, Heidelberg, Germany.

2.2. Cell Culture. Murine hematopoietic precursor cell-7 (HPC-7 [34]) and BA/F3 pro B cells [35] were cultured as previously described [36]. To analyze the effect of the ROS generator 2,3-dimethoxy-1,4-naphthalenedione (DMNQ) [37], the cells were plated in 6-well plates and treated with 10 μ M DMNQ (solved in DMSO) or DMSO (control) for 2 to 8 h.

2.3. Mice and Approval of Animal Studies. PON2-deficient mice were generated by insertion of a loxP-site flanked, β -geo-containing gene trap vector into *Pon2* intron 2 [38]. Consequently, *Pon2* protein expression is reduced by about 95%. These *Pon2*-deficient mice are referred to as *Pon2*^{-/-} mice. Wild-type (WT), C57BL/6J, C57BL/6-Ly5.1, and *Pon2*^{-/-} mice were housed in the translational animal research center of the JGU Mainz. All strains had access to water and standard chow diet ad libitum. Experimental mice were 10-14 weeks old when called “young” or more than 9 months old when called “aged.” The animals were sacrificed by i.p. injection of 2% pentobarbital (0.4 ml/25 g body weight). All animal studies were approved by the Ethical Committee and Landesuntersuchungsamt Rheinland-Pfalz (#23177-07/G13-1-055).

2.4. Blood Drawing and Analysis. After injecting a lethal dose of pentobarbital intraperitoneally (i.p.), intracardial blood was obtained for later analysis on the Sysmex XP Hematology Analyzer or HEMAVET using a syringe coated with citrate solution (Sigma) and a 26 G needle.

For smaller amounts of blood at multiple points in time, e.g., for analyzing erythrocyte turnover and stress erythropoiesis, mice were gently restrained, while blood was drawn by scratching the *Vena caudalis mediana* and immediately transferred to an EDTA-coated reaction vessel.

2.5. In Vivo Biotinylation for Analysis of the Erythroid Lifespan/Turnover. The erythroid lifespan/turnover was analyzed using biotin labeling according to published protocols [39, 40].

For the erythroid cell biotinylation *in vivo*, WT and *Pon2*^{-/-} mice were injected into the tail vein (i.v.) using a 26 G ½ cannula with 100 μ l of a sulfo-NHS-LC-biotin solution (30 mg/ml), resulting in a labeling rate of 80-95% of the circulating erythrocytes. The first blood sample was taken after 30 minutes in order to determine the individual starting value of the biotinylation of each mouse. Subsequent blood samples were taken daily (first 5 days) and then at intervals of 5 days, from day 20 at intervals of 7 days. Approximately 10 μ l blood was drawn and PBS+2% FCS as well as streptavidin APC-Cy7 (1:250) and Ter119 APC (1:500) (both from eBioscience Thermo Fisher Scientific) was added. After incubating for 15 minutes in the dark and on ice, samples were washed and analyzed on the FACSCanto™ II flow cytometer.

2.6. Induction of Hemolytic Anemia by Phenylhydrazine. Approximately 80 μ l blood was drawn from WT and *Pon2*^{-/-} mice by scratching the *Vena caudalis mediana*, transferred to an EDTA-coated reaction vessel, and examined using the Sysmex XP Hematology Analyzer. The mice

were then injected with 50 mg/kg phenylhydrazine hydrochloride (Sigma-Aldrich) or PBS (for control animals) i.p. Injection was performed at days 1 and 3.

2.7. Flow Cytometry and Cell Sorting. Cell suspensions from the liver were obtained by pushing the organ through a 100 μ m cell strainer. Single-cell suspensions from BM were obtained by flushing tibial and femoral bones using RPMI/2% FCS and subsequently filtering the suspension through a cell strainer cap. The targets for the antibodies (all from eBioscience Thermo Fisher Scientific, Dreieich, Germany, unless stated otherwise) used for staining of differentiated BMCs were B220 (CD45R) (APC); CD3e (PE); CD4 (APC); CD8 (Ly2) (PE); ckit (PerCP-eFluor710); CD11b (APC); Gr1 (Ly6G/C) (PE); CD19 (PE, BioLegend, San Diego, U.S.A.); Ter119 (APC); CD71 (PE); and CD138 (Brilliant violet 421, BD Biosciences). For identification of hematopoietic stem and progenitor cells (LT-HSCs, ST-HSCs, MPPs, CMPs, GMPs, and MEPs), cells were incubated with a lineage cocktail of biotin-conjugated antibodies directed against CD3, CD4, CD5, CD8 (Ly2), CD11b (only LT-HSCs, ST-HSCs, and MPPs), CD127 (only CMPs, GMPs, and MEPs; BioLegend), B220 (CD45R), Gr1 (Ly6G/C), and Ter119. After washing, cells were incubated with streptavidin (APC-Cy7), Sca-1 (PECy7), ckit (APC), CD135 (PE, only LT-HSCs, ST-HSCs, and MPPs, BioLegend), CD150 (Alexa Fluor 488, only LT-HSCs, ST-HSCs, and MPPs, BioLegend), CD16/32 (PE, only CMPs, GMPs, and MEPs, BD), and CD34 (Alexa Fluor 488, only CMPs, GMPs, and MEPs, BD). For quantification of apoptotic HSCs, CD135 (PE) was replaced by annexin V (PE), and for measurement of total ROS via H₂DCF-DA staining, CD150 (Alexa Fluor 488) was replaced by CD150 (Brill. violet 421). Data acquisition was done with a FACSCanto II (BD Biosciences) and analyzed using BD FACSDiva™ Software.

For sorting, HSPCs were enriched using EasyStep™ Mouse Hematopoietic Progenitor Cell Isolation Kit (Stem-Cell Technologies, Cologne, Germany), stained with the antibodies mentioned before, and sorted on a FACSARIA™ II SORP Flow Cytometer Cell Sorter (BD Biosciences). All gating strategies are shown in Figure S4.

2.8. Reciprocal Bone Marrow (BM) Transplantation. BM cells (BMCs) of WT or *Pon2*^{-/-} donor mice were isolated by flushing tibial and femoral bones using RPMI/2% FCS/1% penicillin-streptomycin followed by BM cell resuspension in DMEM. By injection of 5 \times 10⁶ BMCs intravenously into recipient mice of the respective genotype 24 hours after lethal irradiation (Cs137, one dose of 9 Gy; this radiation dosage was confirmed to be lethal after 8-10 days), *Pon2*^{-/-} and WT BM chimeras were generated. BM-transplanted mice were analyzed after confirmation of blood cell *Pon2* mRNA expression by qRT-PCR, no earlier than 21 days after BM cell injection.

2.9. Competitive BM Transplantation. BMCs were isolated from CD45.2-positive WT and *Pon2*^{-/-} mice and mixed 1:1 with BMCs isolated from CD45.1 WT mice. Afterwards, 8 \times 10⁶ WT CD45.1/WT CD45.2 (control) or WT

CD45.1/*Pon2*^{-/-} CD45.2 mixed BMCs were intravenously injected into irradiated WT CD45.2 recipient mice. About 50 μ l blood from competitive transplanted mice was taken 3, 7, 11, 15, 19, and 22 weeks after injection and stained with CD45.1 and CD45.2 antibodies to detect HSPC engraftment using congenic C57BL/6 mice that differ at the Ly5 locus [41]. Irradiated mice were treated with Borgal for about 4 weeks after irradiation. All gating strategies are shown in Figure S4.

2.10. Serial Transplantation of Aged BMCs. 5×10^6 BMCs, isolated from aged WT and *Pon2*^{-/-} mice, were separately *i.v.* injected into irradiated, young WT recipient mice. 21 days after transplantation, the BMCs were isolated by flushing tibial and femoral bones of the recipient mice and then resuspended in DMEM and once more *i.v.* injected into irradiated, young WT recipient mice. During the next 21 days, the survival rate of recipient mice was determined.

2.11. Measurement of Total ROS by H₂DCF-DA Staining. After BM isolation and staining of HSPCs using cell surface markers as described above, cells were incubated with 0.5 μ M fluorescent ROS indicator CM-H₂DCF-DA (Molecular Probes/Thermo Fisher Scientific, Dreieich, Germany) for 30 min at 37°C. Subsequent to washing of cells using Krebs HEPES buffer (Noxygen, Elzach, Germany), total ROS was assessed by analyzing H₂DCF-DA signal intensity on a FACSCanto II (BD Biosciences) flow cytometer with BD FACSDiva™ Software (excitation/emission CM-H₂DCF-DA: 488/520 nm). All gating strategies are shown in Figure S4.

2.12. Measurement of ROS Production via L-012. ROS production was determined using the luminol derivative L-012 (8-amino-5-chloro-7-phenylpyridol [3,4-d] pyridazine-1,4 (2H,3H) dione; Wako Chemicals, Richmond, U.S.A.) as previously described for tissue homogenates, whole blood, and isolated leukocytes [42]. Freshly isolated BMCs of WT and *Pon2*^{-/-} mice were centrifuged and resuspended in modified Krebs HEPES buffer at a concentration of 1×10^7 cells/ml. 50 μ l of cell suspension per well (containing 5×10^5 cells) was loaded in a 96-well plate. Chemiluminescence was recorded after addition of 40 μ M L-012 and in some cases 10 μ M DMNQ (2,3-dimethoxy-1,4-naphthoquinone), a redox-cycling agent that induces intracellular superoxide anion and hydrogen peroxide formation. L-012 chemiluminescence was measured simultaneously for the two experimental groups for about 75 minutes every 4 minutes using a Microplate Centro LB960 Luminometer (Berthold Technologies, Sprenglingen, Germany). The photon counts were normalized to chemiluminescence of L-012 in modified Krebs HEPES buffer only.

2.13. Cell Cycle Analysis of BM Populations. Cell surface staining was performed as described above. Subsequently, samples were incubated in Cytofix/Cytoperm (BD Biosciences) for 15 minutes. Cells were washed using Perm/Wash, resuspended in a buffer containing an anti-Ki-67 antibody (Alexa Fluor 647, diluted 1:30 in Perm/Wash), and incubated for at least 30 minutes. After washing with Perm/Wash,

cells were resuspended in 100 μ l Hoechst 33342 (diluted 1:500 in PBS) and incubated for 15 minutes. Analyses were performed using BD LSR II Flow Cytometer, and data were analyzed using BD FACSDiva™ or FlowJo Software. All gating strategies are shown in Figure S5.

2.14. Colony-Forming-Unit Assays (CFUs). 3×10^4 BMCs from WT and *Pon2*^{-/-} mice were cultured in MethoCult™ GF M3434 (StemCell Technologies, Cologne, Germany) in accordance with the manufacturer's instructions. 10-12 days after plating, the colonies were quantified and identified using a Leitz DM IL microscope (Leica, Wetzlar, Germany).

2.15. Homing. Homing of hematopoietic cells to the bone marrow was analyzed as described in Yusuf and Scadden [43], but the BMCs were isolated by flushing instead of crushing the bones.

2.16. Assessing Gamma-H2AX Levels of LSK Cells. Cell surface staining was performed using the lineage cocktail of biotin-conjugated antibodies described above as well as streptavidin (APC-Cy7), Sca-1 (PECy7), and ckit (APC). Cells were fixed and permeabilized using Cytofix/Cytoperm (BD Biosciences) and then stained with γ H2AX antibody (Alexa Fluor 488, BioLegend, San Diego, U.S.A.) for 2 hours on ice. Data acquisition was performed on a FACSCanto II (BD Biosciences), and histogram overlay images were created using CellQuest Pro Software (BD Biosciences).

2.17. Gene Expression Analyses. According to previous studies, *PON2* expression levels are the highest in the lung, intestine, heart, and liver [44]. To prove *Pon2* mRNA expression as well as determine cell-specific *Pon2* expression in HSPCs, we isolated mRNA from FACS-sorted LT-HSCs, ST-HSCs, multipotent progenitor cells (MPPs), common myeloid progenitors (CMPs), granulocyte-macrophage progenitors (GMPs), and megakaryocyte-erythroid progenitors (MEPs) and performed two-step qRT-PCR analyses. To analyze the effect of the redox-cycler DMNQ on CXCR4 mRNA expression, RNA was isolated from HPC7 and BA/F3 cells treated with or without 10 μ M DMNQ for 2 to 8 h. The RNA was reverse transcribed using the SuperScript™ VILO™ Master Mix (Invitrogen/Thermo Fisher Scientific, Dreieich, Germany). Then, qPCRs were performed using primers and double-labeled probes (5'-FAM->3'-TAMRA; all from Eurofins Genomics, Hamburg Germany; listed in Table S1) or with PrecisionPLUS 2x qPCR MasterMix with SYBR green (Primer Design, Chandler's Ford, United Kingdom) as described by the manufacturer. mRNA expression levels were analyzed according to previously established protocols [45], generally applying 2 housekeeping genes (*Gapdh*, *Actb*; for primer used, see Table S1).

2.18. Total RNA Sequencing. For total RNA sequencing (RNA-seq) analyses, Lin⁻, Sca¹⁺, ckit⁺, CD135⁻, and CD150⁺ cells (which represent a mixture of LT-HSC and MPP2 cells—for a better discrimination hereafter referred to as HSCs) [46] were isolated from BM of young WT or *Pon2*^{-/-} mice ($n = 6$ each) by FACS as described above. 10 HSCs per well and a total of 8 wells per mouse were FACS

sorted into a 96-well plate (8 RNA-seq per mouse and 48 RNA-seq per genotype), containing lysis buffer (Qiagen, Hilden Germany). Subsequently, cells were handed over to the genomics core facility of the Institute of Molecular Biology (Mainz, Germany) for RNA-seq using Smart-seq2-protocol for library preparation and NextSeq® 500/550 High Output Kit v2 (Illumina, Cambridge, United Kingdom) for sequencing. Quality of raw sequencing reads was assessed using FastQC (Babraham Bioinformatics), and adapters were trimmed using Trimmomatic (v0.36 [47]). Raw RNA-seq reads were then mapped to mouse reference genome (genome release M12 GRCm38.p5) using the STAR aligner (v2.5.3a [48]), with an option of “-quantModeGeneCounts” to count the number of reads mapped per gene. The numbers of high-quality reads were 21.1 to 32.6 million reads. Between 67 and 76% of the reads were aligned to the mouse genome. DESeq2 (v1.18.1 [49]) was used to identify genes differentially expressed after *Pon2* knockout. Genes with fold change higher than 2 and FDR below 0.05 were considered as differentially expressed. Overrepresentation analysis was performed using the ConsensusPathDataBase release 34 [50].

2.19. RNA-seq or Microarray Analyses. All analyses of public RNA-seq or microarray data from the literature were performed using the software CLC genomic workbench (version 21.0.03) using parameters as recommended by the manufacturer.

2.20. Statistics. GraphPad Prism software (version 9) was used, applying 2-tailed Student’s *t*-test (normally distributed data, skewness < 1) for comparison of two groups. For more than 2 groups, 1-way ANOVA with Tukey’s multiple comparisons test or 2-way ANOVA with Bonferroni’s multiple comparisons test was applied. Numbers of mice in the experimental groups or analyzed numbers of independent cell experiments are indicated in the figures. $P < 0.05$ was considered significant.

3. Results

3.1. *Pon2* mRNA Expression Levels Vary between HSCs and Progenitor Cells in Young and Old Mice. *Pon2* mRNA expression was measured in subsets of BMCs while liver cells, that are known to express high *Pon2* mRNA levels, were used as a positive control. Our results (Figure 1) indicate differential, cell-specific *Pon2* expression levels between 0.15- and 1.35-fold compared to liver cells as well as changes of *Pon2* expression in HSPCs as a function of age. In young animals (10-14 weeks), LT- and ST-HSCs showed low *Pon2* mRNA expression levels, which slightly increased in committed progenitor cells (multipotent progenitor cells (MPPs), common myeloid progenitors (CMPs)) and significantly increased in megakaryocyte-erythroid progenitors (MEPs) (Figures 1 and S1A). In contrast, expression analysis in HSPCs of aged animals (>9 months) revealed the lowest *Pon2* mRNA levels in MEPs, CMPs, and MPPs, but higher in LT- and ST-HSCs (Figures 1 and S1B). No changes in *Pon2* expression as a function of age were observed in hepatic control cells. Analysis of available RNA-seq data sets of HSCs

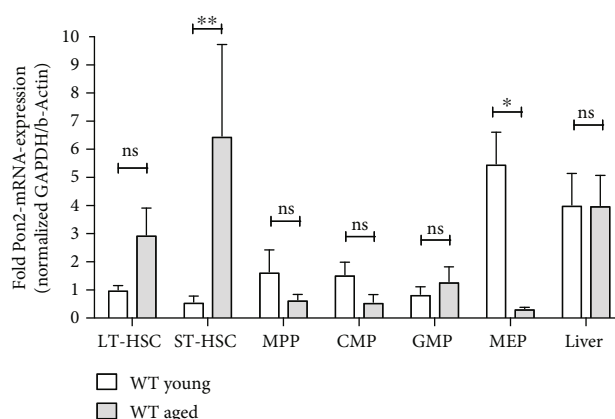


FIGURE 1: *Pon2* mRNA expression level in WT mice changes upon aging. LT-HSCs, ST-HSCs, MPPs, CMPs, GMPs, MEPs, and liver cells were obtained from young (2-3 months) and aged (>9 months) WT mice. *Pon2*, *Gapdh*, and *Actb* mRNA expression was analyzed by qRT-PCR. *Pon2* mRNA expression was normalized to *Gapdh* and *Actb* mRNA expression. The relative *Pon2* mRNA expression in LT-HSCs from young WT mice was set to 1. Shown are the mean + SEM of $n = 3 - 6$ experiments using 2-6 mice per group (** $P < 0.01$, * $P < 0.05$, ns: not significant vs. WT cells; 2-way ANOVA with Bonferroni’s multiple comparisons test).

and progenitor cells of young mice (PRJNA603283 [51], PRJNA665066) demonstrated similar patterns of *Pon2* mRNA expression as those observed in our experiments (Figures 1 and S1C). Finally, analysis of available RNA-seq (PRJNA524895 [52], PRJNA528500 [53], and PRJNA635499 or microarray data sets (GSE76276) [54]; see Figure S1D) revealed no difference in *Pon2* mRNA expression levels between LT-HSCs of young, aged, or old animals.

3.2. Young *Pon2*^{-/-} Mice Show Quantitative Changes in HSPCs but an Unaltered Myeloid/Lymphoid Ratio. Analysis of different HSPC subpopulations using flow cytometry (Figures 2(a)-2(g)) revealed a significant increase of LT-HSCs and decreased numbers of MPPs in BM of young *Pon2*^{-/-} mice compared to WT animals. No significant changes were observed for total Lin⁻Sca-1⁺c-Kit⁺ (LSK) cells, ST-HSCs, CMPs, GMPs, and MEPs. We also determined the ratio of myeloid and lymphoid cells in the peripheral blood (Figure 2(h)). No difference in the myeloid/lymphoid ratio between WT and *Pon2*^{-/-} mice was detected.

3.3. *Pon2*^{-/-} Mice Show Quantitative Changes in Blood Counts. We next tested the consequences of *Pon2* deficiency on the peripheral blood populations by performing blood counts of young *Pon2*^{-/-} and WT mice using a Sysmex Automated Hematology Analyzer.

Compared with WT, *Pon2*^{-/-} mice had similar leukocyte (WBC, Figure 3(a)) and erythrocyte (RBC, Figure 3(c)) counts, but increased hemoglobin (Hb, Figure 3(b)). Furthermore, *Pon2*^{-/-} erythrocytes displayed several qualitative abnormalities, such as enhanced mean corpuscular volume (MCV, Figure 3(d)), mean corpuscular hemoglobin (MCH,

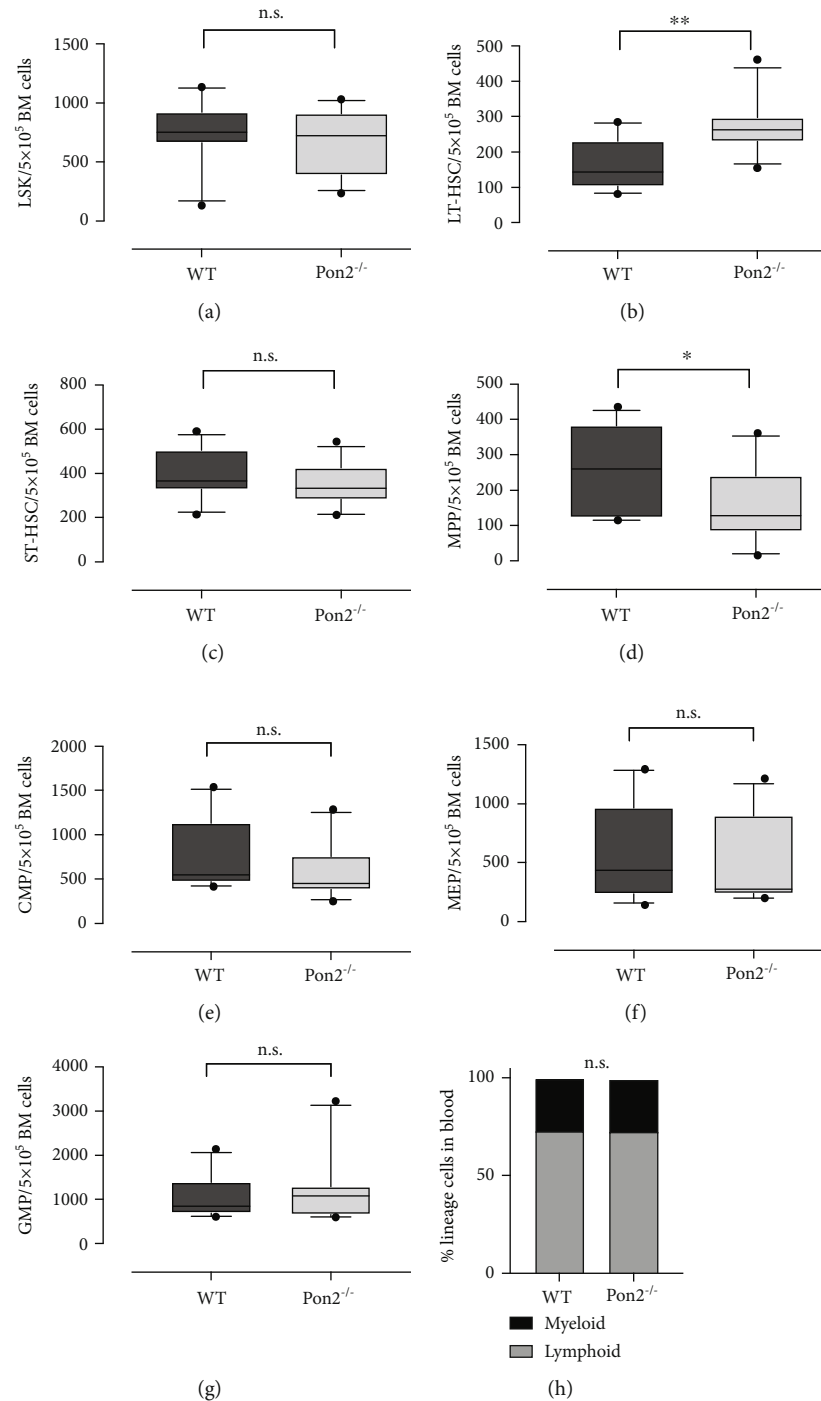


FIGURE 2: Young *Pon2*^{-/-} mice show quantitative abnormalities in HSPCs but unaltered myeloid/lymphoid ratio. Graphs showing absolute cell numbers per 0.5 10^5 whole bone marrow cells (WBMC) of (a) LSK cells, (b) LT-HSCs, (c) ST-HSCs, (d) MPPs, (e) CMPs, (f) MEPs, and (g) GMPs of young WT and *PON2*^{-/-} mice. $n = 11/\text{group}$, box and whiskers; whiskers: 10-90 percentile. *** $P < 0.001$, ** $P < 0.01$, * $P < 0.05$, n.s.: not significant; two-tailed unpaired t -test. (h) Percentage of myeloid and lymphoid cells in blood of young WT and *PON2*^{-/-} mice ($n = 37 - 50$). n.s.: not significant; two-tailed unpaired t -test.

Figure 3(e)), and mean corpuscular hemoglobin concentration (MCHC, Figure 3(f)) and reduced red cell width distribution (RWD, Figure 3(g)).

3.4. *Pon2* Deficiency Associates with a Bias towards Erythropoiesis Both in Physiological and Stress Conditions.

In opposition with bone marrow HSPC subpopulations, in which abnormalities were moderate and limited to LT-HSCs and MPPs only, peripheral blood of *Pon2*-deficient mice had severe erythroid irregularities. We therefore next tested whether the *Pon2*^{-/-}-associated erythroid progenitors are likewise subject to numerical aberrancies. Indeed, as

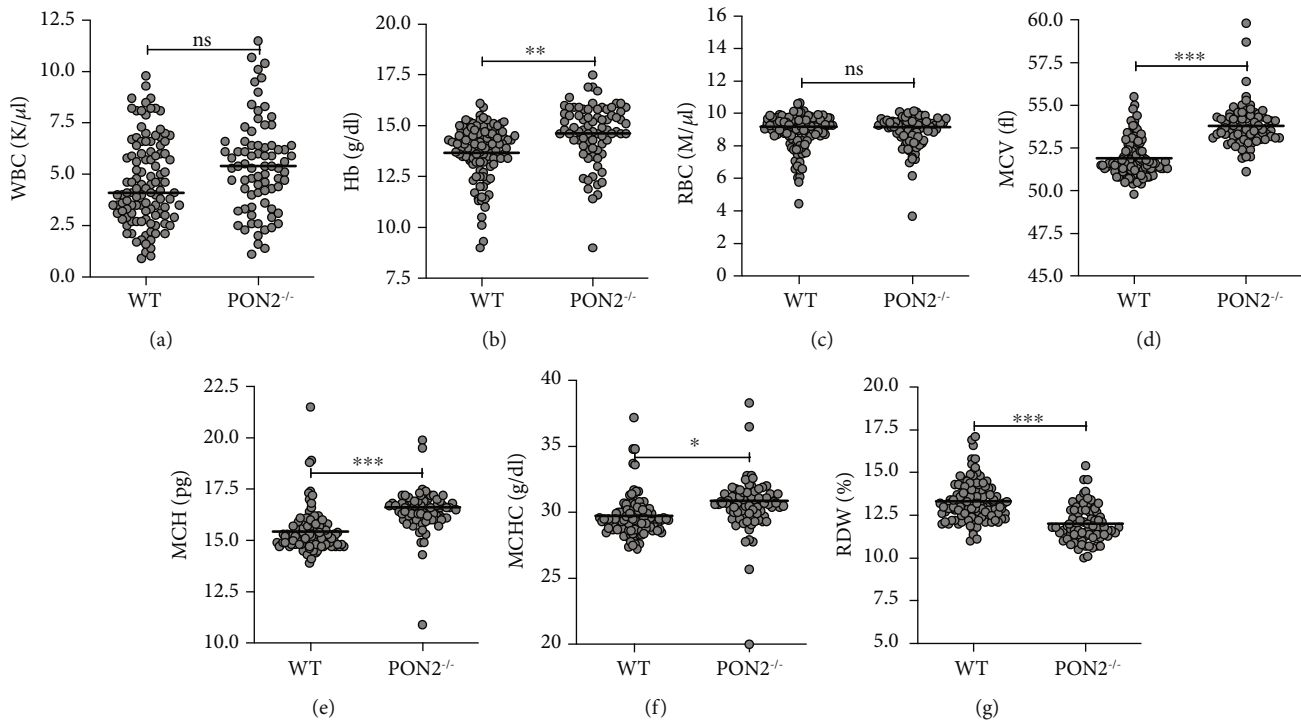


FIGURE 3: Analysis of peripheral blood from young *Pon2*^{-/-} mice compared to WT mice of the same age. Shown are (a) the white blood cell count (WBC), (b) hemoglobin (Hb), (c) red blood cell count (RBC), (d) mean corpuscular volume (MCV), (e) mean corpuscular hemoglobin (MCH), (f) mean corpuscular hemoglobin concentration (MCHC), and (g) red cell distribution width (RDW), in blood of young WT and *PON2*^{-/-} mice. Dot plot diagram. Median, dot each animal; $n = 78 - 113$. * $P < 0.05$, ** $P < 0.01$, *** $P < 0.001$; n.s. = not significant; t -test.

shown in Figures 4(a)–4(c), flow cytometry staining analyses of erythroblasts of *Pon2*^{-/-} BMs demonstrated increased counts at all stages of differentiation. We also analyzed the lifespan of erythroid cells using an *in vivo* biotinylation assay coupled to flow cytometry. Of importance, Ter119-positive erythroid cells from *Pon2*^{-/-} mice had a significantly enhanced lifespan ($t_{1/2} = 16$ days) compared to those in WT controls ($t_{1/2} = 11$ days) (Figure 4(d)).

Finally, we assessed the dynamics of stress erythropoiesis in *Pon2*^{-/-} and WT mice after induction of hemolysis via intraperitoneal application of phenylhydrazine or the control substance PBS. Phenylhydrazine caused a strong decrease of erythrocyte counts in WT mice by day 5 posttreatment commencement (Figure 4(e)). In contrast, the expected hemolysis was weaker in *Pon2*^{-/-} mice, in which the percentage of erythrocytes in blood remained significantly higher (Figure 4(e)). In control-treated animals, no significant changes between WT and *Pon2*^{-/-} animals were seen (Figure 4(f)).

Altogether, these data demonstrate a specific role for *Pon2* to limit erythroid commitment and lifespan.

3.5. In Young *Pon2*^{-/-} Mice, Reciprocal BM Transplantation Reveals Cell Intrinsic as well as Extrinsic Phenotypes. We next aimed to assess the functional importance of the observed quantitative changes in HSPC compartments. To determine whether the effects of *Pon2* deficiency on HSPCs are cell intrinsic or niche derived, we performed reciprocal BM transplantations (see Figure S2A), resulting in four experimental groups: WT recipient (r)/WT donor (d) and

Pon2^{-/-}(r)/*Pon2*^{-/-}(d) as well as chimeras comprising *Pon2*^{-/-}(r)/WT(d) and WT(r)/*Pon2*^{-/-}(d). Successful reconstitution or depletion of *Pon2* in hematopoietic cells of recipient mice was verified by qRT-PCR (Figure S2B). Subsequent flow cytometric analyses of HSPC count showed cell-specific and mixed effects (cell specific + niche effect). Reciprocal BM transplantation revealed increased LT-HSC, CMP, and MEP numbers (Figures S2C, S2F, and S2G) in the *Pon2*^{-/-} animals receiving *Pon2*^{-/-} BM. No major differences were seen in the chimeras, which indicate complementary cell intrinsic and extrinsic effects.

3.6. *Pon2* Deficiency in Young Mice Leads to Oxidative Stress, but Does Not Induce Apoptosis or Cause DNA Double-Strand Breaks. Using two approaches to analyze basal ROS production, we examined murine BMCs under steady-state conditions in *Pon2*^{-/-} mice compared to WT animals. First, we analyzed superoxide/hydrogen peroxide in BMC using detection with the chemiluminescent probe L-012. In accordance with previously published inhibition of superoxide/hydrogen peroxide production by *PON2* [10], we detected markedly increased L-012 chemiluminescence signals in BMCs of young *Pon2*^{-/-} mice compared to WT mice (Figure 5(a)). Furthermore, we analyzed total ROS levels in WT or *Pon2*^{-/-} HSPCs with the fluorescent dye CM-H₂DCF-DA by flow cytometry. The measurements demonstrated significantly enhanced ROS formation in *Pon2*^{-/-} ST-HSCs and numerically enhanced ROS in *Pon2*^{-/-} MPPs of young animals (Figure 5(b)). Interestingly, no differences were observed in LT-HSCs.

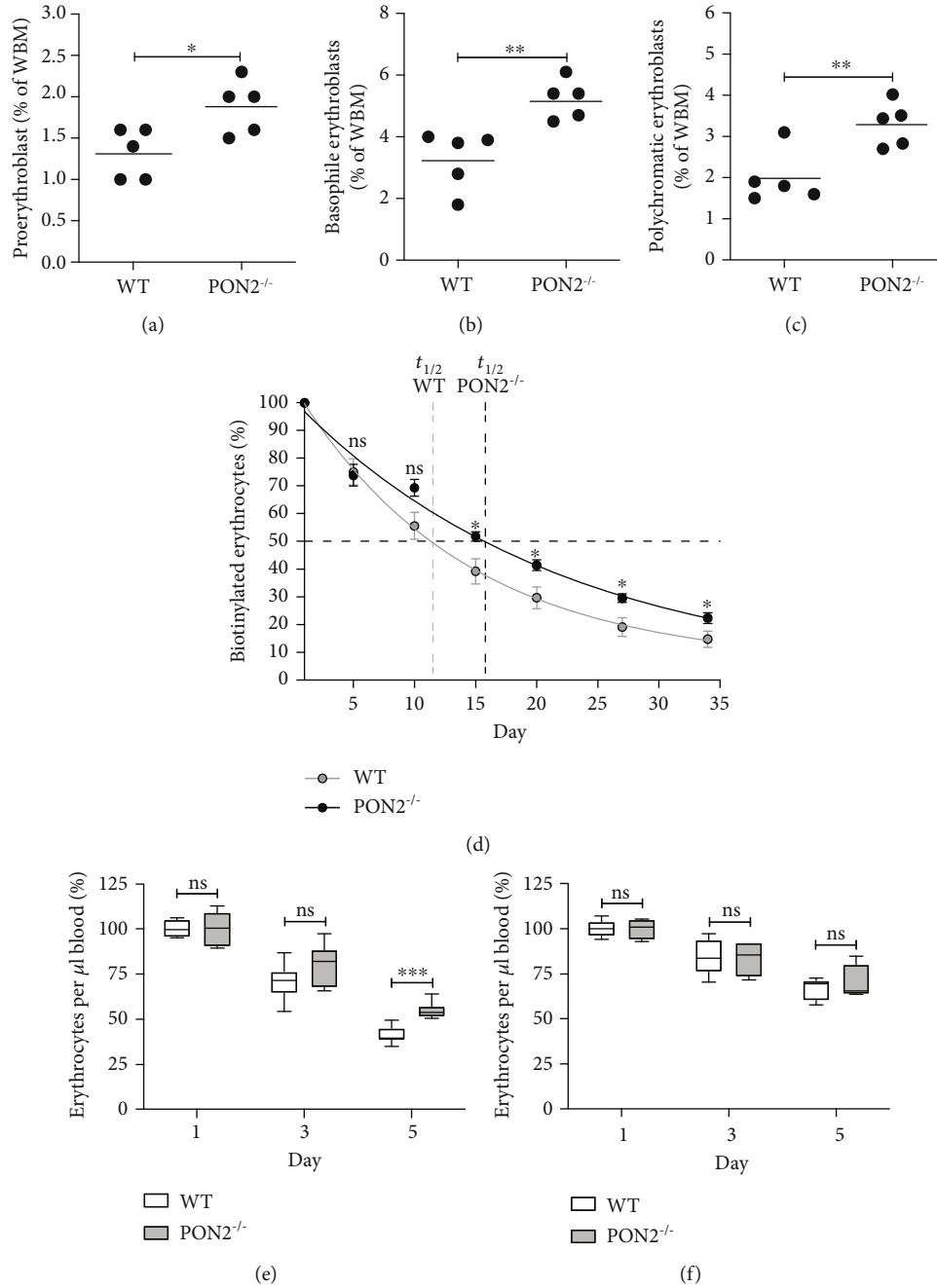


FIGURE 4: Effects of PON2-inactivation on erythropoiesis. (a–c) Analysis of 3 different stages of erythrocyte development in the bone marrow of WT and Pon2^{-/-} mice. Following the isolation of the bone marrow, cells were stained with the antibodies CD71 and Ter119 and analyzed by flow cytometry. The graphs show the percentage of (a) proerythroblasts (CD71 high/Ter119 mid), (b) basophilic erythroblasts (CD71 high/Ter119 high), and (c) polychromatic erythroblasts (CD71 mid/Ter119 mid). Dot plot diagram. Dot each individual animal; $n = 5$. * $P < 0.05$, ** $P < 0.01$; t -test. (d) Lifespan of erythrocytes in young Pon2^{-/-} mice. Erythrocyte degradation and regeneration were analyzed using in vivo biotinylation. Young Pon2-deficient and WT mice were injected with sulfo-NHS-biotin (intravenous), and small blood samples were taken every few days over a total of 34 days. Afterwards, isolated blood cells were stained with fluorescence-conjugated streptavidin as well as the erythrocyte specific marker Ter119 and analyzed using flow cytometry to determine the number of biotinylated erythrocytes. Results are shown as percentage of biotinylated erythrocytes at day 1, immediately after biotin injection; mean \pm SEM, $n = 7 - 8$. A nonlinear regression was calculated (R^2 erythrocytes = 0.90); vertical dashed lines represent the half-life ($t_{1/2}$) of the respective cells from WT (light gray) or Pon2^{-/-} (black) mice. * $P < 0.05$; n.s.: not significant; t -test. (e, f) Percentage of red blood cells in the blood of Pon2^{-/-} and WT mice during the induction of hemolytic anemia by phenylhydrazine. Pon2-deficient and wild-type mice were i.p. injected with either phenylhydrazine or PBS (control group) on days 1 and 3. On day 1 (before the start of treatment) and on days 3 and 5, a small amount of blood was taken from the test animals by scratching the *Vena caudalis mediana* in order to analyze the number of erythrocytes. The percentage of erythrocytes in the blood (e) of the phenylhydrazine group and (f) of the control group is shown in comparison to the mean value of the respective starting amount. $n = 4 - 8$; mean \pm SEM. *** $P < 0.001$; ns = not significant; t -test.

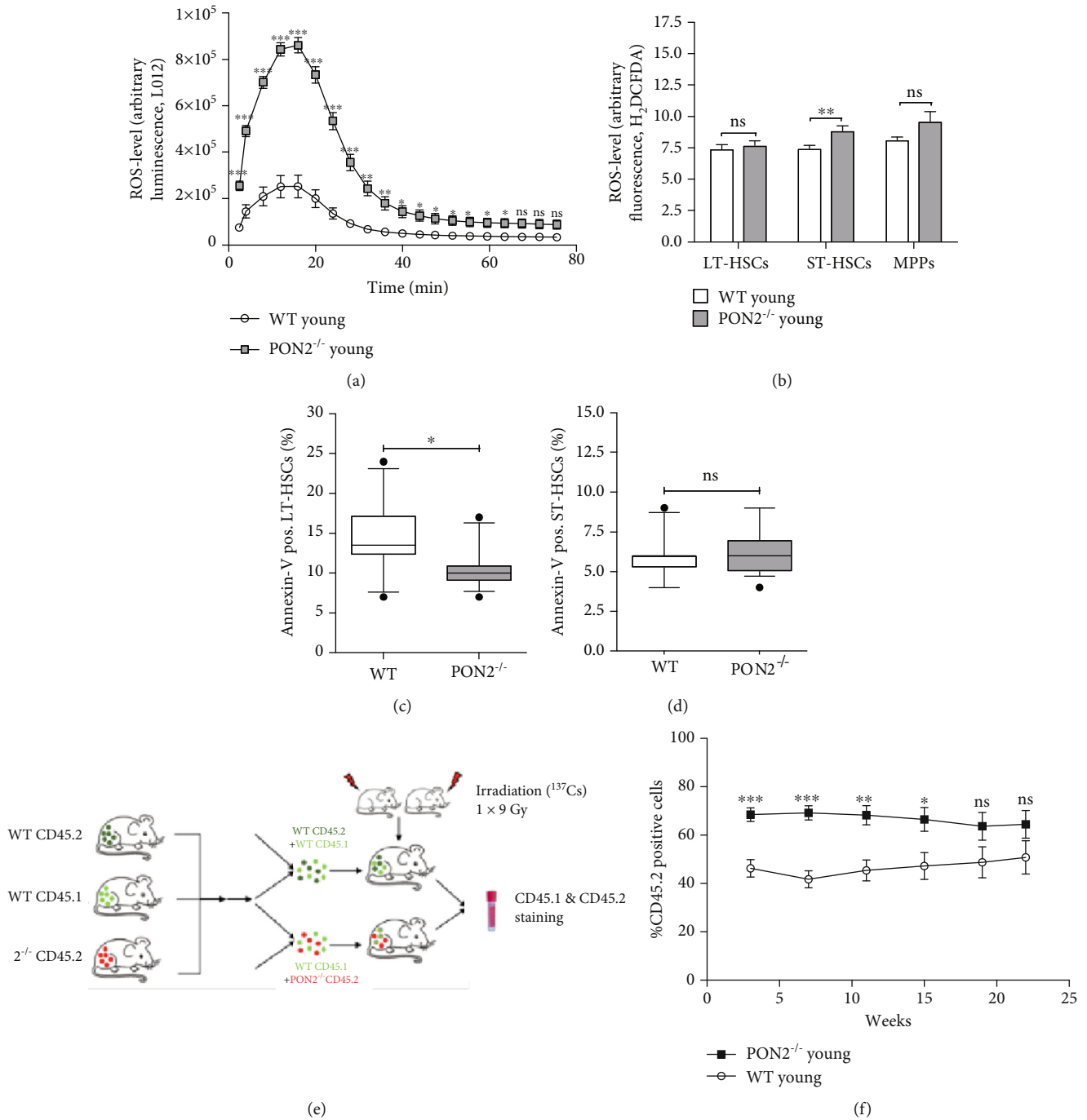


FIGURE 5: PON2 deficiency causes oxidative stress, but does not impair but rather improve HSC function. (a) L-012 chemiluminescence signal of freshly isolated BMCs from young WT and *Pon2*^{-/-} mice quantified over time for ROS formation (representative graph); mean ± SEM. **P* < 0.05, ***P* < 0.01, ****P* < 0.001, ns: not significant vs. WT; two-tailed unpaired *t*-test. (b) Total ROS level in LT-HSCs, ST-HSCs, and MPPs of young (2-3 months) WT and *Pon2*^{-/-} mice stained with cell-specific markers (LT-HSCs: Lin⁻, Sca1⁺, ckit⁺, CD135⁻, and CD150⁻; ST-HSCs: Lin⁻, Sca1⁺, ckit⁺, CD135⁻, and CD150⁻; MPPs: Lin⁻, Sca1⁺, ckit⁺, CD135⁺, and CD150⁻) and H₂DCF-DA, analyzed by FACS (*n* = 12 – 13); mean + SEM. ***P* < 0.01, ns: not significant vs. WT; two-tailed unpaired *t*-test (representative histograms showing the DCF-DA data comparing WT and *Pon2*^{-/-} mice, see Figure S6). BMCs isolated from young WT and *Pon2*^{-/-} mice stained with cell-specific markers for (c) LT-HSCs or (d) ST-HSCs and annexin V for quantification of apoptotic cells (*n* = 12 – 16). Box and whiskers; whiskers: 10-90 percentile; **P* < 0.05, ns: not significant vs. WT; two-tailed unpaired *t*-test. (e) Experimental scheme for competitive bone marrow transplantation. (f) Percentage of CD45.2-positive cells in the blood of competitive transplanted young mice 3, 7, 11, 15, 19, and 22 weeks after transplantation (*n* = 9); mean ± SEM. **P* ≤ 0.05, ***P* ≤ 0.01, ****P* < 0.001, ns: not significant; two-tailed unpaired *t*-test.

We hypothesized that PON2 deficiency leads to increased apoptotic cell death in HSCs. Using annexin V staining, we analyzed the percentage of apoptotic LT- and ST-HSCs in BM of *Pon2*^{-/-} and WT mice by flow cytometry. These measurements revealed significantly less annexin V-positive LT-HSCs but no differences in annexin V-positive ST-HSCs in young *Pon2*^{-/-} mice compared to WT (Figures 5(c) and 5(d)). We also detected no changes in fluorescence signal intensity of gamma-H2AX antibody in *Pon2*-deficient LSK cells compared to WT cells (Figure S3A), indicating genetic stability in WT and *Pon2*^{-/-} mice, despite higher ROS levels in *Pon2*^{-/-} mice.

3.7. Young *Pon2*^{-/-} BM Cells Outcompete WT Cells at Early but Not at Later Time Points. To analyze whether the increased number of LT-HSCs in *Pon2*^{-/-} animals confers increased fitness, we performed competitive BM transplantation assays. Engraftment of WT and *Pon2*^{-/-} BMCs was analyzed by flow cytometry using the cell surface markers CD45.1 and CD45.2, respectively (Figure 5(e)) as described [41]. Competitive transplantation of WT and *Pon2*^{-/-} BMCs in a 1:1 ratio revealed significant advantages of *Pon2*^{-/-} BMCs in multilineage reconstitution at early time points (Figure 5(f)) whereas engraftment was similar between WT and *Pon2*^{-/-} cells after week 15.

3.8. Young *Pon2*^{-/-} and WT HSPCs Show No Differences in Cell Cycle Status, Colony-Forming Ability, and Homing. Since increased ROS level disrupts the quiescent state of HSCs and can stimulate them to proliferate and differentiate [18], we performed cell cycle analysis using Hoechst 33342 and Ki-67 to distinguish between cells in G0- and G1- as well as G2-, S-, and M-phase. We detected no difference in cell cycle status of *Pon2*^{-/-} LSK cells or LT-HSCs compared to WT cells (Figures S4A and S4B). Similarly, colony-forming assays revealed no difference in colony-forming ability of WT or *Pon2*^{-/-} BMCs after 10 days of incubation. Besides the equal amounts of total colonies (Figure S4C), there was also no change in the number of specific colonies (Figure S4D), indicating no Pon2-mediated impact on colony forming and differentiation.

We also analyzed the homing ability of BMCs. We examined homing efficiency using the fluorescent dye DiI and analyzing BM of lethally irradiated recipient mice 48 h after injecting stained *Pon2*^{-/-} or WT BMCs (Figure S4E). Flow cytometric analysis revealed no differences in homing ability of WT and *Pon2*^{-/-} BMCs (Figure S3F). Therefore, we speculate that the higher frequency of *Pon2*^{-/-}-derived cells upon competitive BM transplantation at early time points (Figure 5(f)) was likely caused by the increased number of LT-HSCs in *Pon2*^{-/-}-derived BM cells (Figure 2(b)) and not due to increased fitness of *Pon2*^{-/-} HSCs.

3.9. Aged *Pon2*^{-/-} Mice Reiterate the Increased LT-HSCs Proportion, but Also Exhibit Changes Leading to an Altered Myeloid/Lymphoid Ratio. In accordance with the analysis in young mice, flow cytometry on BMC of aged *Pon2*^{-/-} mice demonstrated an increase of LT-HSCs. Additionally, a sur-

prising increase in the proportion of GMPs was noted, while all other committed progenitors remained at comparable levels with those in control mice (Figures 6(a)–6(g)). These increased GMP levels indicate potential intensified myeloid skewing compared to age-matched WT mice, which could be confirmed by a significantly shifted myeloid/lymphoid ratio in the peripheral blood of aged *Pon2*^{-/-} mice (Figure 6(h)).

3.10. Similar Total ROS Levels in Old *Pon2*^{-/-} HSCs Compared to WT HSCs, but Significantly Decreased Baseline Apoptosis. Total ROS in HSPCs of aged *Pon2*^{-/-} mice was assessed by flow cytometry using H₂DCF-DA staining. Similar to young *Pon2*^{-/-} HSCs, no major differences in ROS levels were observed in all subpopulations of the LSK fraction compared to WT cells (Figure 7(a)). Again, the number of annexin V-positive cells was significantly decreased in *Pon2*^{-/-} LT- and ST-HSCs (Figures 5(b) and 5(c)), whereas DNA damage analyses did not reveal higher levels of DNA double-strand breaks compared to WT cells (Figure S3B).

3.11. In Serial Transplantation Experiments, Recipients of BM from Aged *Pon2*^{-/-} Mice Show No Reduced Survival Rate. To analyze the functionality of aged *Pon2*^{-/-} BMC, we performed serial transplantation experiments to induce decent proliferative stress. The BMCs were isolated from aged WT and *Pon2*^{-/-} mice. HSCs from aged animals have been described to have a reduced ability to repopulate recipient mice in *in vivo* transplantation assays [55]. Therefore, we performed 2 rounds of transplantations (Figure 7(d)). Of note, aiming to create a condition of higher stress levels upon the bone marrow repopulation, we shortened the time between the primary and secondary retransplantation to 3 weeks. These experiments revealed no statistical differences in the survival rate of the animals transplanted with *Pon2*^{-/-} or WT BMCs, albeit at a low sample size (5 vs. 6 animals). However, and in line with the observed increased number of LT-HSCs and decreased levels of apoptosis, more recipient mice transplanted with BMCs of aged *Pon2*^{-/-} donors were alive at day 21 of the second transplantation round compared to recipients of BMCs from wild-type animals (Figure 7(e)).

3.12. RNA-seq Analyses Show Enhancement of the Expression of Survival Genes in HSCs of Young *Pon2*^{-/-} Mice. Although increased ROS levels in progenitor cells, in particular in aged mice, caused a premature aging phenotype with increased frequencies of myeloid progenitors and a shifted myeloid-to-lymphoid ratio in the peripheral blood of aged *Pon2*^{-/-} mice, we did not observe an exhaustion phenotype under conditions of stress. This observation might be the consequence of increased LT-HSC numbers or the reduction of baseline apoptotic cell death in *Pon2*^{-/-} LT-HSCs. We hypothesized that depletion of Pon2 induces a compensatory program during the earliest hematopoietic stages to overcome the harmful effects of supraphysiological ROS levels that we discovered in whole BM. To address this hypothesis, we performed RNA-seq analyses of Lin⁻, Sca1⁺, kkit⁺, CD135⁻, and CD150⁺ cells (representative for a mixture of

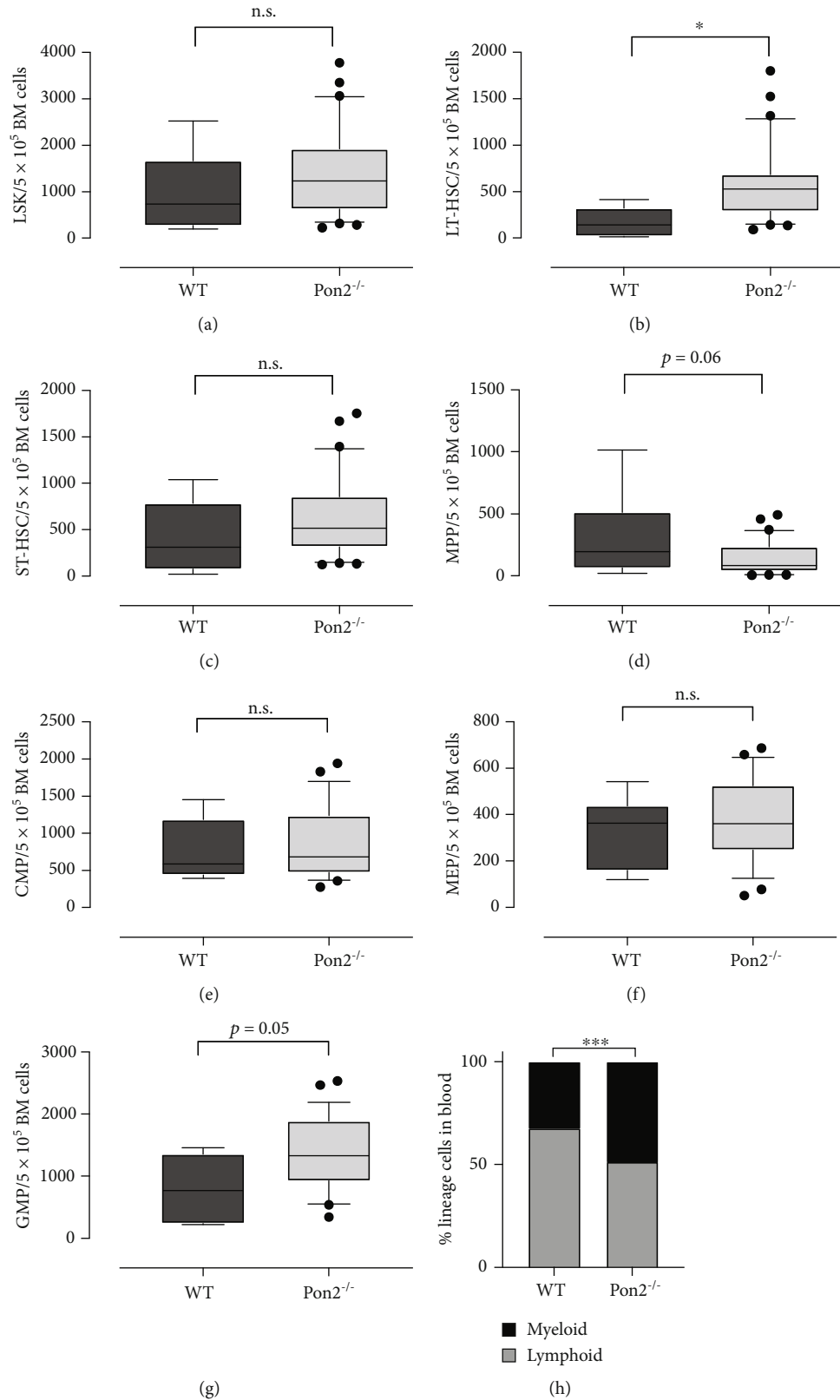


FIGURE 6: Aged *Pon2*^{-/-} mice show increased cell count of HSPCs and altered myeloid/lymphoid ratio in the blood. Graphs showing absolute cell numbers per 0.5 × 10⁵ whole bone marrow cells (WBMC) of (a) LSK cells, (b) LT-HSCs, (c) ST-HSCs, (d) MPPs, (e) CMPs, (f) MEPs, and (g) GMPs of old WT and *PON2*^{-/-} mice. *n* = 6 – 30, box and whiskers; whiskers: 10-90 percentile. ****P* < 0.001, ***P* < 0.01, **P* < 0.05, n.s.: not significant; two-tailed unpaired *t*-test. (h) Percentage of myeloid and lymphoid cells in the blood of aged WT and *Pon2*^{-/-} mice (*n* = 37 – 50). ****P* < 0.001 vs. WT; two-tailed unpaired *t*-test.

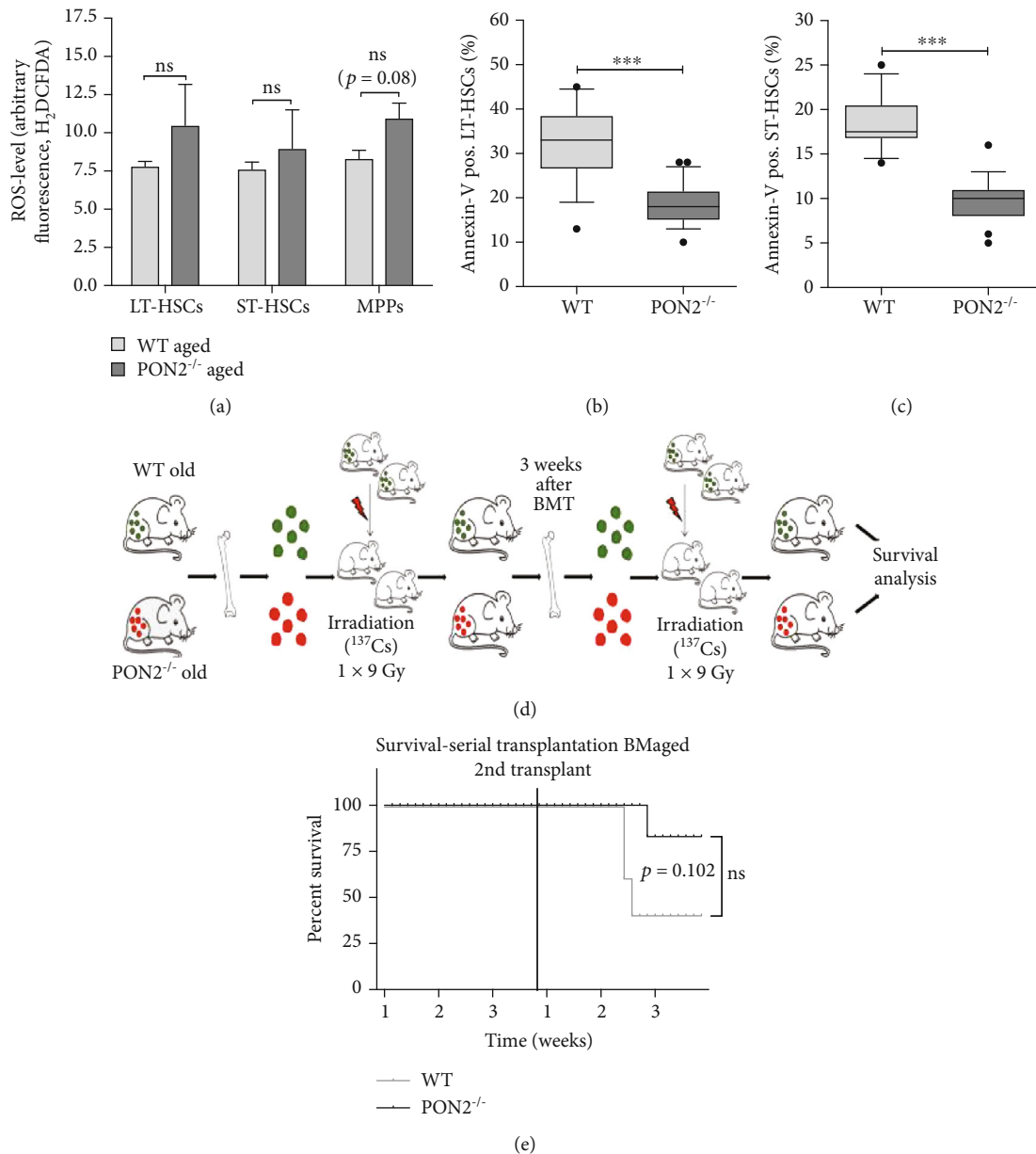


FIGURE 7: Aged *Pon2*^{-/-} mice show numeric increased total ROS level in HSPCs, but significantly decreased apoptotic rate and increased functionality. (a) Total ROS level in LT-HSCs, ST-HSCs, and MPPs of aged (≥ 9 months) WT and *Pon2*^{-/-} mice stained with cell-specific markers (LT-HSCs: Lin⁻, Sca1⁺, ckit⁺, CD135⁻, and CD150⁺; ST-HSCs: Lin⁻, Sca1⁺, ckit⁺, CD135⁻, and CD150⁻; MPPs: Lin⁻, Sca1⁺, ckit⁺, CD135⁺, and CD150⁻) and H₂DCF-DA, analyzed by FACS ($n = 3$); mean + SEM, ns: not significant vs. WT; two-tailed unpaired *t*-test. BMCs isolated from aged WT and *Pon2*^{-/-} mice stained with cell surface markers for (b) LT-HSCs or (c) ST-HSCs and annexin V for quantification of apoptotic cells ($n = 14 - 29$); box and whiskers; whiskers: 10-90 percentile. *** $P < 0.001$; two-tailed unpaired *t*-test. (d) Experimental scheme for serial transplantation of aged BMCs. (e) Percent survival of mice after serial transplantation of aged WT or *Pon2*^{-/-} BMCs ($n = 5 - 6$); ns: not significant vs. WT; survival rates are shown as a Kaplan-Meier plot; log rank (Mantel-Cox) test ($P = 0.102$).

LT-HSCs and MPP2—hereafter referred to as HSC) isolated from young WT or *Pon2*^{-/-} mice ($n = 6$ per genotype). The comparison of whole transcriptomes of HSCs isolated from young WT or *Pon2*^{-/-} mice using DESeq2 identified 341 differentially expressed genes. Of these, 168 genes were down-regulated and 157 genes were up-regulated in *Pon2*^{-/-} HSCs compared to WT HSCs (see Table S2 and Figure 6(b)). Sample distance analysis (see Figure 8(a)) revealed no

distinct clustering between the *Pon2*^{-/-} and WT groups, and this coincided with similar spreading profiles in the first principal component (PC1) of the principal component analysis (PCA). Nonetheless, *Pon2*^{-/-} and WT groups clearly clustered separately in the second principal component (PC2), which led us to believe that a rather discrete number of cellular processes/pathways differ between HSCs of young *Pon2*^{-/-} and WT animals.

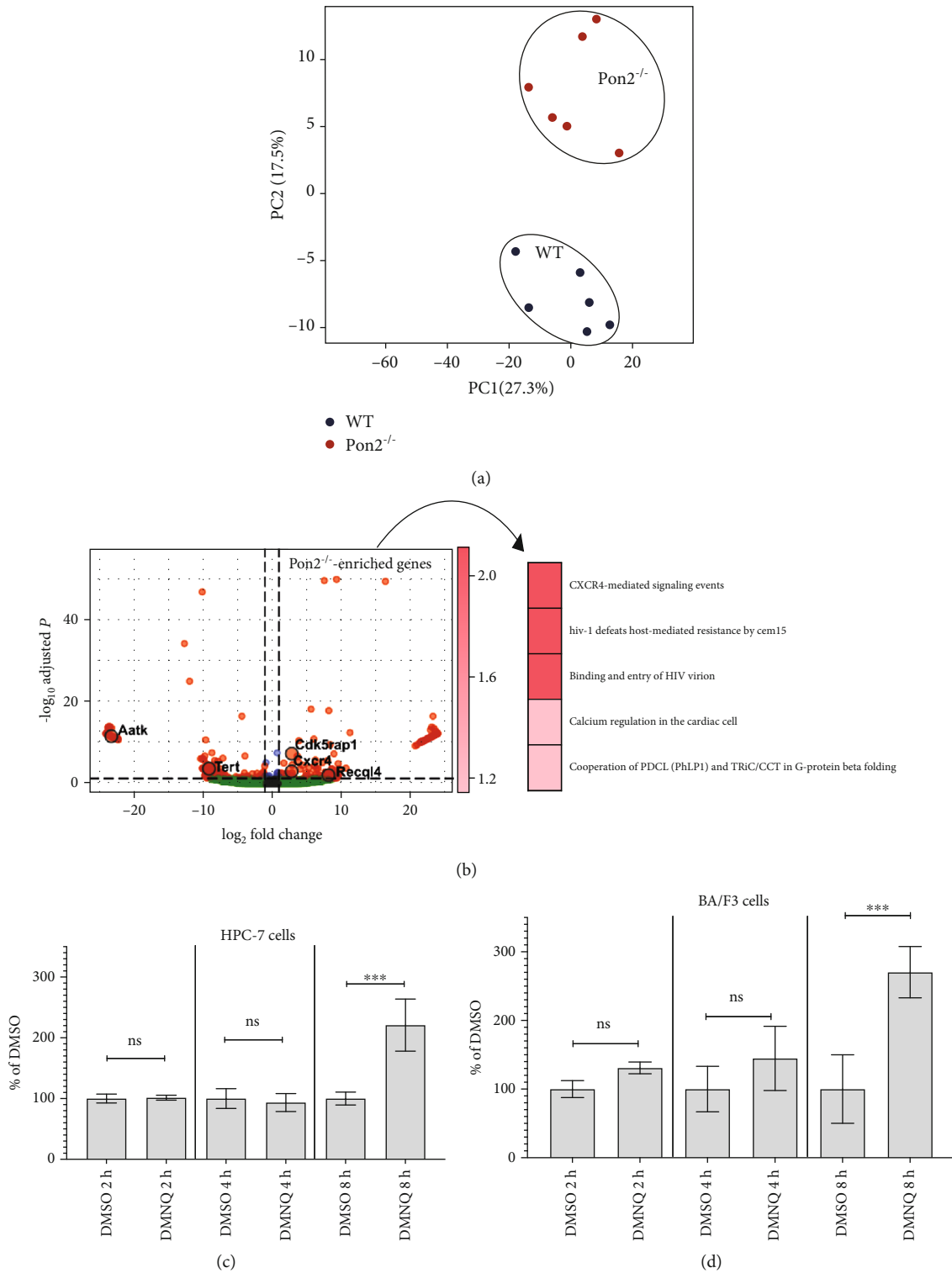


FIGURE 8: *Cxcr4* and *Cxcr4* pathway-related genes are upregulated in young *Pon2*^{-/-} HSCs and upon treatment with DMNQ in murine hematopoietic stem cell lines. (a) PCA plot displaying the variance of gene expression in 5 *Pon2*^{-/-} HSCs and 5 matched WT LT-HSCs. (b) Left panel: volcano plot of gene expression differences between *Pon2*^{-/-} and matched WT HSCs. Genes whose expression is significantly upregulated in *Pon2*^{-/-} LT-HSCs are marked in red, while genes whose expression is significantly downregulated in *Pon2*^{-/-} HSCs are marked in blue. Right panel: heat map showing the top 5 overrepresented pathways in *Pon2*^{-/-} HSCs. The scale was calculated as -log₁₀ FDRq. (c) HPC-7 or (d) BA/F3 cells were treated with DMSO (control) or 10 μM DMNQ for 2 to 8 h. *CXCR4* and *Gapdh* mRNA expression was analyzed by qRT-PCR. *CXCR4* mRNA expression was normalized to *Gapdh* mRNA expression. The relative *CXCR4* mRNA levels in DMSO-treated cells were set to 100%. Shown are the mean ± SEM of *n* = 3–6 experiments (****P* < 0.001, ns: not significant vs. DMSO-treated cells; two-sided *t*-test).

We noted differential expression of several important regulators of cell survival, such as Telomerase (*Tert*) [56, 57] or the NRF2 pathway genes *Nfe2l2* and *Abcc2* [58, 59] and CXCR4 involved in the regulation of homing, quiescence/proliferation, or migration [60]. Of note, overrepresentation analysis of genes that were upregulated in *Pon2*^{-/-} HSCs demonstrated significant enrichment of only a discrete number of pathways (Figure 8(b)). Most importantly, the CXCR4-mediated signaling event pathway reached the highest level of significance (FDRq 0.02) among the whole database (Figure 6(b); Tables S3 and S4). Moreover, treatment with the ROS generator DMNQ resulted in enhanced (around 2.5-fold) CXCR4 mRNA expression in HPC-7 hematopoietic stem cells and BA/F3 pro B cells (see Figures 8(c) and 8(d)).

4. Discussion

In this study, we comprehensively investigated the function of PON2 in the hematopoietic system. PON2 has been linked to therapy resistance and poor prognosis in different types of leukemia, but the biological function of PON2 in hematopoiesis has not been investigated. Our *in vivo* studies demonstrate that PON2 is involved in the regulation of normal hematopoiesis. First, we determined *Pon2* mRNA expression levels in different HSPC subpopulations of young (<3 months) and aged (>9 months) mice. In young mice, *Pon2* mRNA levels were increased in committed progenitor cells, in particular in CMPs and MEPs, compared to the HSC compartment. Surprisingly, but at least in line with the high expression levels putatively linked to a specific functional importance in MEPs, *Pon2* deficiency in young mice associated with a propensity to a more robust erythropoiesis both in physiological and stress conditions. While this remains to be demonstrated in subsequent works, we believe that *Pon2* deficiency might activate an (over) compensatory mechanism to maintain the erythropoiesis.

Meanwhile, expression levels of *Pon2* declined with proceeding differentiation in aged mice. Interestingly, in aged mice, depletion of *Pon2* caused an increase of GMPs accompanied by a skewed myeloid-to-lymphoid ratio pointing to at least partly accelerated aging of *Pon2*^{-/-} HSCs in comparison to WT cells. An age-related expansion of different HSPC subpopulations has been described in different HSC aging studies [55, 61]. The enhanced myeloid skewing in aged *Pon2*^{-/-} mice may be caused by a small increase in ROS levels as detected in MPPs [62, 63].

Since studies on cell culture models after PON2 knockdown as well as *Pon2*^{-/-} endothelial cells have shown enhanced ROS formation [12, 13], we determined total ROS level and superoxide/hydrogen peroxide level in BMCs of young animals. Due to their low metabolic activity, HSCs are vulnerable to cellular damage caused by oxidative stress. In physiological quantities, ROS act as signal molecules that regulate stem cell proliferation, differentiation, and mobilization. Even a comparatively minor increase of ROS in HSCs can lead to the malfunction of self-renewal activity and HSC senescence, which can cause premature exhaustion of the HSC pool and hematopoietic dysfunctions [64]. Analysis

of superoxide/hydrogen peroxide production showed markedly enhanced formation rates in whole BMC of young *Pon2*^{-/-} animals. However, total ROS levels were not affected in LT-HSCs in young and old *Pon2*^{-/-} animals. PON2 has been shown to reduce superoxide production mainly at the inner membrane of mitochondria [10], but LT-HSCs demand low amounts of energy, which are almost entirely produced via glycolysis [19]. The increase of mitochondrial superoxide production in *Pon2*^{-/-} LT-HSC may therefore be minimal or not even existent. Meanwhile, already with the first step of differentiation into cycling cells—that of ST-HSCs—cells shift from glycolysis to mitochondrial ATP production [20]. The increase of superoxide/hydrogen peroxide (e.g., in ST-HSCs and numerically in MPPs) likely reflects higher ROS level in *Pon2*^{-/-} progenitor cells, finally contributing to the observed phenotype resembling premature aging. A mechanism involved in HSC aging is reduction of the activity of the telomerase enzyme, which leads to a limitation of cell proliferation in HSCs [26]. In our studies, we observed a reduction of *Tert* gene expression in HSC isolated from young *Pon2*^{-/-} mice.

Interestingly, quantitative analysis of different HSPC subpopulations in BM of WT and *Pon2*^{-/-} mice revealed an increased percentage of LT-HSCs. Further, we observed an advantage over WT-BMCs in competitive repopulation assays at early time points in young animals, likely due to the increased percentage of *Pon2*^{-/-} LT-HSCs as a consequence of diminished apoptotic cell death in young and old *Pon2*^{-/-} LT-HSCs. Interestingly, gene inactivation of the enzymatically active subunit of the NADPH oxidase holoenzyme subunit gp91phox (NOX2) resulting in reduced ROS generation produced an opposite result. In competitive transplantation with WBM cells from NOX2^{-/-} animals, a reduced engraftment was seen [17]. These data indicate that *Pon2*-dependent mechanisms additional to ROS detoxification might be involved in mediating the observed phenotype. RNA-seq analyses in HSCs of young animals identified a number of differentially expressed genes described to regulate cell death and proliferation. For example, we observed enhanced expression of the ATP-dependent DNA helicase Q4 (*Recq14*, DNA repair), the makorin ring finger protein 2 (*Mkrn2*, antiapoptotic), and the cyclin-dependent kinase 5 regulatory subunit-associated protein 1 (*Cdk5rap1*) as well as decreased levels of apoptosis-associated tyrosine kinase (*Aatk*, proapoptotic). RECQL4 is essentially involved in DNA-repair [65, 66] and inactivation of this gene resulted in bone marrow failure due to increased apoptotic rates [67]. In primary leukemia cells and in different leukemia cell lines, enhanced MKRN2 expression results in reduced apoptotic rates and enhanced cell proliferation [68]. In human breast cancer MCF-7 cells, CDK5RAP1 deficiency induces cell cycle arrest and apoptosis indicating an antiapoptotic function of this protein [69]. AATK has been described to be important for the induction of growth arrest and/or apoptosis of myeloid precursor cells [70]. In previous studies, PON2 has been shown to induce antiapoptotic properties [71, 72]. We speculate that in our *Pon2*^{-/-} knockout model, a positive feedback is activated at the LT-HSC levels to compensate the increased demand of progenitor cells and

accelerated aging phenotype resulting in an increased number of LT-HSCs. In addition to the above-mentioned genes, we detected a significant induction of the expression of *Cxcr4*. The CXCL12/CXCR4 axis is involved in the regulation of homing, quiescence/proliferation, or migration [60]. In young mice with inactivated aryl hydrocarbon receptor (*Ahr*), a small but significant enhancement of the ROS production was seen, similar upon *Pon2* depletion. In microarray experiments, the authors detected a 2.91-fold enhancement of the *Cxcr4* expression (*P* value 0.045) [54]. Moreover, treatment with the ROS generator DMNQ resulted in enhanced CXCR4 mRNA expression in HPC-7 hematopoietic stem cells and BA/F3 pro B cells. One important mechanism of CXCL12/CXCR4 signaling in the maintenance of HSC homeostasis is the protection against (oxidative) stress [73]. So it is likely that the enhanced *Cxcr4* expression in *Pon2*^{-/-} HSC protects these cells from transplantation-induced stress at early time points. In line with previous data [73], this finding allows us to speculate that the CXCR4/CXCL12 axis is upregulated as a result of increased ROS to counteract hematopoietic stem cell exhaustion upon *Pon2* loss. While *Pon2* depletion causes increased ROS and cell exhaustion in more mature progenitor cells of young mice, compensatory upregulation of *Cxcr4* may protect LT-HSCs of these mice, leading to increased cell numbers and decreased apoptosis providing adequate supply of committed progenitors, a hypothesis that remains to be explored in future investigations.

5. Conclusion

In conclusion, our current data indicate that PON2 is involved in the regulation of HSC functions. Enhanced ROS levels in *Pon2*^{-/-} progenitor cells correlate with increased frequencies of CMPs and GMPs as well as a skewed myeloid-to-lymphoid ratio in aged mice. Loss of *Pon2* activated an antiapoptotic program in LT-HSCs but also caused increased expression of genes involved in stem cell maintenance, e.g., *Cxcr4*, *Recql4*, and *Aatk*. We speculate that the induction of a “maintenance” program upon *Pon2* depletion counteracts a ROS-mediated premature aging phenotype and ensures proper supply of committed progenitor cells in aged mice. However, further experiments are required to address this hypothesis.

Data Availability

Raw RNA-seq data are available via the gene expression omnibus (GEO) repository [74] by accession number GSE122553.

Conflicts of Interest

The authors have no conflict of interest.

Authors' Contributions

LS designed the study, performed the research, analyzed the data, and wrote the manuscript; JE, VS, MM, PSH, VP, AS,

DS, PM, and NC-W performed the research, analyzed the data, and wrote the manuscript; SH, AP, and AD designed the study, analyzed the data, and wrote the manuscript; IW, DS, TK, and HK designed and supervised the study, analyzed the data, and wrote the manuscript. LS and IW as well as DS, TK, and HK contributed equally to this work.

Acknowledgments

The authors thank the Institute of Molecular Biology gGmbH (IMB), Mainz, Germany, for the possibility to use the FACSARIA™ II SORP Flow Cytometer Cell Sorter (BD Biosciences) of the IMB Flow Cytometry Core Facility in our experiments. We thank the genomics core facility at the IMB, Mainz, for providing the sequencing facility. This work was supported by the DFG grant WI3897/3-1 to IW and HK and Center for Thrombosis and Hemostasis Mainz (BMBF funding allocation ID 01E01003, project TRPX2 to SH and HK).

Supplementary Materials

Figure S1: *Pon2* mRNA expression in different bone marrow cells of WT mice. Figure S2: in young *Pon2*^{-/-} mice, reciprocal BM transplantation reveals cell intrinsic as well as extrinsic phenotypes. Figure S3: *Pon2*^{-/-} BMCs show no enhanced amount of DNA double-strand breaks in LSK cells. Figure S4: bone marrow cells of young *Pon2*^{-/-} and WT mice show no differences in cell cycle status, colony-forming ability, and homing. Figure S5: gating strategies. Figure S6: representative histograms showing the DCF-DA data of LT- and ST-HSC as well as MPP isolated from young WT and *Pon2*^{-/-} mice. Table S1: sequences of primers and probes used for qRT-PCR-based quantification of *Pon2* mRNA expression. Table S2: differentially expressed genes identified using DESeq2 and whole genome RNA-seq data from HSCs isolated from WT and *Pon2*^{-/-} animals. Table S3: pathways enriched in HSCs isolated from *Pon2*^{-/-} animals. Table S4: pathways decreased in HSCs isolated from *Pon2*^{-/-} animals. (*Supplementary Materials*)

References

- [1] R. Prieto-Bermejo, M. Romo-Gonzalez, A. Perez-Fernandez, C. Ijurko, and A. Hernandez-Hernandez, “Reactive oxygen species in haematopoiesis: leukaemic cells take a walk on the wild side,” *Journal of Experimental & Clinical Cancer Research*, vol. 37, no. 1, p. 125, 2018.
- [2] W. Droge, “Free radicals in the physiological control of cell function,” *Physiological Reviews*, vol. 82, no. 1, pp. 47–95, 2002.
- [3] Y. M. Mosaad, “Hematopoietic stem cells: an overview,” *Transfusion and Apheresis Science*, vol. 51, no. 3, pp. 68–82, 2014.
- [4] A. Valdivia, S. Perez-Alvarez, J. D. Aroca-Aguilar, I. Ikuta, and J. Jordan, “Superoxide dismutases: a physiopharmacological update,” *Journal of Physiology and Biochemistry*, vol. 65, no. 2, pp. 195–208, 2009.
- [5] P. Wenzel, S. Kossmann, T. Munzel, and A. Daiber, “Redox regulation of cardiovascular inflammation - immunomodulatory

- function of mitochondrial and Nox-derived reactive oxygen and nitrogen species,” *Free Radical Biology & Medicine*, vol. 109, pp. 48–60, 2017.
- [6] T. E. S. Kauppila, J. H. K. Kauppila, and N. G. Larsson, “Mammalian mitochondria and aging: an update,” *Cell Metabolism*, vol. 25, no. 1, pp. 57–71, 2017.
- [7] T. Bacchetti, G. Ferretti, and A. Sahebkar, “The role of paraoxonase in cancer,” *Semin Cancer Biol*, vol. 56, 2017.
- [8] C. J. Ng, D. J. Wadleigh, A. Gangopadhyay et al., “Paraoxonase-2 is a ubiquitously expressed protein with antioxidant properties and is capable of preventing cell-mediated oxidative modification of low density lipoprotein*,” *The Journal of Biological Chemistry*, vol. 276, no. 48, pp. 44444–44449, 2001.
- [9] C. J. Ng, N. Bourquard, V. Grijalva et al., “Paraoxonase-2 deficiency aggravates atherosclerosis in mice despite lower apolipoprotein-B-containing lipoproteins,” *The Journal of Biological Chemistry*, vol. 281, no. 40, pp. 29491–29500, 2006.
- [10] S. Altenhöfer, I. Witte, J. F. Teiber et al., “One enzyme, two functions,” *The Journal of Biological Chemistry*, vol. 285, no. 32, pp. 24398–24403, 2010.
- [11] H. Hagmann, A. Kuczkowski, M. Ruehl et al., “Breaking the chain at the membrane: paraoxonase 2 counteracts lipid peroxidation at the plasma membrane,” *The FASEB Journal*, vol. 28, no. 4, pp. 1769–1779, 2014.
- [12] S. Horke, I. Witte, P. Wilgenbus, M. Kruger, D. Strand, and U. Foerstermann, “Paraoxonase-2 reduces oxidative stress in vascular cells and decreases endoplasmic reticulum stress-induced caspase activation,” *Circulation*, vol. 115, no. 15, pp. 2055–2064, 2007.
- [13] J. Ebert, P. Wilgenbus, J. F. Teiber et al., “Paraoxonase-2 regulates coagulation activation through endothelial tissue factor,” *Blood*, vol. 131, no. 19, pp. 2161–2172, 2018.
- [14] E. M. Schweikert, A. Devarajan, I. Witte et al., “PON3 is upregulated in cancer tissues and protects against mitochondrial superoxide-mediated cell death,” *Cell Death and Differentiation*, vol. 19, no. 9, pp. 1549–1560, 2012.
- [15] S. H. Orkin and L. I. Zon, “Hematopoiesis: an evolving paradigm for stem cell biology,” *Cell*, vol. 132, no. 4, pp. 631–644, 2008.
- [16] R. Schofield, “The relationship between the spleen colony-forming cell and the haemopoietic stem cell,” *Blood Cells*, vol. 4, no. 1-2, pp. 7–25, 1978.
- [17] B. Adane, H. Ye, N. Khan et al., “The hematopoietic oxidase NOX2 regulates self-renewal of leukemic stem cells,” *Cell Reports*, vol. 27, no. 1, pp. 238–254.e6, 2019.
- [18] Y. Cao, Y. Fang, J. Cai et al., “ROS functions as an upstream trigger for autophagy to drive hematopoietic stem cell differentiation,” *Hematology*, vol. 21, no. 10, pp. 613–618, 2016.
- [19] N. Shyh-Chang, G. Q. Daley, and L. C. Cantley, “Stem cell metabolism in tissue development and aging,” *Development*, vol. 140, no. 12, pp. 2535–2547, 2013.
- [20] L. Papa, M. Djedaini, and R. Hoffman, “Mitochondrial role in stemness and differentiation of hematopoietic stem cells,” *Stem Cells International*, vol. 2019, Article ID 4067162, 10 pages, 2019.
- [21] B. A. Anthony and D. C. Link, “Regulation of hematopoietic stem cells by bone marrow stromal cells,” *Trends in Immunology*, vol. 35, no. 1, pp. 32–37, 2014.
- [22] Z. Tothova, R. Kollipara, B. J. Huntly et al., “FoxOs are critical mediators of hematopoietic stem cell resistance to physiologic oxidative stress,” *Cell*, vol. 128, no. 2, pp. 325–339, 2007.
- [23] J. Lee, S. R. Yoon, I. Choi, and H. Jung, “Causes and mechanisms of hematopoietic stem cell aging,” *International Journal of Molecular Sciences*, vol. 20, no. 6, p. 1272, 2019.
- [24] D. J. Rossi, D. Bryder, J. M. Zahn et al., “Cell intrinsic alterations underlie hematopoietic stem cell aging,” *Proceedings of the National Academy of Sciences of the United States of America*, vol. 102, no. 26, pp. 9194–9199, 2005.
- [25] E. M. Pietras, “Inflammation: a key regulator of hematopoietic stem cell fate in health and disease,” *Blood*, vol. 130, no. 15, pp. 1693–1698, 2017.
- [26] M. L. Porto, B. P. Rodrigues, T. N. Menezes et al., “Reactive oxygen species contribute to dysfunction of bone marrow hematopoietic stem cells in aged C57BL/6 J mice,” *Journal of Biomedical Science*, vol. 22, no. 1, p. 97, 2015.
- [27] S. Ghaffari, “Oxidative stress in the regulation of normal and neoplastic hematopoiesis,” *Antioxidants & Redox Signaling*, vol. 10, no. 11, pp. 1923–1940, 2008.
- [28] J. Barminko, B. Reinholt, and M. H. Baron, “Development and differentiation of the erythroid lineage in mammals,” *Developmental and Comparative Immunology*, vol. 58, pp. 18–29, 2016.
- [29] B. Zhao, Y. Mei, J. Yang, and P. Ji, “Erythropoietin-regulated oxidative stress negatively affects enucleation during terminal erythropoiesis,” *Experimental Hematology*, vol. 44, no. 10, pp. 975–981, 2016.
- [30] J. S. Friedman, V. I. Rebel, R. Derby et al., “Absence of mitochondrial superoxide dismutase results in a murine hemolytic anemia responsive to therapy with a catalytic antioxidant,” *The Journal of Experimental Medicine*, vol. 193, no. 8, pp. 925–934, 2001.
- [31] Y. Kong, S. Zhou, A. J. Kihm et al., “Loss of alpha-hemoglobin-stabilizing protein impairs erythropoiesis and exacerbates beta-thalassemia,” *The Journal of Clinical Investigation*, vol. 114, no. 10, pp. 1457–1466, 2004.
- [32] J. M. Lee, K. Chan, Y. W. Kan, and J. A. Johnson, “Targeted disruption of Nrf2 causes regenerative immune-mediated hemolytic anemia,” *Proceedings of the National Academy of Sciences of the United States of America*, vol. 101, no. 26, pp. 9751–9756, 2004.
- [33] I. Witte, U. Foerstermann, A. Devarajan, S. T. Reddy, and S. Horke, “Protectors or traitors: the roles of PON2 and PON3 in atherosclerosis and cancer,” *J Lipids*, vol. 2012, article 342806, pp. 1–12, 2012.
- [34] P. O. Pinto do, A. Kolterud, and L. Carlsson, “Expression of the LIM-homeobox gene LH2 generates immortalized steel factor-dependent multipotent hematopoietic precursors,” *The EMBO Journal*, vol. 17, no. 19, pp. 5744–5756, 1998.
- [35] R. Palacios, G. Henson, M. Steinmetz, and J. P. McKearn, “Interleukin-3 supports growth of mouse pre-B-cell clones in vitro,” *Nature*, vol. 309, no. 5964, pp. 126–131, 1984.
- [36] D. Sasca, H. Yun, G. Giotopoulos et al., “Cohesin-dependent regulation of gene expression during differentiation is lost in cohesin-mutated myeloid malignancies,” *Blood*, vol. 134, no. 24, pp. 2195–2208, 2019.
- [37] N. Watanabe and H. J. Forman, “Autoxidation of extracellular hydroquinones is a causative event for the cytotoxicity of menadione and DMNQ in A549-S cells,” *Archives of Biochemistry and Biophysics*, vol. 411, no. 1, pp. 145–157, 2003.
- [38] C. J. Ng, S. Y. Hama, N. Bourquard, M. Navab, and S. T. Reddy, “Adenovirus mediated expression of human paraoxonase 2 protects against the development of atherosclerosis in

- apolipoprotein E-deficient mice,” *Molecular Genetics and Metabolism*, vol. 89, no. 4, pp. 368–373, 2006.
- [39] J. Y. Chan, M. Kwong, M. Lo, R. Emerson, and F. A. Kuypers, “Reduced oxidative-stress response in red blood cells from p45NFE2-deficient mice,” *Blood*, vol. 97, no. 7, pp. 2151–2158, 2001.
- [40] S. F. Libregts, L. Gutierrez, A. M. de Bruin et al., “Chronic IFN- γ production in mice induces anemia by reducing erythrocyte life span and inhibiting erythropoiesis through an IRF-1/PU.1 axis,” *Blood*, vol. 118, no. 9, pp. 2578–2588, 2011.
- [41] M. Mardiney 3rd and H. L. Malech, “Enhanced engraftment of hematopoietic progenitor cells in mice treated with granulocyte colony-stimulating factor before low-dose irradiation: implications for gene therapy,” *Blood*, vol. 87, no. 10, pp. 4049–4056, 1996.
- [42] A. Daiber, M. Oelze, M. August et al., “Detection of superoxide and peroxynitrite in model systems and mitochondria by the luminol analogue L-012,” *Free Radical Research*, vol. 38, no. 3, pp. 259–269, 2004.
- [43] R. Z. Yusuf and D. T. Scadden, “Homing of hematopoietic cells to the bone marrow,” *Journal of Visualized Experiments*, vol. 25, no. 25, 2009.
- [44] G. Giordano, T. B. Cole, C. E. Furlong, and L. G. Costa, “Paraoxonase 2 (PON2) in the mouse central nervous system: a neuroprotective role?,” *Toxicology and Applied Pharmacology*, vol. 256, no. 3, pp. 369–378, 2011.
- [45] I. Witte and S. Horke, “Assessment of endoplasmic reticulum stress and the unfolded protein response in endothelial cells,” *Methods in Enzymology*, vol. 489, pp. 127–146, 2011.
- [46] E. M. Pietras, D. Reynaud, Y. A. Kang et al., “Functionally distinct subsets of lineage-biased multipotent progenitors control blood production in normal and regenerative conditions,” *Cell Stem Cell*, vol. 17, no. 1, pp. 35–46, 2015.
- [47] A. M. Bolger, M. Lohse, and B. Usadel, “Trimmomatic: a flexible trimmer for Illumina sequence data,” *Bioinformatics*, vol. 30, no. 15, pp. 2114–2120, 2014.
- [48] A. Dobin, C. A. Davis, F. Schlesinger et al., “STAR: ultrafast universal RNA-seq aligner,” *Bioinformatics*, vol. 29, no. 1, pp. 15–21, 2013.
- [49] M. I. Love, W. Huber, and S. Anders, “Moderated estimation of fold change and dispersion for RNA-seq data with DESeq2,” *Genome Biology*, vol. 15, no. 12, p. 550, 2014.
- [50] A. Kamburov, U. Stelzl, H. Lehrach, and R. Herwig, “The ConsensusPathDB interaction database: 2013 update,” *Nucleic Acids Research*, vol. 41, no. D1, pp. D793–D800, 2013.
- [51] W. Pei, F. Shang, X. Wang et al., “Resolving fates and single-cell transcriptomes of hematopoietic stem cell clones by PolylloxExpress barcoding,” *Cell Stem Cell*, vol. 27, no. 3, pp. 383–395.e8, 2020.
- [52] M. Yamashita and E. Passegue, “TNF- α coordinates hematopoietic stem cell survival and myeloid regeneration,” *Cell Stem Cell*, vol. 25, no. 3, pp. 357–372.e7, 2019.
- [53] M. Grigoriou, A. Banos, A. Filia et al., “Transcriptome reprogramming and myeloid skewing in haematopoietic stem and progenitor cells in systemic lupus erythematosus,” *Annals of the Rheumatic Diseases*, vol. 79, no. 2, pp. 242–253, 2020.
- [54] J. A. Bennett, K. P. Singh, S. L. Welle, L. A. Boule, B. P. Lawrence, and T. A. Gasiewicz, “Conditional deletion of Ahr alters gene expression profiles in hematopoietic stem cells,” *PLoS One*, vol. 13, no. 11, article e0206407, 2018.
- [55] S. J. Morrison, A. M. Wandycz, K. Akashi, A. Globerson, and I. L. Weissman, “The aging of hematopoietic stem cells,” *Nature Medicine*, vol. 2, no. 9, pp. 1011–1016, 1996.
- [56] R. C. Allsopp, G. B. Morin, J. W. Horner, R. DePinho, C. B. Harley, and I. L. Weissman, “Effect of TERT over-expression on the long-term transplantation capacity of hematopoietic stem cells,” *Nature Medicine*, vol. 9, no. 4, pp. 369–371, 2003.
- [57] E. Sahin and R. A. Depinho, “Linking functional decline of telomeres, mitochondria and stem cells during ageing,” *Nature*, vol. 464, no. 7288, pp. 520–528, 2010.
- [58] L. Hu, Y. Zhang, W. Miao, and T. Cheng, “Reactive Oxygen Species and Nrf2: Functional and Transcriptional Regulators of Hematopoiesis,” *Oxidative Medicine and Cellular Longevity*, vol. 2019, Article ID 5153268, 11 pages, 2019.
- [59] S. Murakami, T. Suzuki, H. Harigae, P. H. Romeo, M. Yamamoto, and H. Motohashi, “NRF2 activation impairs quiescence and bone marrow reconstitution capacity of hematopoietic stem cells,” *Molecular and Cellular Biology*, vol. 37, no. 19, 2017.
- [60] T. Nagasawa, “CXCL12/SDF-1 and CXCR4,” *Frontiers in Immunology*, vol. 6, p. 301, 2015.
- [61] M. Kim, H. B. Moon, and G. J. Spangrude, “Major age-related changes of mouse hematopoietic stem/progenitor cells,” *Annals of the New York Academy of Sciences*, vol. 996, no. 1, pp. 195–208, 2003.
- [62] C. Mantel, S. Messina-Graham, A. Moh et al., “Mouse hematopoietic cell-targeted STAT3 deletion: stem/progenitor cell defects, mitochondrial dysfunction, ROS overproduction, and a rapid aging-like phenotype,” *Blood*, vol. 120, no. 13, pp. 2589–2599, 2012.
- [63] M. Sattler, S. Verma, G. Shrikhande et al., “The BCR/ABL tyrosine kinase induces production of reactive oxygen species in hematopoietic cells*,” *The Journal of Biological Chemistry*, vol. 275, no. 32, pp. 24273–24278, 2000.
- [64] L. Shao, H. Li, S. K. Pazhanisamy, A. Meng, Y. Wang, and D. Zhou, “Reactive oxygen species and hematopoietic stem cell senescence,” *International Journal of Hematology*, vol. 94, no. 1, pp. 24–32, 2011.
- [65] H. Lu, R. A. Shamanna, G. Keijzers et al., “RECQL4 promotes DNA end resection in repair of DNA double-strand breaks,” *Cell Reports*, vol. 16, no. 1, pp. 161–173, 2016.
- [66] R. A. Shamanna, D. K. Singh, H. Lu et al., “RECQ helicase RECQL4 participates in non-homologous end joining and interacts with the Ku complex,” *Carcinogenesis*, vol. 35, no. 11, pp. 2415–2424, 2014.
- [67] M. F. Smeets, E. DeLuca, M. Wall et al., “The Rothmund-Thomson syndrome helicase RECQL4 is essential for hematopoiesis,” *The Journal of Clinical Investigation*, vol. 124, no. 8, pp. 3551–3565, 2014.
- [68] K. Y. Lee, K. Y. Chan, K. S. Tsang et al., “Ubiquitous expression of MAKORIN-2 in normal and malignant hematopoietic cells and its growth promoting activity,” *PLoS One*, vol. 9, no. 3, article e92706, 2014.
- [69] H. Wang, L. Wei, C. Li, J. Zhou, and Z. Li, “CDK5RAP1 deficiency induces cell cycle arrest and apoptosis in human breast cancer cell line by the ROS/JNK signaling pathway,” *Oncology Reports*, vol. 33, no. 3, pp. 1089–1096, 2015.
- [70] E. Gaozza, S. J. Baker, R. K. Vora, and E. P. Reddy, “AATYK: a novel tyrosine kinase induced during growth arrest and apoptosis of myeloid cells,” *Oncogene*, vol. 15, no. 25, pp. 3127–3135, 1997.

- [71] S. Horke, I. Witte, P. Wilgenbus et al., "Protective effect of paraoxonase-2 against endoplasmic reticulum stress-induced apoptosis is lost upon disturbance of calcium homeostasis," *The Biochemical Journal*, vol. 416, no. 3, pp. 395–405, 2008.
- [72] I. Witte, S. Altenhofer, P. Wilgenbus et al., "Beyond reduction of atherosclerosis: PON2 provides apoptosis resistance and stabilizes tumor cells," *Cell Death & Disease*, vol. 2, no. 1, article e112, 2011.
- [73] Y. Zhang, M. Depond, L. He et al., "CXCR4/CXCL12 axis counteracts hematopoietic stem cell exhaustion through selective protection against oxidative stress," *Scientific Reports*, vol. 6, no. 1, p. 37827, 2016.
- [74] R. Edgar, M. Domrachev, and A. E. Lash, "Gene Expression Omnibus: NCBI gene expression and hybridization array data repository," *Nucleic Acids Research*, vol. 30, no. 1, pp. 207–210, 2002.

Research Article

Preparation, Biosafety, and Cytotoxicity Studies of a Newly Tumor-Microenvironment-Responsive Biodegradable Mesoporous Silica Nanosystem Based on Multimodal and Synergistic Treatment

Zelai He,¹ Huijun Zhang,² Hongwei Li,¹ Yanyan Wang,¹ Jing Qian,¹ Xixi Cai,³ Li Sun,¹ and Jingwen Huang¹ 

¹The First Affiliated Hospital of Bengbu Medical College & Tumor Hospital Affiliated to Bengbu Medical College, Bengbu 233004, China

²Department of Cardiothoracic Surgery, Huashan Hospital of Fudan University, Shanghai 200040, China

³The Second Affiliated Hospital of Bengbu Medical College, Bengbu 233004, China

Correspondence should be addressed to Jingwen Huang; byfyhjw@163.com

Received 10 July 2020; Accepted 28 July 2020; Published 5 November 2020

Guest Editor: Ciprian Tomuleasa

Copyright © 2020 Zelai He et al. This is an open access article distributed under the Creative Commons Attribution License, which permits unrestricted use, distribution, and reproduction in any medium, provided the original work is properly cited.

Patients with triple negative breast cancer (TNBC) often suffer relapse, and clinical improvements offered by radiotherapy and chemotherapy are modest. Although targeted therapy and immunotherapy have been a topic of significant research in recent years, scientific developments have not yet translated to significant improvements for patients with TNBC. In view of these current clinical treatment shortcomings, we designed a silica nanosystem (SNS) with Nano-Ag as the core and a complex of MnO₂ and doxorubicin (Dox) as the surrounding mesoporous silica shell. This system was coated with anti-PD-L1 to target the PD-L1 receptor, which is highly expressed on the surface of tumor cells. MnO₂ itself has been shown to act as chemodynamic therapy (CDT), and Dox is cytotoxic. Thus, the full SNS system presents a multimodal, potentially synergistic strategy for the treatment of TNBC. Given potential interest in the clinical translation of SNS, the biological safety and antitumor activity of SNS were evaluated in a series of studies that included physicochemical characterization, particle stability, blood compatibility, and cytotoxicity. We found that the particle size and zeta potential of SNS were 94.6 nm and -22.1 mV, respectively. Ultraviolet spectrum analysis showed that Nano-Ag, Dox, and MnO₂ were successfully loaded into SNS, and the drug loading ratio of Dox was about 10.2%. Stability studies found that the particle size of SNS did not change in different solutions. Hemolysis tests showed that SNS, at levels far exceeding the anticipated physiologic concentrations, did not induce red blood cell lysis. Further *in vitro* and *in vivo* experiments found that SNS did not activate platelets or cause coagulopathy and had no significant effects on the total number of blood cells or hepatorenal function. Cytotoxicity experiments suggested that SNS significantly inhibited the growth of tumor cells by damaging cell membranes, increasing intracellular ROS levels, inhibiting the release of TGF- β 1 cytokines by macrophages, and inhibiting intracellular protein synthesis. In general, SNS appeared to have favorable biosafety and antitumor effects and may represent an attractive new therapeutic approach for the treatment of TNBC.

1. Introduction

Nanoparticle (NP) systems have arisen as a popular strategy among researchers seeking to improve methods of diagnosis and treatment for a wide range of diseases and have resulted in a number of approved diagnoses/therapies

such as Ferumoxytol, albumin-bound paclitaxel, and Onivyde [1–6]. Nanosystems are primarily used as drug loading or delivery carriers (e.g., for small molecules, proteins/peptides, or gene therapies) or directly as imaging agents [7–9]. Nanosystems as drug carriers for anticancer therapeutics have become a particularly popular field of

research, given the potential benefits of targeted delivery to the tumor environment and a corresponding possibly reduction in systemic toxicities [10–12]. Nanomaterials have unique physical, chemical, and biological characteristics that allow them to effectively be loaded with chemotherapeutics or gene therapies [7–9]. Through active or passive transport that leads to preferential accumulation at the target site *in vivo*, the effective dose of chemotherapy drugs delivered to nontarget tissues can be significantly reduced, enabling either higher dosage to the tumor or reduced toxicity to the rest of the body [10, 11]. The PEGylated liposomal formulation of doxorubicin (Dox) reduces the toxicities and side effects of Dox through the enhanced permeability and retention effect (EPR) in the treatment of triple negative breast cancer (TNBC) [13, 14]. Similarly, nanocarrier-encapsulated indocyanine green (ICG) and Dox have allowed for combined treatment of hyperthermia and chemotherapy [15]. However, most of these new technologies are designed for systemic applications, raising biocompatibility as an important issue [16, 17].

In order to improve the poor prognosis of patients with TNBC that lacks specific, targetable receptors, our team designed a silica nanosystem (SNS) with a core made of Nano-Ag and an outer shell composed of mesoporous silica containing MnO_2 blocked Dox, with anti-PD-L1 as a targeting group. The inclusion of anti-PD-L1 was aimed at capitalizing upon the highly expressed PD-L1 receptor on the surface of tumor cells and tumor-infiltrating lymphocytes (TIL) [18–20]. MnO_2 itself has a role in chemodynamic therapy (CDT), and Dox is cytotoxic [21, 22]. Combined, this platform offers the potential for multimodal, synergistic treatment of TNBC. Prior preliminary studies showed that SNS can successfully target TNBC. In this work, to enable further potential clinical development of SNS, we investigated the biosafety and antitumor activity of SNS.

2. Materials and Methods

2.1. Materials. Assay kits for phorbol 12-myristate 13-acetate (PMA), reactive oxygen species (ROS), Triton X-100, BCA, IL-1 β , and TGF- β 1 were obtained from Beyotime Biotechnology (Shanghai, China). Kits for the measurement of adenosine diphosphate (ADP), lactate dehydrogenase (LDH), anti-PD-L1 (spartalizumab), and Dox were purchased from TOMUMS life science Co., Ltd. (Guangzhou, China). Cell Counting Kit-8 (CCK8) was obtained from Dojindo Laboratories (Shanghai) Co., Ltd. (Shanghai, China). Fetal bovine serum (FBS), penicillin, and streptomycin, Roswell Park Memorial Institute (RPMI) 1640 medium and Dulbecco modified Eagle medium (DMEM) were purchased from Thermo Fisher Scientific, Inc. (Waltham, USA). Other reagents not specifically listed here were obtained from Sino-pharm (Beijing, China).

2.2. Cell Culture and Animal Experiments. Human Monocyte Leukemia Cell line THP-1, TNBC cell lines MDA-MB-231, and 4T1 were kindly provided by Stem Cell Bank of the Chinese Academy of Sciences. All cells were cultured at 37°C in

5% CO_2 , and the culture media for 4T1 and MDA-MB-231 cells was high-glucose DMEM with 1% penicillin-streptomycin and 10% FBS [2, 21]. The medium of THP-1 cells was RPMI 1640 medium with 1% penicillin-streptomycin and 10% FBS [16]. All animal studies met the Ethical Committee requirements of Bengbu College.

2.3. Preparation of SNS. (a) 7.5 mL glucose solution (30 mg/mL) was added to 40 mL of CTAB aqueous solution (1.25 mg/mL) and stirred at 80°C and 500 rpm for 30 min. Then, we slowly added 1.5 mL of a mixed solution containing 54 mg AgNO_3 and 56 mg arginine. After 3 min, we added, in turn, 50 mg CTAB and 424 μL TEOS and continued stirring for 3 h. Next, we added 15 mL of isopropanol, 30 mL of hydrochloric acid (5 N), and 20 mL of hexamethyldisilicylether (HMDO), which was then heated to 80°C and stirred for 30 min. The colored solution on the upper layer was collected, centrifuged, and washed many times with ethanol to obtain the silver-containing mesoporous silica NPs (MSN). (b) Next, we combined 25 mg of silver-loaded MSN and 1 mL of Dox-HCl (2.78 mg/mL and pH 7.0), which was stirred in the dark for 24 hours at room temperature to allow Dox adsorption to reach equilibrium. (c) The silver-loaded MSN and Dox were collected by centrifugation; then, we added 1 mL of KMnO_4 solution (0.79 mg/mL) and 1.25 mL of MES (100 mm and pH 6.0) and mixed for 30 min by ultrasound. Then, the oxidation-reduction reaction between KMnO_4 and MES formed brown MnO_2 , which would be loaded into the MSN-COOH shell to block Dox. Finally, MSN loaded with Nano-Ag, Dox, and MnO_2 was obtained and precipitated by centrifugation and three washes (15,000 rpm and 15 min). (d) 20 mg MSN was dispersed in 5 mL MES (100 mm and pH 6), 1 mg anti-PD-L1 was added, and 0.2 mg EDC was added to crosslink for 4 h. Then, it was centrifuged and washed another 3 times (15,000 rpm and 15 min) and then freeze dried to obtain the final SNS.

2.4. Physicochemical Characterization. The diameter and size distribution of NPs were determined by dynamic light scattering (DLS) on a ZetaSizer Nano ZS (Malvern Instruments Ltd., UK). Zeta potential (ζ) was characterized using an He-Ne laser beam ($\lambda = 633.8$ nm) [23–26]. All measurements were made at 25°C, and the concentration of the sample in PBS solution was 40 $\mu\text{g}/\text{mL}$. Ten microliters of NPs (40 $\mu\text{g}/\text{mL}$) were dropped on a copper grid and dried at room temperature, then sputter-coated with gold and observed using an H-800 transmission electron microscope (TEM) (Hitachi, Tokyo, Japan) (acceleration voltage: 200 kV) [24–27]. The UV-Vis absorbance of different NP formulations was detected by GS54T UV-Vis spectrophotometer (Tianjin Tuopu Instrument Co., Ltd., Tianjin, China). All samples were analyzed in triplicate batches ($n = 3$).

2.5. Stability Evaluation of SNS. The size of SNS in PBS (pH 7.4), 2% BSA, and 5% FBS solution (NPs' final concentration: 40 $\mu\text{g}/\text{mL}$) was detected using a ZetaSizer Nano ZS system after 6 h, 12 h, 24 h, 2 d, and 3 days of incubation at 37°C. We also measured the size of SNS in PBS of varying pH (5.0, 7.4, and 9.1) by DLS [25, 28].

2.6. Blood Compatibility

2.6.1. Hemolysis Rate. Blood samples were collected from healthy male volunteers into an anticoagulant tube (BD EDTA routine blood tube) according to the anticoagulant tube instructions and diluted with normal saline (8 mL anticoagulant blood plus 10 mL normal saline). The prepared NPs were added to the diluted blood, and the final concentrations of NPs were 20, 50, 100, and 200 $\mu\text{g}/\text{mL}$. After incubation for 1 h at 37°C, blood samples were centrifuged at 2,500 rpm for 5 min. The supernatant was collected, and the absorbance was measured using a UV-Vis spectrophotometer at 540 nm. Then, we calculated the hemolysis rate as the following formula (1):

$$\text{Hemolysis rate(\%)} = (\text{ODt} - \text{ODnc})/\text{ODpc} \times 100\%, \quad (1)$$

where ODt is the absorbance value of the NP group; ODnc is the absorbance value of the negative control (normal saline); ODpc is the absorbance value of the positive control (distilled water), and hemolysis rate was 100%. A hemolysis rate $\leq 5\%$ indicated that the material met our safety requirements; a hemolysis rate $> 5\%$ indicated that the material could induce rupture of red blood cells (RBCs), thus failing requirements for clinical use [17, 23].

2.6.2. Platelet Activation Analysis. To determine the platelet activation, fresh blood samples from healthy male volunteers were collected into sodium citrate anticoagulant tubes (BD Biosciences-China, China). Then, the blood was incubated with NPs at 37°C (final concentration: 200 $\mu\text{g}/\text{mL}$). After 30 min, we assessed the degree of platelet activation by flow cytometry (FCM) (BD Biosciences, USA). For this, we measured the presence of fluorescently labeled platelet activation marker anti-CD62P and the platelet pan-marker anti-CD42a using FCM [11, 17]. 0.9% NaCl and 0.2 μM ADP were used as negative control (NC) and positive control (PC), respectively.

2.6.3. Effect of NPs on Blood Coagulation. Fresh blood samples were collected from healthy male volunteers into anticoagulation tubes with 109 mmol/L sodium citrate ($V_{\text{blood}} : V_{\text{anticoagulant}} = 9 : 1$). NPs were added to this blood sample to a final concentration of 200 $\mu\text{g}/\text{mL}$. After incubation for 30 min at 37°C, the blood was centrifuged at 2,500 rpm for 10 min. Then, according to standard protocols, the activated partial thromboplastin time (APTT), prothrombin time (PT), thrombin time (TT), and fibrinogen (FIB) was measured on a Sysmex CS5100 Automatic Coagulation Analyzer (Xisen Meikang Medical Electronics (Shanghai) Co., Ltd., Shanghai, China) [29]. PBS and hemocoagulase atrox (0.1 unit/mL) were used as NC and PC, respectively.

2.6.4. Effect of NPs In Vivo on Blood Cells and Biochemical Parameters. NPs (1.5 mg/kg) were injected into the tail vein of female SD mice (7-8 weeks) once every 7 d. We used PBS and Dox (4.5 mg/kg) as the NC and PC. After 14 d, the mice were sacrificed, and fresh blood was collected into an anticoagulant tube with 109 mmol/L sodium citrate ($V_{\text{blood}} : V_{\text{anticoagulant}} = 9 : 1$). A complete blood count and

clinical blood chemistries (to assess liver and kidney functions) were measured using a Sysmex pocH-100i Automated Hematology Analyzer (Sysmex Medical Electronics (Shanghai) Co., Ltd., China) and an AU480 Beckman Automatic Biochemical Analyzer (Beckman Coulter, Inc., Miami, USA), as instructed by the manufacturer [16].

2.7. Cell Compatibility

2.7.1. LDH Release Experiment. The integrity of cell membranes was determined by an LDH release experiment. An appropriate amount of 4T1 and MDA-MB-231 cells were cultured in 96-well plates, per kit instructions. After adherence, the culture medium was aspirated and 200 μL of DMEM containing NPs (5 $\mu\text{g}/\text{mL}$) was added into each well of the 96-well plates. DMEM medium containing 1% Triton X-100 was used as the PC, and DMEM medium alone was used as the NC [2, 16]. After 24 h, the LDH concentration in the supernatant was determined according to the LDH kit instructions.

2.7.2. Intracellular ROS Level Assay. Intracellular ROS levels were determined using 2,7-dichlorodihydrofluorescein diacetate (DCFH-DA) as the indicator. In brief, an appropriate amount of 4T1 and MDA-MB-231 cells were incubated in 6-well plates. After adherence, DMEM medium containing NPs (5 $\mu\text{g}/\text{mL}$) was added and cells were cultured. DMEM medium containing H_2O_2 (50 μM) was used as the PC. PBS was used as the NC [16, 30]. After 6 h, the cells were washed 3 times using PBS. Then, the effect of NPs on intracellular ROS levels was determined per the kit's instructions.

2.8. Immunocompatibility. PMA was added into RPMI 1640 medium containing THP-1 cells in the logarithmic phase of growth to a final concentration of 50 ng/mL. Then, the cell suspension medium was added to 96-well plates at 200 μL per well and incubated for 48 h to induce THP-1 cells to differentiate into macrophages. Then, the RPMI 1640 was carefully aspirated and replaced by 200 μL of RPMI 1640 medium containing NPs (concentration: 5 $\mu\text{g}/\text{mL}$). In this experiment, 200 μL RPMI 1640 medium was used as the NC, and 200 μL RPMI 1640 medium containing 2.5 mg/mL of inulin was used as the PC. Cells were cultured for another 24 h, and the supernatant was measured for absorbance at 450 nm according to the IL-1 β and TGF- β 1 quantitative enzyme-linked assay kit instructions [16]. We used a standard curve to determine the contents of IL-1 β and TGF- β 1 in the medium.

2.9. Protein Synthesis Experiment. 4T1 cells and MDA-MB-231 cells were cultured in 6-well plates. After adherence, the culture medium in the 6-well plates was aspirated, and 1,000 μL DMEM containing NPs (concentration: 5 $\mu\text{g}/\text{mL}$) was added to each well. PBS and free Dox (10 $\mu\text{g}/\text{mL}$) were used as the NC and PC, respectively. After incubation for 24 h, protein concentration was measured according to the instructions of the BCA kit to evaluate the effects of different NPs on protein synthesis and cytotoxicity [31, 32].

2.10. Statistical Analysis. Data were presented as mean \pm standard deviation (SD). One-way ANOVA and an unpaired Student's *t*-test were used to determine the statistical significance of cross-group comparisons. A threshold of $p < 0.05$ was considered statistically significant.

3. Results

3.1. Physicochemical Characterization. During the preparation of SNS, the particle size of the intermediate NPs was about 50–80 nm (Figure 1(a)). After loading MnO_2 , the size of NPs obviously increased, indicating that MnO_2 played a role of sealing mesoporous on the surface of mesoporous silica. After NPs were conjugated with anti-PD-L1, the hydrodynamic diameter also slightly increased (by about 94.6 nm). The Dox loaded into NPs was fully encapsulated after the addition of MnO_2 , and the zeta potential of the intermediate NPs was between -20 and -30 mV. The zeta potential of full SNS was -22.1 mV (Figure 1(b)). TEM images of SNS showed that the size distribution of the black core Nano-Ag was uniform, and the morphology of the SNS with 90–100 nm diameter was uniformly spherical, in good agreement with the DLS findings of 94.6 nm (Figure 1(c)). In the UV-Vis absorption spectra, SNS without anti-PD-L1 and SNS evinced high signal peaks are representing Nano-Ag (408 nm), Dox (272 nm), and MnO_2 (380 nm) (Figure 1(d)). The signal peaks of Dox/-Ag@SNS had Nano-Ag (408 nm) and Dox (272 nm). As expected, Ag@SNS only had peaks for Nano-Ag (408 nm). These findings indicated that the Nano-Ag, Dox, and MnO_2 were successfully coloaded into SNS prior to anti-PD-L1 grafting. After SNS preparation, the content of Dox in the supernatant was detected by a UV-Vis spectrophotometer, and the drug-loading rate of Dox was determined to be about 10.2%. As seen in Figure 1(e), the SNS without Nano-Ag was dark blue, and the SNS without Dox was yellow green. SNS, SNS without MnO_2 , and SNS without anti-PD-L1 were color of MnO_2 ; light brown.

3.2. Stability of SNS. When NPs are injected to systemic circulation, they adsorb plasma proteins that change the size of NPs and extent of phagocytosis by macrophages, thus affecting *in vivo* distribution and retention time [33, 34]. Before SNS incubation with PBS, 2% BSA, and 5% FBS, the particle size was 94.6 nm by DLS. In a PBS alone, PBS with 5% FBS, and PBS with 2% BSA, the particle sizes of SNS at 12 h were 98.52 nm, 114.11, nm and 103.04 nm, respectively; at 72 h, the average diameters were 109.39 nm, 126.92 nm, and 121.41 nm, respectively (Figure 2(a)). Thus, protein contents in buffer appeared to slightly increase mean particle size, potentially due to protein adsorption. However, these differences were not statistically significant. With prolonged incubation time, the particle size of SNS in different pH values of PBS solution gradually increased (Figure 2(b)). At 12 h, in PBS solutions with pH of 5.0, 7.4, and 9.1, the size of SNS was 95.16 nm, 98.52 nm, and 101.09 nm, respectively; at 72 h, the sizes were 101.73 nm, 109.39 nm, and 113.74 nm, respectively. The lower the pH value, the smaller the increase in SNS particle size; the larger the pH value, the larger the increase in SNS particle size. However, compared with the

preincubation of SNS diameters, there was no statistically significant difference, potentially due to the accelerated degradation of MnO_2 in acidic solution [31]. These results suggest that SNS is stable over a range of physiologic buffer conditions.

3.3. Blood Compatibility

3.3.1. Hemolysis Rate. *In vitro* hemolysis tests are considered an important and reliable method to evaluate the hemocompatibility of drugs [35]. In these hemolysis experiments, we assessed for a linear relationship between SNS concentration and hemolysis rate. The fitted linear equation of SNS without Dox was $y = 0.7612 + 0.00966x$ ($R^2 = 0.96$); for SNS without MnO_2 group was $y = 1.7471 + 0.01053x$ ($R^2 = 0.88$); SNS without Nano-Ag group was $y = 1.1693 + 0.01460x$ ($R^2 = 0.87$); SNS without anti-PD-L1 group was $y = 1.8149 + 0.007144x$ ($R^2 = 0.99$); and, finally, SNS group was $y = 1.2731 + 0.009075x$ ($R^2 = 0.99$). When the above NPs reached 5% hemolysis rate, the concentrations were 438.80, 308.92, 262.38, 445.84, and 410.68 $\mu\text{g}/\text{mL}$, respectively, significantly higher than the maximum experimental concentration of 200 $\mu\text{g}/\text{mL}$ used in this experiment. Moreover, when the maximum experimental concentration of NPs was 200 $\mu\text{g}/\text{mL}$, the hemolysis rate of all NPs was less than 4% (Figure 3(a)). These experiments suggest that the extent of RBC rupture induced by SNS over the relevant concentration range (5–10 $\mu\text{g}/\text{mL}$) is likely to be far less than 5%. According to the standard of American Society for Materials Testing (ASTM F756-00, 2000), SNS and other NPs are not typically hemolytic [25].

3.3.2. Platelet Activation Test. Platelet activation is a complicated process involving many physiological and pathological processes, including thrombosis events, inflammation, tumor growth, and metastasis [11, 17]. When foreign NPs are introduced to the blood, the degree of platelet activation is a key indicator of hemocompatibility. We performed a platelet activation test to study the hemocompatibility of SNS, by FCM (Figure 3(b)). The platelet activation results suggested that NPs were not significantly different than NC, which had very low platelet activation ($p > 0.05$). The PC, however, induced clear platelet activation, and there was a significant difference between PC and NC ($p < 0.001$). These results indicated that SNS likely has good platelet compatibility.

3.3.3. Effects of SNS on Coagulation. PT is the coagulation status screening test for extrinsic coagulation system and assesses for the function of each coagulation factor. The PT is an important index for monitoring patients on anticoagulation treatment. When the test value is more than 3 s greater than the control value, it is considered abnormal [16]. Similarly, APTT is a test that reflects the coagulation status of the intrinsic coagulation system and is often used as a screening test [25]. TT is a simple test to detect the function of the coagulation, anticoagulation, and fibrinolysis systems [25]. In addition, when a platelet is activated, it will release a coagulation activator, which catalyzes prothrombin to turn into

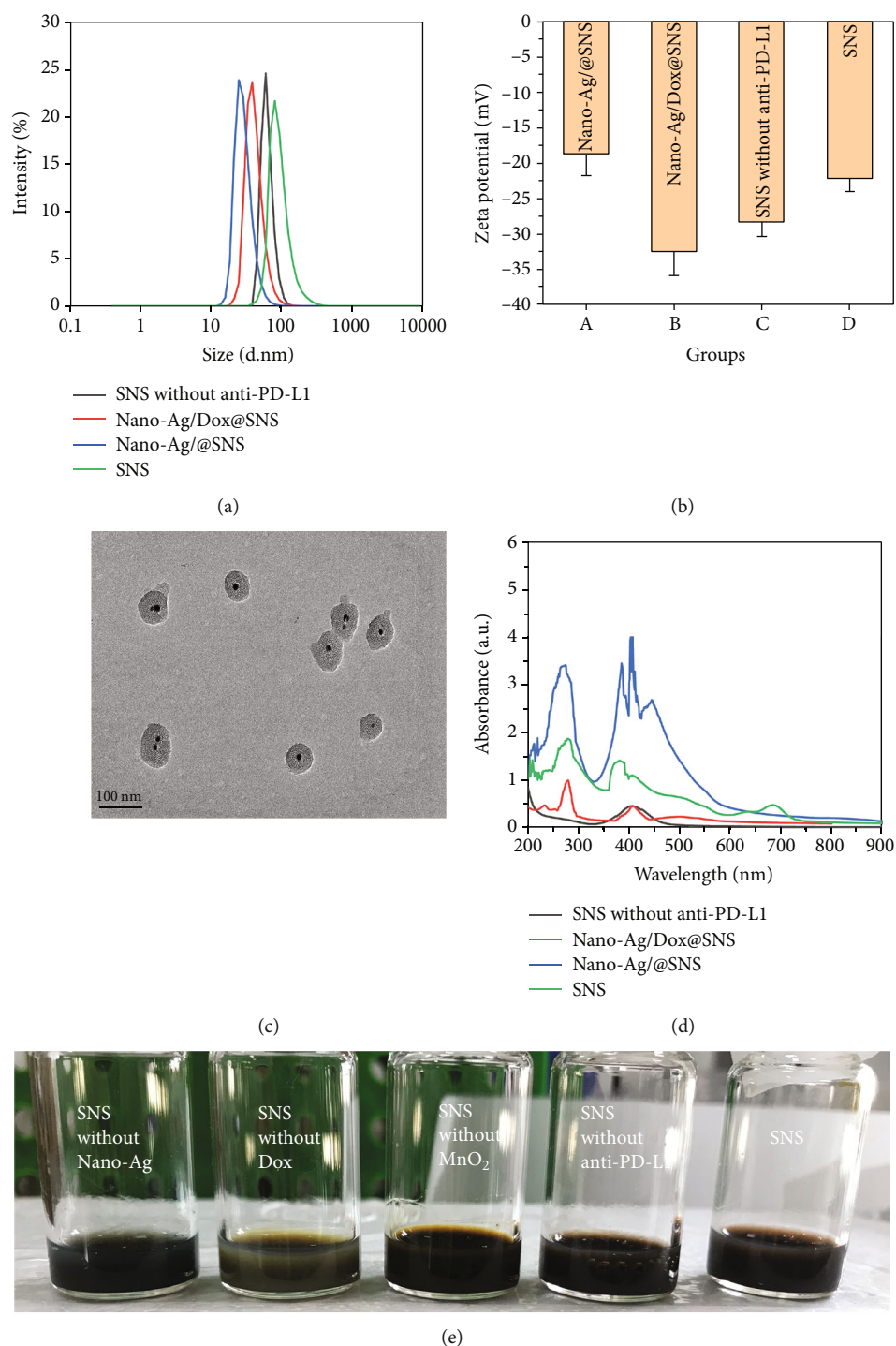


FIGURE 1: Characterization of different NPs during SNS preparation. (a) The particle size and (b) zeta potential of NPs at different stages of SNS preparation; (c) TEM of SNS showed that SNSs were uniform spheres with no aggregation; (d) UV-Vis absorption spectra of NPs in different stages of SNS preparation; (e) the appearance of different NPs in distilled water.

thrombin in a manner dependent on calcium ions. Thrombin converts water-soluble FIB in the plasma into water-insoluble fibrin. FIB accumulates around blood cells, binding them together to form a mass which results in a clot [16]. The normal concentration of FIB (cFIB) is 2-4 g/L. In the clinic, PT, APTT, TT, and cFIB are generally used as convenient indices for coagulation screening. In our study, when com-

paring NC and different NP groups, there was no significant difference in results from PT, APTT, TT, and cFIB (Table 1). Comparing the PC and NC, the PT and TT were not significantly different, but the APTT and cFIB in the PC were significantly lower than NC ($p < 0.05$). Together, these results suggest that SNS did not obviously affect the coagulation system. These results are also in accordance with the mechanism

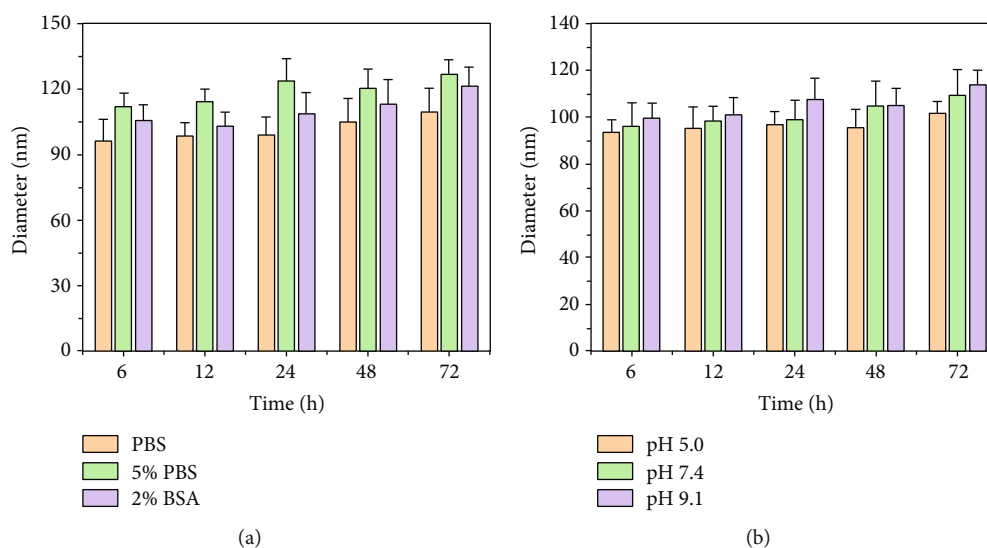


FIGURE 2: The stability of SNS in various buffers was determined by DLS. The change in size of SNS in (a) different media and (b) PBS of varying pH, over various incubation times. The size of SNS did not significantly change relative to preincubation SNS.

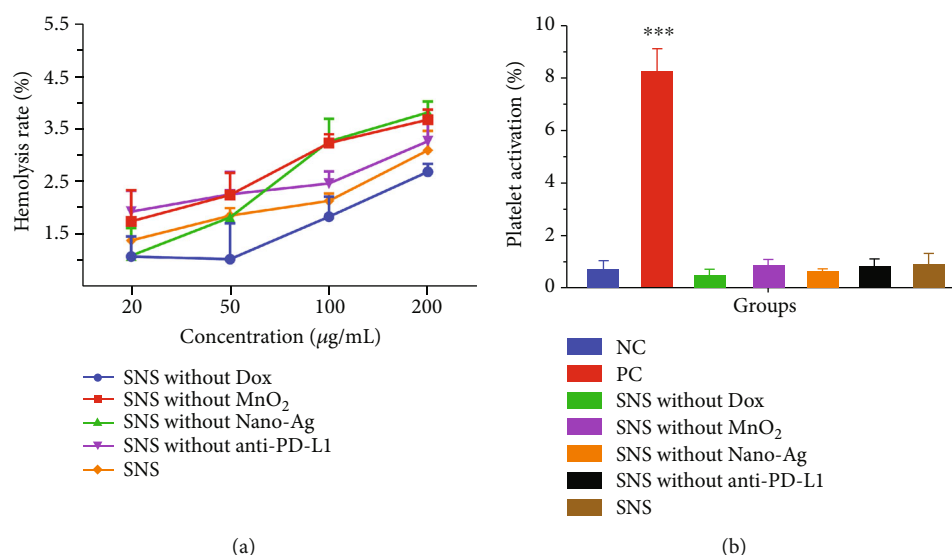


FIGURE 3: Blood compatibility of NPs. (a) The hemolysis rate of NPs at different concentrations and different stages of preparation. The hemolysis rate of all NPs at $200 \mu\text{g/mL}$ was less than 4%, suggesting that SNS had no significant effect on RBC rupture. (b) The effect of different forms of NPs on platelet activation. Treatment with $200 \mu\text{g/mL}$ NPs led to no significant induction of platelet activation, and there was no significant difference compared with the NC (0.9% NaCl), but the NPs and NC were far lower than the PC ($0.2 \mu\text{M}$ ADP). *** indicates that, compared with NC, $p < 0.001$.

of action of hemocoagulase atrox, which contains two enzymes that coagulate blood: thrombin-like and thrombokinase-like. The former promotes platelet aggregation at the site of bleeding to form white thrombus (platelet thrombus) and produce hemostasis. The latter is activated by platelet factor III (phospholipid), which converts prothrombin into thrombin and further activates fibrinogen to become fibrin [36]. Therefore, it is fitting that hemocoagulase atrox would primarily affect APTT and cFIB.

3.3.4. Effect of NPs on Blood Component Results. The effects of treatment on blood cells and biochemical parameters are

listed in Table 2. Between the NC and NP groups, there was no significant difference in white blood cells (WBC), hemoglobin (HB), platelet (PLT), alanine aminotransferase (ALT), aspartate aminotransferase (AST), serum creatinine (Scr), and blood urea nitrogen (BUN) over the course of treatment. In the PC, compared with NC, the biochemical parameters (ALT, AST, BUN, and Scr) were significantly increased ($p < 0.05$), and the blood cell counts (WBC, HB, and PLT) were significantly decreased ($p < 0.05$). These results indicated that the SNS did not significantly affect blood cells or biochemical parameters, suggesting that SNS is not likely to be toxic *in vivo*.

TABLE 1: The effects of NPs on coagulation test results.

Groups	PT (s)	APTT (s)	TT (s)	cFIB (g/L)
NC	10.33 ± 0.17	25.60 ± 0.56	18.40 ± 0.68	2.79 ± 0.55
PC	9.40 ± 0.14	11.40 ± 0.08**	17.05 ± 2.38	1.65 ± 0.42*
SNS without anti-PD-L1	10.55 ± 0.13	27.45 ± 0.52	20.20 ± 0.25	2.68 ± 0.08
SNS without Nano-Ag	10.35 ± 0.13	27.95 ± 0.41	19.08 ± 0.99	2.66 ± 0.15
SNS without Dox	10.48 ± 0.10	28.45 ± 1.37	17.78 ± 0.30	2.63 ± 0.10
SNS without MnO ₂	10.38 ± 0.10	28.05 ± 0.52	18.00 ± 0.35	2.62 ± 0.06
SNS	10.65 ± 0.06	28.00 ± 0.47	18.65 ± 0.42	2.64 ± 0.01

Note: * and **, indicate that, compared with NC, $p < 0.05$ and $p < 0.01$, respectively.

TABLE 2: The effects of NPs on blood cells and biochemical parameters.

Groups	WBC ($\times 10^9/L$)	HB (g/L)	PLT ($\times 10^9/L$)	ALT (IU/L)	AST (IU/L)	BUN (mmol/L)	Scr ($\mu\text{mol/L}$)
NC	7.36 ± 1.54	143.15 ± 18.97	462.35 ± 42.78	52.47 ± 7.84	43.86 ± 5.79	13.42 ± 2.81	124.68 ± 14.57
PC	3.14 ± 1.98**	97.07 ± 16.48*	231.92 ± 37.54**	132.59 ± 15.88**	87.63 ± 11.74**	35.81 ± 9.06**	189.82 ± 33.28*
SNS without anti-PD-L1	8.06 ± 2.19	126.08 ± 24.63	407.11 ± 64.55	48.69 ± 5.72	38.61 ± 8.71	16.44 ± 2.57	138.44 ± 23.61
SNS without Nano-Ag	6.93 ± 1.72	157.03 ± 19.46	459.32 ± 34.03	57.53 ± 4.88	41.56 ± 3.89	12.69 ± 3.78	114.65 ± 17.56
SNS without Dox	7.91 ± 2.41	135.39 ± 14.16	506.16 ± 89.97	46.05 ± 3.21	44.75 ± 6.09	15.06 ± 2.14	146.37 ± 19.72
SNS without MnO ₂	6.74 ± 2.83	161.54 ± 28.91	531.06 ± 79.58	51.06 ± 6.54	39.56 ± 4.88	17.01 ± 3.22	109.81 ± 22.43
SNS	8.25 ± 1.79	149.44 ± 12.09	493.05 ± 67.52	56.43 ± 5.01	46.77 ± 5.16	11.76 ± 3.08	133.66 ± 26.78

Note: * and ** indicated that compared with NC, $p < 0.05$ and $p < 0.01$, respectively.

3.4. Cell Compatibility

3.4.1. LDH Release Experiment. LDH is an endoenzyme that cannot pass through the intact cell membrane. Therefore, LDH release experiments can be used to determine whether treatment with SNS leads to cell membrane damage. The LDH concentration in medium at 24 h is shown in Figure 4(a) and Figure 4(b). The LDH concentrations of the NC in the 4T1 cells (87.56 U/mL) were significantly lower than the PC (442.52 U/mL) ($p < 0.01$). The LDH concentrations of SNS without Dox, SNS without MnO₂, SNS without Nano-Ag, SNS without anti-PD-L1, and SNS in 4T1 cells were 159.66, 213.04, 178.23, 256.81, and 274.09 U/mL, respectively. The LDH concentration of these NP groups was significantly higher than NC ($p < 0.01$) and significantly lower than PC ($p < 0.05$). Moreover, SNS was associated with the highest extent of LDH release. We observed similar behavior in the MDA-MB-231 cells, except that the LDH concentration of the SNS group was not significantly different compared to the PC. The high LDH release after treatment with NPs was indicative of NP-induced damage to the cell membrane. These results suggest that SNS alone leads to the most significant damage to the cell membrane.

3.4.2. Intracellular ROS Assay. Excessive ROS in cells can destroy proteins, DNA, phospholipids, and other biological macromolecules. The generation of ROS is one main anticancer mechanism of radiotherapy and several therapeutic

agents [1, 37–39]. Therefore, it is of great clinical and theoretical significance to measure the effect of NPs on intracellular ROS production. DCFH-DA has no fluorescence and can freely pass through the cell membrane. After entering the cell, DCFH-DA in the cells can be hydrolyzed by esterase to generate DCFH. Importantly, DCFH cannot penetrate the cell membrane, so the DCFH-DA probe remains inside the cell. Intracellular ROS oxidizes the nonfluorescent DCFH to produce fluorescent DCF [1, 31]. Thus, the intracellular ROS level can be measured by detecting the fluorescence of intracellular DCF. The intracellular ROS levels are shown in Figure 4(c) and Figure 4(d). The intracellular ROS of 4T1 cells treated with NC (91.39%) was significantly lower than that of PC (628.65%) ($p < 0.01$). The intracellular ROS level produced after treatment with SNS without Dox, SNS without MnO₂, SNS without Nano-Ag, SNS without anti-PD-L1, and SNS in 4T1 cells was 225.89%, 413.54%, 194.33%, 289.37%, and 357.09%, respectively. The intracellular ROS levels after treatment with each of these NP groups were significantly higher than NC ($p < 0.01$) but lower than PC ($p < 0.01$). SNS without MnO₂ led to the highest intracellular ROS level among all SNS variants, perhaps due to the ability of MnO₂ to react directly with ROS. We found similar trends in the MDA-MB-231 cells. These results indicate that SNS may have antitumor activity by producing ROS.

3.5. Immunocompatibility. The polypeptide IL-1 β is mainly produced by monocytes and macrophages and contributes

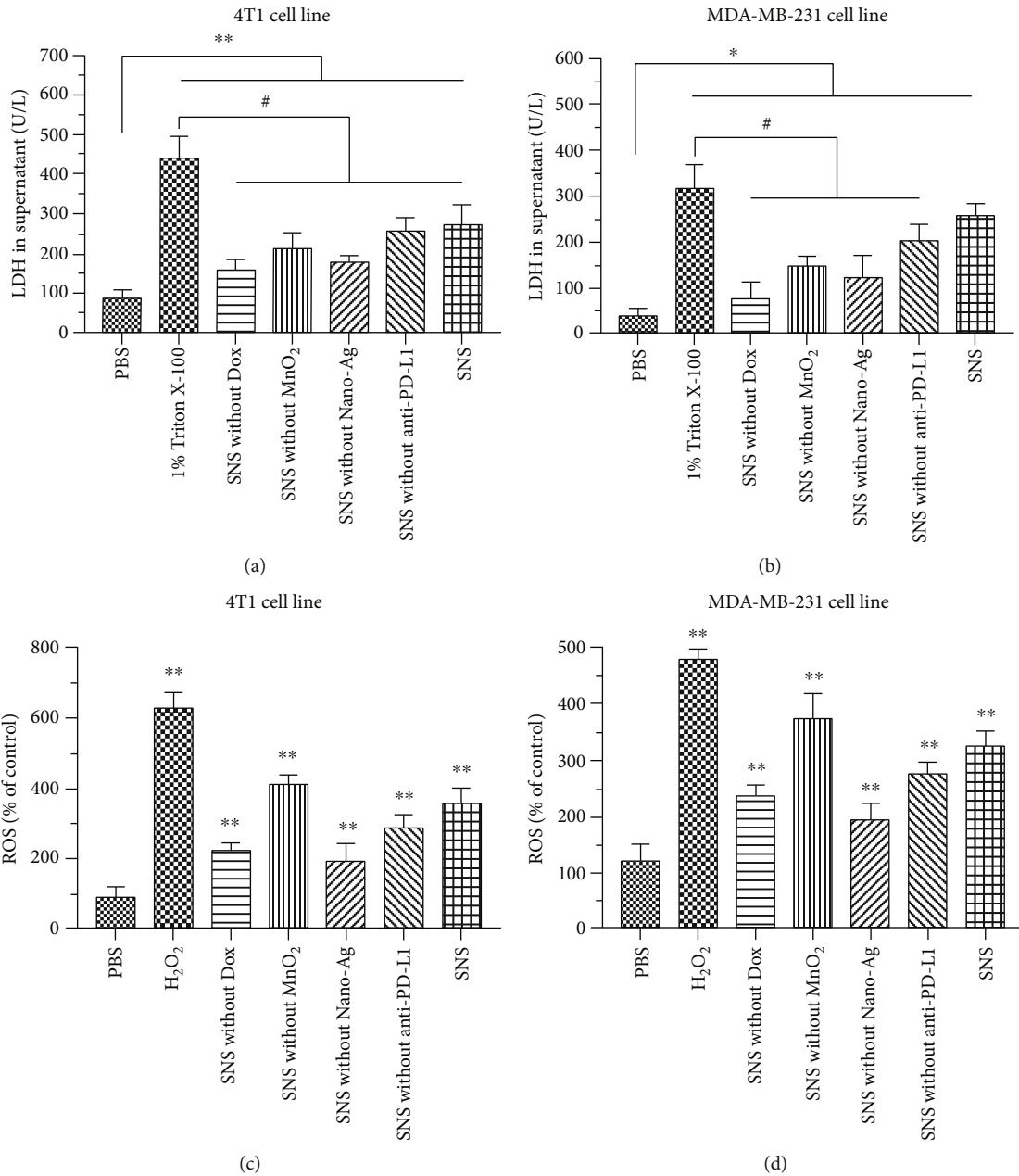


FIGURE 4: LDH release and intracellular ROS assays. The extent to which NPs induced LDH release in (a) 4T1 cells and (b) MDA-MB-231 cells. The extent to which NPs induced intracellular ROS in (c) 4T1 cells and (d) MDA-MB-231 cells. * and ** indicate that, compared with NC, $p < 0.05$ and $p < 0.01$, respectively. # indicates that $p < 0.05$ relative to PC.

to inflammation that can result in fever. However, in the tumor microenvironment, it can cause tumor growth and metastasis [2, 39]. TGF- β 1 is mainly expressed by endothelial cells, blood cells, connective tissue cells, and epithelial cells. TGF- β 1 blocks the differentiation of immature T cells into Th1 cells, promotes their transformation into Treg subsets, and inhibits the antigen-presenting function of dendritic cells, thus interfering with normal immune regulation and potentiating immune escape of tumor cells [24, 40]. Therefore, it is of great significance to evaluate the effects of SNS on the release of IL-1 β and TGF- β 1 by monocytes and macrophages.

THP-1 monocytes were induced to differentiate by treatment with PMA for 48 h, and we observed fusiform, elliptical, or irregular adherent cells (Figure 5(a)). This observation suggests that THP-1 cells were successfully differentiated into macrophages. In the following immunocompatibility test, the medium IL-1 β concentrations after treatment with NC (72.08 ± 27.44 pg/mL) were significantly lower than PC (266.98 ± 32.47 pg/mL) ($p < 0.01$) (Figure 5(b)). The IL-1 β level after treatment with SNS without Dox, SNS without MnO₂, SNS without Nano-Ag, SNS without anti-PD-L1, and SNS was 87.03 ± 33.61 , 87.93 ± 49.95 , 78.16 ± 36.02 , 70.93 ± 31.64 , and 76.17 ± 11.51 pg/mL, respectively. The

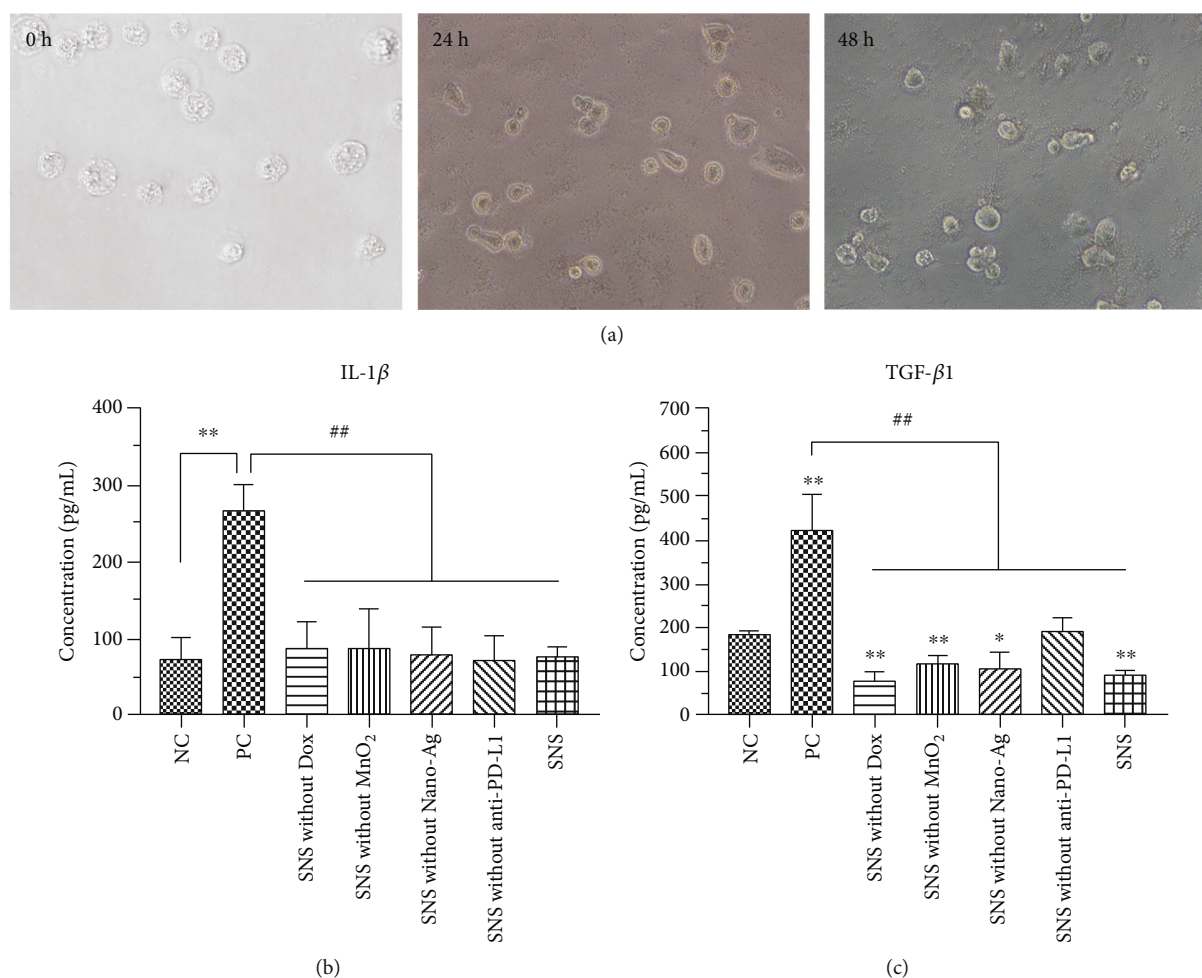


FIGURE 5: The effects of NPs on cytokine release. (a) THP-1 cells were induced and differentiated into macrophages by treatment with PMA for 0, 24, and 48 h. (b) Macrophages were incubated with the different NPs for 24 h, and the concentrations of (b) IL-1 β and (c) TGF- β 1 released from cells were significantly lower than that of PC. For IL-1 β , there was no significant difference between the NC and NP groups. For TGF- β 1, there was a significant difference between NC and SNS ($p < 0.01$). * and ** indicate $p < 0.05$ and $p < 0.01$, respectively, compared with NC. ## indicates $p < 0.01$ compared with PC.

IL-1 β concentrations of these NP groups had similar concentrations as the NC ($p > 0.05$), but significantly lower than the PC ($p < 0.01$). These results suggested that treatment of macrophages with SNS did lead to the synthesis and release of IL-1 β . The TGF- β 1 concentrations after incubation with NC (183.24 ± 7.90 pg/mL) were significantly lower than after treatment with PC (421.59 ± 79.61 pg/mL) ($p < 0.01$) (Figure 5(c)). The TGF- β 1 concentrations after treatment with SNS without Dox, SNS without MnO₂, SNS without Nano-Ag, SNS without anti-PD-L1, and SNS were 79.13 ± 19.14 , 118.01 ± 16.74 , 92.67 ± 40.08 , 164.80 ± 66.10 , and 91.34 ± 8.91 pg/mL, respectively. The TGF- β 1 concentrations of these NP groups (except SNS without anti-PD-L1) were significantly lower than NC ($p < 0.05$) and PC ($p < 0.01$). The TGF- β 1 concentrations resulting from treatment with SNS without anti-PD-L1, however, was slightly higher than after treatment with the NC ($p > 0.05$). These indicated that targeting with anti-PD-L1 leads to decreased release of TGF- β 1, potentially further enhancing the immunotherapy benefits of SNS. However, anti-PD-L1 in SNS did not affect the release of IL-1 β .

3.6. Intracellular Protein Synthesis. The intracellular protein concentrations are shown in Figure 6. 4T1 cells had significantly different intracellular protein after treatment with NC, relative to after treatment with PC or NPs ($p < 0.05$). The intracellular protein levels after treatment with SNS without Dox, SNS without MnO₂, or SNS without Nano-Ag were significantly higher than PC ($p < 0.01$). There was no significant difference between PC with SNS and SNS without anti-PD-L1 ($p > 0.05$). These findings indicate that SNS without anti-PD-L1 and SNS groups have a comparable antitumor activity as the PC. Moreover, the cytotoxicity of SNS (as indicated by impact on intracellular protein concentration) was the highest in all SNS variants. In the MDA-MB-231 cells, the intracellular protein concentration after treatment with SNS without Dox, SNS without MnO₂, SNS without Nano-Ag, and SNS without anti-PD-L1 was significantly higher than after treatment with PC ($p < 0.01$). The cells treated with SNS had similar intracellular protein concentrations as cells treated with PC ($p > 0.05$). The intracellular protein concentration of all NP-treated cells was lower than that of the NC ($p < 0.01$). These results indicated that all

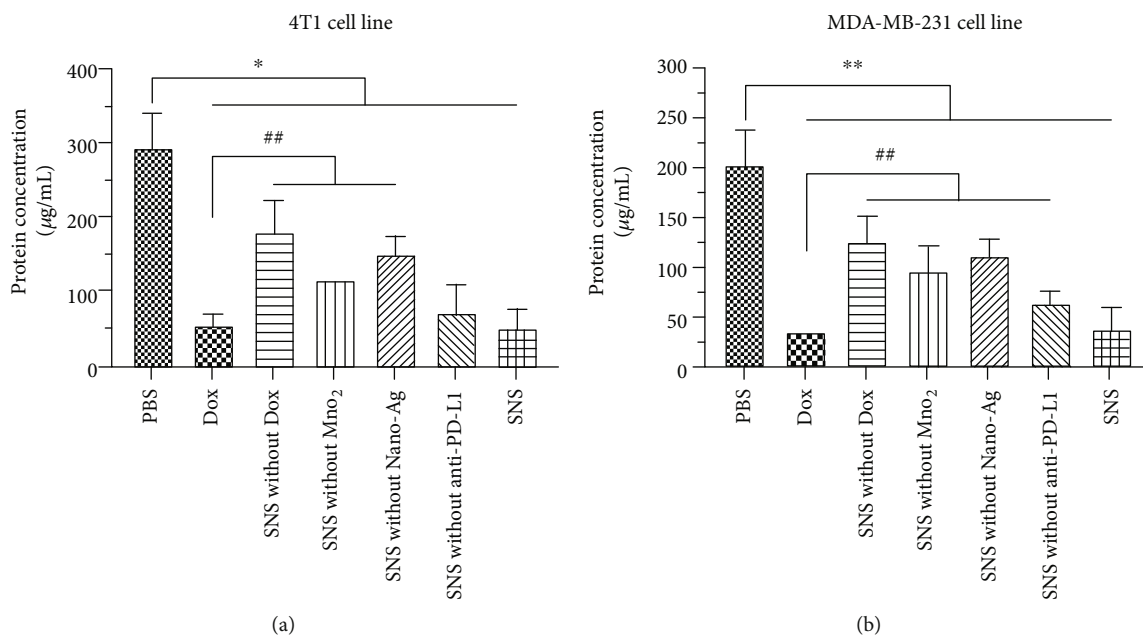


FIGURE 6: After (a) 4T1 cells and (b) MDA-MB-231 cells were treated with different NPs (5 µg/mL), the effects of NPs for intracellular protein synthesis were evaluated. * and ** indicate that intracellular protein concentrations were significantly lower than that of cells treated with NC, at $p < 0.05$ and $p < 0.01$, respectively. ## indicates that the intracellular protein concentration was significantly higher than PC, $p < 0.01$. The intracellular protein content of the SNS-treated group was the lowest, and SNS had the strongest antitumor activity among all NP groups.

NPs had some level of cytotoxicity, but the final formulation of SNS (with targeting ligand) had the strongest antitumor activity. This may be due to the targeting and immunotherapy activity of anti-PD-L1. This result further confirmed the data obtained in the LDH release.

4. Discussion

In recent years, immunotherapies and targeted therapies for the treatment of malignant tumors have been an area of rapid scientific and clinical development [6, 18]. However, these approaches have not yet been translated to meaningful improvements in outcomes for patients with TNBC [41, 42]. Therefore, in this work, we sought to test a new nanodelivery system to potentially leverage anti-PD-L1 activity to achieve targeted immunotherapy. Prior indications were supporting the potential effectiveness of this approach, so we required a better understanding of the biocompatibility of SNS.

In this study, we used DLS to analyze the stability of SNS, as indicated by changes in particle size. Upon injection, plasma proteins are adsorbed to NPs, forming a hydrodynamic corona on the NPs' surface and thus affecting the particle size and zeta potential of NPs, ultimately changing the retention time of NPs by altering interactions with the reticuloendothelial system (RES) and renal filtration [43, 44]. Generally, smaller particles are less likely to be removed by the RES, leading to a more favorable pharmacokinetic and biodistribution profile. Additionally, smaller particles also have a more hydrophilic surface, potentially decreasing protein adsorption [34]. However, if particles are too small, such as below 10 nm, they are more likely to extravasate from the liver and kidney. It has been reported that NPs with a particle

size of about 100 nm are most efficient at avoiding scavenging by the RES and benefiting from the EPR effect to distribute into tumor tissue [44, 45]. We found that when the incubation time was prolonged, the size of about 100 nm SNS did not change regardless of incubation in PBS, 5% FBS, and 2% BSA suggesting good stability. The average particle size of SNS incubated in 2% BSA was slightly smaller than those incubated in 5% FBS, potentially because BSA is an extracted albumin (583 amino acid residues, molecular weight 66.43 kDa) from bovine serum, and its molecular weight is smaller than that of the full proteins found in FBS. We found that incubation in buffers with lower pH led to smaller SNS, potentially because MnO₂ decomposed more quickly and could improve the state of cell hypoxia. This phenomenon may help improve the antitumor effects of SNS in acidic organelles of tumor cells.

Since it would likely be administered via infusion to the systemic circulation, understanding the hemocompatibility of SNS is crucial to understand its safety profile *in vivo*. According to the international standard (ISO 10933-4), the blood compatibility of synthetic materials is mainly considered in the following two respects: (1) whether the therapeutic does not damage blood components (such as by changing hemolysis rate, hepatorenal function, or blood cell counts); (2) whether the therapeutic does not cause thrombosis (i.e., by induction platelet activation and coagulation) [16, 46].

In this paper, the total blood hemoglobin (TBH) and plasma-free hemoglobin (PFH) released into the plasma were determined by quantitative colorimetry [47]. For these toxicity studies, we tested concentrations of NPs in vast excess of what we might expect to use during treatment. Generally, the experimental concentration of NPs should be at least 30 times of the expected treatment concentration. The expected

therapeutic concentration of SNS is roughly $5 \mu\text{g/mL}$, so we tested at a concentration of $200 \mu\text{g/mL}$.

In our study, the hemolysis rate reached 5% when the concentration of NPs was $262.38 \mu\text{g/mL}$ according to the linear regression. Therefore, SNS at therapeutic concentrations ($5 \mu\text{g/mL}$) likely has no significant effect on hemolysis. This was an expected result, because RBC damage typically would result from electrostatic adsorption and hydrophobic interactions. However, in this study, the hydrophobic mesoporous silica surface contains hydrophilic carboxyl groups and can be really dissolved in water. Although SNS has a negative charge, the hydrophobic interactions between SNS and RBCs are greater than the electrostatic repulsions between SNS and RBCs. Therefore, at high concentrations, SNS can induce the rupture of RBC membranes.

During chemotherapy for malignant tumors, myelosuppression is a common serious side effect. This is because chemotherapy leads to a decrease in bone marrow hematopoietic capacity, decreasing the number of peripheral blood cells. Second, due to the varying half-lives of various blood cells, the initial manifestation of myelosuppression is usually leukopenia, especially neutropenia, followed by PLT and a reduction in hemoglobin [48]. Therefore, it is of great significance to monitor changes in RBCs, white blood cells, and platelets after the administration of cytotoxic drugs.

ALT is mainly present in hepatocytes (but not in their mitochondria). On the other hand, AST is mainly distributed in the mitochondria of cells in the heart and liver. The plasma concentrations of these two enzymes are very low under healthy conditions. However, when hepatocytes are damaged, the permeability of cell membranes increases, leading to the release of these two enzymes from the liver cells. The kidney is primarily responsible for blood filtration and waste removal, so it plays a key role in the transport and removal of NPs. When NPs enter the body and are phagocytosed by the RES, NPs are primarily concentrated in the liver, spleen, and kidney, potentially affecting the liver and kidney function and resulting in abnormal increase of ALT, AST, Scr, and BUN [16]. We found that after 14 days of PC treatment in mice, blood cell counts were significantly reduced and biochemical parameters were significantly increased. However, treatment with SNS or NC did not lead to significant differences in blood cells or biochemical parameters, despite loading with Dox and Ag. This is likely because of the protective effects of drug encapsulation by the mesoporous silica carrier, which prevented direct contact between Dox, Ag, and normal tissue.

Platelet activation can result from three main mechanisms. (1) ADP pathway: ADP, thrombin, adrenaline, etc. induce platelets to release endogenous ADP and cause platelet aggregation; (2) TXA₂ pathway: PGG₂ and TXA₂ induce platelet aggregation; (3) PAF pathway. SNS, as an exogenous substance entering the blood, may induce platelet activation and aggregation through any of the above pathways to cause thrombosis. In addition, NPs with negative charges have been shown to induce platelet aggregation more strongly than cationic or neutral NPs [2, 11]. The zeta potential of SNS is negative, so it was important to evaluate the platelet aggregation effects of SNS. In our study, SNS and 0.9% NaCl

solution did not induce platelet aggregation, but PC did, indicating that SNS had no significant effect on the platelet coagulation pathway.

Next, we further studied the effects of SNS on coagulation. Blood vessel damage or the introduction of exogenous substances can cause activation of the coagulation cascade, leading to the generation of thrombin, and the conversion of fibrinogen into fibrin, which promotes coagulation [49]. This can be divided into three basic steps: the formation of the prothrombin complex, the activation of prothrombin, and the formation of fibrin. Coagulation function is mainly divided into the endogenous coagulation system, exogenous coagulation system, and fibrinolysis system. In the clinic, APTT, PT, TT, and cFIB are common tests used to evaluate coagulation function [25, 49]. In our study, the APTT and cFIB of hemocoagulase atrox (our PC) were significantly higher than that of the NPs and NC, suggesting that the coagulation assay was functioning correctly. However, the coagulation function was not significantly different between the NP group and NC group, suggesting that SNS had no significant effect on coagulation function. This could be due to the hydrophilicity of the SNS shell, which may reduce the phagocytosis of NPs. Further, SNS has the same charge as many plasma proteins, potentially decreasing opsonization.

LDH is a NAD-dependent kinase. It can be divided into NAD-dependent-L-lactate dehydrogenase and NAD-dependent-D-lactate dehydrogenase. LDH mainly exists in the cytoplasm and cannot penetrate the cell membrane under normal conditions. When the cell membrane is damaged, however, LDH can exit the cell [16, 50]. Thus, LDH activity in culture medium is reflective of the cytotoxicity of NPs. In our study, SNS resulted in the largest amount of LDH release among all NP groups and was significantly higher than NC. These results are consistent with our finding that SNS also led to the greatest decrease in intracellular protein concentration. Thus, the observed increase of LDH release is likely due to cell death, not just cell membrane damage.

ROS consists of free and nonfree radicals from oxygen sources, including superoxide anion (O_2^-), H_2O_2 , hydroxyl radical ($\text{OH}\cdot$), ozone (O_3), and singlet oxygen ($^1\text{O}_2$). These each possess unpaired electrons, resulting in high chemical reactivity. In the natural biological setting, ROS is a by-product of oxygen metabolism and plays an important role in cell signaling and homeostasis [51, 52]. However, ROS levels can dramatically increase during environmental pressures (e.g., after UV or heat exposure), potentially causing oxidative stress or serious damage to cell structures [1, 31]. Thus, we can measure possible cytotoxicity by determining the effect of SNS on ROS production and metabolism. Among all tested NPs, SNS without MnO_2 led to the highest level of intracellular ROS, likely because the MnO_2 reacts with H_2O_2 in acid environments to produce O_2 , increasing ROS consumption and leading to a state of oxygen deficiency [31]. SNS without Nano-Ag resulted in the lowest level of intracellular ROS, potentially because Nano-Ag can also generate ROS. SNS has MnO_2 and Nano-Ag, so the ROS resulting from treatment with SNS was at a level between that induced by SNS without MnO_2 and SNS without Nano-Ag. The ROS resulting from treatment with SNS without anti-

PD-L1 was lower than that of SNS, further supporting the cytotoxic effects of the anti-PD-L1 targeting moiety, in good agreement with results from the LDH release test and intracellular protein assays.

IL-1 β family cytokines play an important role in host defense mechanisms as well as the pathogenesis of various immune diseases. Local overexpression of IL-1 β in the early chronic inflammatory environment promotes tumor development. After tumorigenesis, IL-1 β interacts with vascular endothelial growth factor (VEGF) in the tumor microenvironment to drive angiogenesis and enable tumor metastasis and diffusion [53, 54]. In addition, IL-1 β also supports metastasis by promoting the transformation of cancer stem cells and the epithelial mesenchymal transition (EMT). In the tumor microenvironment, tumor cells also produce IL-1 β and act on other cells through autocrine function, thereby avoiding apoptosis and promoting proliferation and invasion [55]. At the tumor site, low-level IL-1 β expression usually induces immunosuppression at the early stage of disease, but high-level IL-1 β usually leads to cell invasion [40].

As a growth factor, TGF- β 1 exerts biological functions regulating cell proliferation, differentiation, apoptosis, and immunity. TGF- β 1 induces tumor cell apoptosis and inhibits tumor growth by regulating the downstream signal transduction molecule Smad in the early stages of tumor development [55, 56]. With further development of the tumor, gene mutations in the TGF- β 1 receptor or its downstream Smad pathway accumulate in tumor cells, resulting in the weakening of TGF- β 1 inhibition [55]. The activation of the TGF- β 1 receptor promotes EMT, and polarized epithelial cells can be transformed into active stromal capable of invasion and migration. This process is a crucial stage of tumor occurrence, growth, and metastasis [56, 57]. TGF- β 1 is a chemokine that can attract macrophages and fibroblasts and cause the release of bFGF, PDGF, TNF- α , and other vasoactive factors, thus promoting angiogenesis and inducing tumor metastasis [24, 56]. In this study, THP-1 cells were successfully induced and differentiated into adherent macrophages, and the IL-1 β release of the SNS-treated group was not significantly different from NC groups. However, the extent of TGF- β 1 release in the SNS-treated group was significantly lower than that of the NC groups. The TGF- β 1 had the capability to promote tumor development. These findings indicated that SNS can enhance the antitumor effects by TGF- β 1 pathway. The TGF- β 1 release due to treatment with SNS without anti-PD-L1 was significantly greater than the SNS-treated groups. This finding supports the importance of the anti-PD-L1 targeting moiety in the immunotherapeutic effects of SNS.

Assays of intracellular protein synthesis are interpreted similar to the results of the MTT assay and are a reflection of the cytotoxicity of drugs. The results of intracellular protein and LDH release assays were consistent, suggesting that treatment with SNS led to strong cytotoxicity and may represent a promising strategy for targeted immunotherapy.

5. Conclusions

There remains a strong need for improved therapies of difficult-to-target cancers such as TNBC. In this work, we

assessed the cytotoxicity and biocompatibility of SNS, a new candidate therapeutic platform. The results of TEM and DLS suggested spherical particles of about 95 nm with no tendency for aggregation. UV-Vis spectrum analysis of SNS suggested that SNS was successfully loaded with Nano-Ag, Dox, and MnO₂, and the drug-loading rate of Dox was about 10.2%. Stability tests showed that the particle size of SNS in PBS, 5% FBS, and 2% BSA solution did not significantly change within 72 hours. Meanwhile, we found that incubation in solutions of lower pH led to smaller particles. SNS did not lead to hemolysis or platelet activation and had no significant effect on coagulation or fibrinolysis. Animal experiments suggested that SNS did not affect blood cell counts or hepatorenal function. In cell experiments, SNS increased LDH release and intracellular ROS, which is consistent with intracellular protein assays. An immune compatibility assay found that SNS did not induce the release of IL-1 β from macrophages, but did induce the release of TGF- β 1. In conclusion, SNS appeared to have good biosafety and anti-tumor activities, supporting its potential as an anticancer drug for clinical use.

Data Availability

Any display item and related data are available upon request.

Conflicts of Interest

The authors have declared that no conflicts exist.

Authors' Contributions

H.Z. and Z.H. contributed equally to the implementation and writing; L.H. contributed the figure and language modification; W.Y., Q.J., C.X., and S.L. contributed the support studies and statistics assay; H.J. conceived and supervised the project. Zelai He and Huijun Zhang contributed equally to this work. All authors have reviewed the paper and agreed to publish.

Acknowledgments

This work was financially supported by the National Natural Science Foundation of China (No. 81602545), the First Affiliated Hospital of Bengbu Medical College Science Fund for Distinguished Young Scholars (No. 2019byyfyjq04), the Program of Natural Science Foundation of the Anhui Higher Education Institutions (No. KJ2019A0313), Bengbu Medical College Science Fund for "excellent young teachers in 512 talent development programme (No. BY51201314)", a Bengbu-Bengbu Medical College Joint Research Project (No. BYLK201810), the Translation Medicine Key Project of Bengbu Medical College (No. BYTM2019013), the Scientific Research Project of Huashan Hospital Affiliated to Fudan University (No. 2016Q018), the Scientific Research Project of Huashan North Hospital Affiliated to Fudan University (No. 20151115), and the Natural Science Foundation of Bengbu Medical College (No. BYKY1726ZD).

References

- [1] Y. Ding, Z. Sun, Z. Tong et al., "Tumor microenvironment-responsive multifunctional peptide coated ultrasmall gold nanoparticles and their application in cancer radiotherapy," *Theranostics*, vol. 10, no. 12, pp. 5195–5208, 2020.
- [2] Y. Sun, Q. Wang, J. Chen et al., "Temperature-sensitive gold nanoparticle-coated pluronic-PLL nanoparticles for drug delivery and chemo-photothermal therapy," *Theranostics*, vol. 7, no. 18, pp. 4424–4444, 2017.
- [3] E. D. Lehrman, A. N. Plotnik, T. Hope, and D. Saloner, "Ferumoxytol-enhanced MRI in the peripheral vasculature," *Clinical Radiology*, vol. 74, no. 1, pp. 37–50, 2019.
- [4] D. Adrianzen Herrera, N. Ashai, R. Perez-Soler, and H. Cheng, "Nanoparticle albumin bound-paclitaxel for treatment of advanced non-small cell lung cancer: an evaluation of the clinical evidence," *Expert Opinion on Pharmacotherapy*, vol. 20, no. 1, pp. 95–102, 2019.
- [5] S. Palchetti, D. Caputo, L. Digiacoimo et al., "Protein corona fingerprints of liposomes: new opportunities for targeted drug delivery and early detection in pancreatic cancer," *Pharmaceutics*, vol. 11, no. 1, p. 31, 2019.
- [6] P. Schmid, S. Adams, H. S. Rugo et al., "Atezolizumab and nab-paclitaxel in advanced triple-negative breast cancer," *The New England Journal of Medicine*, vol. 379, no. 22, pp. 2108–2121, 2018.
- [7] X. Zhang, Z. He, L. Xiang et al., "Codelivery of GRP78 siRNA and docetaxel via RGD-PEG-DSPE/DOPA/CaP nanoparticles for the treatment of castration-resistant prostate cancer," *Drug Design, Development and Therapy*, vol. 13, pp. 1357–1372, 2019.
- [8] J. Zhang, H. Zhang, J. Jiang et al., "Doxorubicin-loaded carbon dots lipid-coated calcium phosphate nanoparticles for visual targeted delivery and therapy of tumor," *International Journal of Nanomedicine*, vol. 15, pp. 433–444, 2020.
- [9] M. Chen, L. Wang, F. Wang et al., "Quick synthesis of a novel combinatorial delivery system of siRNA and doxorubicin for a synergistic anticancer effect," *International Journal of Nanomedicine*, vol. Volume 14, pp. 3557–3569, 2019.
- [10] J. Shi, P. W. Kantoff, R. Wooster, and O. C. Farokhzad, "Cancer nanomedicine: progress, challenges and opportunities," *Nature Reviews Cancer*, vol. 17, no. 1, pp. 20–37, 2017.
- [11] W. Lv, B. Cai, Y. Song et al., "Preparation of hemocompatible cellulose paper based on P(DMAPS)-functionalized surface," *Colloids and Surfaces B: Biointerfaces*, vol. 116, pp. 537–543, 2014.
- [12] K. G. K. Deepak, R. Vempati, G. P. Nagaraju et al., "Tumor microenvironment: challenges and opportunities in targeting metastasis of triple negative breast cancer," *Pharmacological Research*, vol. 153, article 104683, 2020.
- [13] A. Schneeweiss, V. Möbus, H. Tesch et al., "Intense dose-dense epirubicin, paclitaxel, cyclophosphamide versus weekly paclitaxel, liposomal doxorubicin (plus carboplatin in triple-negative breast cancer) for neoadjuvant treatment of high-risk early breast cancer (GeparOcto-GBG 84): a randomised phase III trial," *European Journal of Cancer*, vol. 106, pp. 181–192, 2019.
- [14] Y. C. Su, P. A. Burnouf, K. H. Chuang, B. M. Chen, T. L. Cheng, and S. R. Roffler, "Conditional internalization of PEGylated nanomedicines by PEG engagers for triple negative breast cancer therapy," *Nature Communications*, vol. 8, no. 1, article 15507, 2017.
- [15] H. H. Chen, I. L. Lu, T. I. Liu et al., "Indocyanine green/doxorubicin-encapsulated functionalized nanoparticles for effective combination therapy against human MDR breast cancer," *Colloids and Surfaces B: Biointerfaces*, vol. 177, pp. 294–305, 2019.
- [16] J. Huang, X. Zhang, Z. Wu et al., "Preparation and biocompatibility evaluation of PEG-PLL/RGD-PEG-DSPE/phospholipid/CaP nanoparticles," *Journal of Biomedical Nanotechnology*, vol. 14, no. 1, pp. 98–113, 2018.
- [17] D. Sonin, E. Pochkaeva, S. Zhuravskii et al., "Biological safety and biodistribution of chitosan nanoparticles," *Nanomaterials*, vol. 10, no. 4, article E810, p. 810, 2020.
- [18] C. Sun, R. Mezzadra, and T. N. Schumacher, "Regulation and function of the PD-L1 checkpoint," *Immunity*, vol. 48, no. 3, pp. 434–452, 2018.
- [19] X. Shen and B. Zhao, "Efficacy of PD-1 or PD-L1 inhibitors and PD-L1 expression status in cancer: meta-analysis," *BMJ*, vol. 362, article k3529, 2018.
- [20] F. Schütz, S. Stefanovic, L. Mayer, A. von Au, C. Domschke, and C. Sohn, "PD-1/PD-L1 pathway in breast cancer," *Oncology Research and Treatment*, vol. 40, no. 5, pp. 294–297, 2017.
- [21] G. Yang, L. Xu, Y. Chao et al., "Hollow MnO₂ as a tumor-microenvironment-responsive biodegradable nano-platform for combination therapy favoring antitumor immune responses," *Nature Communications*, vol. 8, no. 1, p. 902, 2017.
- [22] C. Liu, X. Ma, J. Zhuang, L. Liu, and C. Sun, "Cardiotoxicity of doxorubicin-based cancer treatment: what is the protective cognition that phytochemicals provide us?," *Pharmacological Research*, vol. 160, article 105062, 2020.
- [23] Z. He, Z. Shi, W. Sun et al., "Hemocompatibility of folic-acid-conjugated amphiphilic PEG-PLGA copolymer nanoparticles for co-delivery of cisplatin and paclitaxel: treatment effects for non-small-cell lung cancer," *Tumour Biology*, vol. 37, no. 6, pp. 7809–7821, 2016.
- [24] L. Wang, L. Jiang, P.-f. Li et al., "Positive expression of programmed death ligand-1 correlates with superior outcomes and might be a therapeutic target in primary pulmonary lymphoepithelioma-like carcinoma," *OncoTargets and Therapy*, vol. 8, pp. 1451–1457, 2015.
- [25] Z. He, Q. Wang, Y. Sun et al., "The biocompatibility evaluation of mPEG-PLGA-PLL copolymer and different LA/GA ratio effects for biocompatibility," *Journal of Biomaterials Science Polymer Edition*, vol. 25, no. 9, pp. 943–964, 2014.
- [26] A. Mehta, E. Dalle Vedove, L. Isert, and O. M. Merkel, "Targeting KRAS mutant lung cancer cells with siRNA-loaded bovine serum albumin nanoparticles," *Pharmaceutical Research*, vol. 36, no. 9, p. 133, 2019.
- [27] R. Mukhopadhyay, R. Sen, B. Paul, J. Kazi, S. Ganguly, and M. C. Debnath, "Gemcitabine co-encapsulated with curcumin in folate decorated PLGA nanoparticles; a novel approach to treat breast adenocarcinoma," *Pharmaceutical Research*, vol. 37, no. 3, p. 56, 2020.
- [28] Z. He, Y. Sun, J. Cao, and Y. Duan, "Degradation behavior and biosafety studies of the mPEG-PLGA-PLL copolymer," *Physical Chemistry Chemical Physics*, vol. 18, no. 17, pp. 11986–11999, 2016.
- [29] O. M. Daraba, A. N. Cadinoiu, D. M. Rata, L. I. Atanase, and G. Vochita, "Antitumoral drug-loaded biocompatible polymeric nanoparticles obtained by non-aqueous emulsion polymerization," *Polymers*, vol. 12, no. 5, article E1018, 2020.
- [30] Z. Wei, F. Xin, J. Zhang et al., "Donor-acceptor conjugated polymer-based nanoparticles for highly effective

- photoacoustic imaging and photothermal therapy in the NIR-II window,” *Chemical Communications*, vol. 56, no. 7, pp. 1093–1096, 2020.
- [31] L. S. Lin, J. Song, L. Song et al., “Simultaneous fenton-like ion delivery and glutathione depletion by MnO₂-based nanoagent to enhance chemodynamic therapy,” *Angewandte Chemie*, vol. 57, no. 18, pp. 4902–4906, 2018.
- [32] S. A. Adeyemi, Y. E. Choonara, P. Kumar et al., “Folate-decorated, endostatin-loaded, nanoparticles for anti-proliferative chemotherapy in esophageal squamous cell carcinoma,” *Biomedicine & Pharmacotherapy*, vol. 119, article 109450, 2019.
- [33] Y. Zhang, J. Pan, H. Li et al., “Albumin based nanomedicine for enhancing tacrolimus safety and lymphatic targeting efficiency,” *Journal of Biomedical Nanotechnology*, vol. 15, no. 6, pp. 1313–1324, 2019.
- [34] A. Huguet-Casquero, M. Moreno-Sastre, T. B. López-Méndez, E. Gainza, and J. L. Pedraz, “Encapsulation of oleuropein in nanostructured lipid carriers: biocompatibility and antioxidant efficacy in lung epithelial cells,” *Pharmaceutics*, vol. 12, no. 5, article E429, 2020.
- [35] B. Hu, J. Wang, J. Li, S. Li, and H. Li, “Superiority of L-tartaric acid modified chiral mesoporous silica nanoparticle as a drug carrier: structure, wettability, degradation, bio-adhesion and Biocompatibility,” *International Journal of Nanomedicine*, vol. 15, pp. 601–618, 2020.
- [36] J. Z. Qin, S. J. Wang, X. P. Zheng et al., “Comparison of hemo-coagulase atrox versus tranexamic acid used in primary total knee arthroplasty: a randomized controlled trial,” *Thrombosis Research*, vol. 188, pp. 39–43, 2020.
- [37] X. Wei, J. Liao, Z. Davoudi et al., “Folate receptor-targeted and GSH-responsive carboxymethyl chitosan nanoparticles containing covalently entrapped 6-mercaptopurine for enhanced intracellular drug delivery in leukemia,” *Mar Drugs*, vol. 16, no. 11, article E439, 2018.
- [38] Z. Wei, M. Wu, S. Lan et al., “Semiconducting polymer-based nanoparticles for photothermal therapy at the second near-infrared window,” *Chemical Communications*, vol. 54, no. 96, pp. 13599–13602, 2018.
- [39] Y. Chen, N. Li, B. Xu et al., “Polymer-based nanoparticles for chemo/gene-therapy: evaluation its therapeutic efficacy and toxicity against colorectal carcinoma,” *Biomedicine & Pharmacotherapy*, vol. 118, article 109257, 2019.
- [40] M. Moniri, A. Boroumand Moghaddam, S. Azizi et al., “In vitro molecular study of wound healing using biosynthesized bacteria nanocellulose/silver nanocomposite assisted by bioinformatics databases,” *International Journal of Nanomedicine*, vol. 13, pp. 5097–5112, 2018.
- [41] R. L. Siegel, K. D. Miller, and A. Jemal, “Cancer statistics, 2020,” *CA: A Cancer Journal for Clinicians*, vol. 70, no. 1, pp. 7–30, 2020.
- [42] C. E. DeSantis, J. Ma, M. M. Gaudet et al., “Breast cancer statistics, 2019,” *CA: A Cancer Journal for Clinicians*, vol. 69, no. 6, pp. 438–451, 2019.
- [43] Y. Chen, Y. Zhang, J. Zhuang et al., “Cell-membrane-cloaked oil nanosponges enable dual-modal detoxification,” *ACS Nano*, vol. 13, no. 6, pp. 7209–7215, 2019.
- [44] Y. Zheng, X. You, L. Chen et al., “Biotherapeutic nanoparticles of poly(ferulic acid) delivering doxorubicin for cancer therapy,” *Journal of Biomedical Nanotechnology*, vol. 15, no. 8, pp. 1734–1743, 2019.
- [45] Z. Wei, M. Wu, Z. Li et al., “Gadolinium-doped hollow CeO₂-ZrO₂ nanoplatform as multifunctional MRI/CT dual-modal imaging agent and drug delivery vehicle,” *Drug Delivery*, vol. 25, no. 1, pp. 353–363, 2018.
- [46] M. Modic and M. Mozetic, “In vitroscreening procedure for characterization of thrombogenic properties of plasma treated surfaces,” *Biointerphases*, vol. 11, no. 2, article 029808, 2016.
- [47] Y. Chen, Y. Zhang, M. Chen et al., “Biomimetic nanosponges suppress in vivo lethality induced by the whole secreted proteins of pathogenic bacteria,” *Small*, vol. 15, no. 6, article e1804994, 2019.
- [48] S. Atkins and F. He, “Chemotherapy and beyond: infections in the era of old and new treatments for hematologic malignancies,” *Infectious Disease Clinics of North America*, vol. 33, no. 2, pp. 289–309, 2019.
- [49] W. Song, Q. Zeng, X. Yin, L. Zhu, T. Gong, and C. Pan, “Preparation and anticoagulant properties of heparin-like electrospun membranes from carboxymethyl chitosan and bacterial cellulose sulfate,” *International Journal of Biological Macromolecules*, vol. 120, Part B, pp. 1396–1405, 2018.
- [50] D. T. Savage, J. Z. Hilt, and T. D. Dziubla, “In vitro methods for assessing nanoparticle toxicity,” *Methods in Molecular Biology*, vol. 1894, pp. 1–29, 2019.
- [51] J. Liu, X. Liu, Y. Sun et al., “High density and super ultramicroporous-activated carbon macrospheres with high volumetric capacity for CO₂Capture,” *Advanced Sustainable Systems*, vol. 2, no. 2, article 1700115, 2018.
- [52] X. Lai, H. Liu, Y. Zheng, Z. Wang, and Y. Chen, “Drug loaded nanoparticles of metal-organic frameworks with high colloidal stability for anticancer application,” *Journal of Biomedical Nanotechnology*, vol. 15, no. 8, pp. 1754–1763, 2019.
- [53] P. Song, C. Yang, J. S. Thomsen et al., “Lipidoid-siRNA nanoparticle-mediated IL-1 β gene silencing for systemic arthritis therapy in a mouse model,” *Molecular Therapy*, vol. 27, no. 8, pp. 1424–1435, 2019.
- [54] J. Wu, Y. Han, X. Zou et al., “Silica nanoparticles as an enhancer in the IL-1 β -induced inflammation cycle of A549 cells,” *Immunopharmacology and Immunotoxicology*, vol. 41, no. 2, pp. 199–206, 2019.
- [55] Y. Yu, T. Zhu, Y. Li et al., “Repeated intravenous administration of silica nanoparticles induces pulmonary inflammation and collagen accumulation via JAK2/STAT3 and TGF- β /Smad3 pathways in vivo,” *International Journal of Nanomedicine*, vol. 14, pp. 7237–7247, 2019.
- [56] Y. Chen, P. Liu, P. Sun et al., “Oncogenic MSH6-CXCR4-TGFB1 feedback loop: a novel therapeutic target of photothermal therapy in glioblastoma multiforme,” *Theranostics*, vol. 9, no. 5, pp. 1453–1473, 2019.
- [57] Q. Zhang, X. Chang, H. Wang et al., “TGF- β 1 mediated Smad signaling pathway and EMT in hepatic fibrosis induced by Nano NiO in vivo and in vitro,” *Environmental Toxicology*, vol. 35, no. 4, pp. 419–429, 2020.

Research Article

Polydatin Attenuates 14.1 MeV Neutron-Induced Injuries via Regulating the Apoptosis and Antioxidative Pathways and Improving the Hematopoiesis of Mice

Jiaming Guo ¹, Tingting Liu,¹ Long Ma,² Wei Hao,³ Hongli Yan,² Taosheng Li,⁴ Yanyong Yang ¹, Jianming Cai ¹, Fu Gao ¹, Zhao Xu ⁴, and Hu Liu ¹

¹Department of Radiation Medicine, College of Naval Medicine, Naval Medical University, Shanghai 200433, China

²Department of Reproductive Medicine Center, Changhai Hospital, Naval Medical University, Shanghai 200433, China

³Department of Endocrinology, Changhai Hospital, Naval Medical University, Shanghai 200433, China

⁴Institute of Nuclear Energy Safety Technology, Chinese Academy of Sciences, Hefei, Anhui 230031, China

Correspondence should be addressed to Fu Gao; gaofusmmu@163.com, Zhao Xu; zhao.xu@inest.cas.cn, and Hu Liu; gzsassliuhu@163.com

Received 30 June 2020; Accepted 1 August 2020; Published 31 August 2020

Guest Editor: Ciprian Tomuleasa

Copyright © 2020 Jiaming Guo et al. This is an open access article distributed under the Creative Commons Attribution License, which permits unrestricted use, distribution, and reproduction in any medium, provided the original work is properly cited.

With more powerful penetrability and ionizing capability, high energetic neutron radiation (HENR) often poses greater threats than photon radiation, especially on such occasions as nuclear bomb exposure, nuclear accidents, aerospace conduction, and neutron-based radiotherapy. Therefore, there emerges an urgent unmet demand in exploring highly efficient radioprotectants against HENR. In the present study, high-throughput 14.1 MeV neutrons were generated by the high-intensity D-T fusion neutron generator (HINEG) and succeeded in establishing the acute radiation syndrome (ARS) mouse model induced by HENR. A series of preclinical studies, including morphopathological assessment, flow cytometry, peripheral complete blood, and bone marrow karyocyte counting, were applied showing much more serious detriments of HENR than the photon radiation. In specific, it was indicated that surviving fraction of polydatin- (PD-) treated mice could appreciably increase to up to 100% when they were exposed to HENR. Moreover, polydatin contributed much in alleviating the HENR-induced mouse body weight loss, spleen and testis indexes decrease, and the microstructure alterations of both the spleen and the bone marrow. Furthermore, we found that the HENR-damaged hematopoiesis was greatly prevented by PD treatment in such aspects as bone marrow hemocytogenesis, splenocytes balancing, or even the peripheral blood cellularity. The additional IHC investigations revealed that PD could exert potent hematopoiesis-promoting effects against HENR via suppressing apoptosis and promoting the antioxidative enzymes such as HO-1.

1. Introduction

Irradiation is being applied in more and more areas such as nuclear plants, radiotherapy, and aerospace, providing us great benefits along with some adverse effects as well [1]. Especially, the neutron radiation poses severer threats than the others due to its powerful penetrability and high ionizing capability. Due to its physical trait and the key role it plays in either initiating the chain fission reactions or participating other kinds of nuclear processes, the neutron exposure exists extensively in our life, ranging from aircrew and the passen-

gers, aerospace, nuclear reactors, particle accelerators, to radiotherapies. Thus, strategy explorations aiming at preventing human from neutron radiation injuries have been attracting a lot of attentions all the time [2].

Neutrons are classified into high linear energy transfer (LET) radiation, which means ionizing more atoms and thus producing more attacking free radicals than the low LET rays such as photons (γ rays or X rays) at the same situation. Indeed, numbers of studies concerning the biological effect of different types of radiation showed that the relative biological effectiveness (RBE) of neutrons was

generally several times as those of low LET rays did in various models regarding with different indicators [3–5]. Furthermore, even the neutrons of different energy levels hold distinct RBEs for the same observation end point. For example, determined on human lymphocyte with either the comet assay or the chromosome aberration rates, RBE values of low-energy neutrons is higher than that of fission neutrons [6]. Thus, necessity is that the biological effect of monoenergetic neutrons should be investigated in detail separately instead of indiscriminately due to their distinct characteristics.

As a kind of noncharged particles, neutrons can penetrate materials with much depth. However, neutrons with different levels of energy have different penetrating power. The more energy confers neutrons' greater tissue-penetrating ability, which have been utilized in clinical tumor radiotherapies by neutron radiation such as boron neutron capture therapy (BNCT) regimen [2]. But as for the neutron radiation protection, it is harder to prevent the high-penetrating neutrons compared to the thermal neutrons of relatively low energy (~ 0.025 eV). After all, taking full advantage of the nuclear reactions prone to occur with the neutrons of different energy levels, the optimized physical shield composed of series nuclides were able to absorb most of the relatively low-energy neutrons. In contrast, high-energy neutrons can penetrate deeply and impose much threats to physical prevention, eliciting the significant demand for exploring the medical countermeasures to high energetic neutron radiation as the last line of defense [7]. Nevertheless, it is not easy to produce enough high-dose rate monoenergetic neutrons with a high level of energy to generate appropriate biological effects for medical research.

After the discovery of neutron in 1935, much progress have been made concerning the neutron biology, the main investigations of which were concentrated in RBE studies, dosimetry studies, BNCT optimizing, and some attempts to make a feel of the underlying neutron injury mechanisms [8]. However, as to the pharmacological prevention exploration, fewer studies were conducted except for several regarding cytokines and natural antioxidants [9, 10]. In the present study, we managed to establish an acute radiation sickness (ARS) mouse model irradiated by high-flux 14.1 MeV neutrons, whereby the world-leading facility named the high-intensity D-T fusion neutron generator (HINEG) [11], and made an effort to develop ideal candidate drugs for the injury.

Polydatin (PD; 3,4,5-trihydroxystibene-3-b-mono-D-glucoside), extracted from *Polygonum cuspidatum*, is a small natural compound exerting various therapeutic activities including antioxidation and anti-inflammation [12]. Previous studies have revealed that PD could also ameliorate γ radiation-induced injuries in multiple organs such as the lung, testis, and intestine through scavenging ROS, activating antioxidation cascades, or regulating apoptosis and many other relevant pathways [13–15]. Since neutron radiation provoked even severer toxic free radicals outbreak and apoptosis imbalance, we made an assumption that PD could still improve the ARS outcomes via its comprehensive bioactivities. Therefore, the established ARS mouse model was adopted to test whether PD administration could exert radio-

protection against high-energy neutrons and to unveil the potential mechanism.

2. Material and Methods

2.1. Animals and Treatments. Male wild type 8-week old Balb/c mice were obtained from Shanghai Laboratory Animal Center of Chinese Academy of Science and maintained at 23°C to 25°C with a 12 h light/dark cycle. Before enrolling into the experiment, mice were firstly housed for a week to accommodate the new environment. All living conditions and protocols were approved by the Naval Medical University Institutional Animal Care and Use Committee in accordance with the Guide for Care and Use of Laboratory Animals published by the US NIH (publication No. 96-01).

Either PD (Sigma-Aldrich, 100 mg/kg in 0.1 ml 5% DMSO) or 0.1 ml DMSO only (5% in PBS) was delivered to the experimental mice in the corresponding groups via intraperitoneal injection one day before IR exposure and continued daily to the last. For the animal survival survey, all the mice were taken carefully and at least observed twice a day (every morning and evening) up to the 30th day post IR to make a good record of the animal state and the survival rate. As for the tissue sampling experiments, mice were anesthetized (chloral hydrate of 10% in physiological saline, intraperitoneal injection) and sacrificed to harvest different kinds of samples which was applied for the next determination on day 1, day 3, day 7, and, if still alive, day 30 post IR. Before tissue sampling, the cardiac perfusion was conducted to avoid the potential interference from blood background when employing the following experiments such as the immunohistological analysis.

2.2. Neutron Irradiation and Dosimetry. We adopted the high-intensity D-T fusion neutron generator (HINEG), located at The Institute of Nuclear Energy Safety Technology, Chinese Academy of Sciences, as the radiation source to provide the fast neutrons. By accelerating the deuterium ions to hit tritium targets, HINEG is designed to produce D-T fusion 14.1 MeV monoenergetic neutrons. Actually, there existed unavoidable contamination of the neutron dose with around 5% γ rays, whose contribution to the biological effect was yet deemed as negligible due to the higher RBE of the neutrons. Mice, which were confined in a plastic box with a certain arc ensuring each cell holding the equal distance to the neutron source, were exposed to a single dose of HENR (Figure S1).

Using the ^{238}U fission chamber, the neutron yield from HINEG device has been measured as 4.00×10^{14} N. The absorbed dose from a beam of neutrons may be computed by considering the energy absorbed by each of the tissue elements that react with the neutrons. The type of reaction, of course, depends on the neutron energy. For fast neutrons up to about 14.1 MeV, the main mechanism of energy transfer is elastic collision. In cases of elastic scattering of fast neutrons, the scattered nuclei dissipate their energy in the immediate vicinity of the primary neutron interaction. The radiation dose absorbed locally in this way is called the first collision dose and is determined entirely by the primary

neutron flux; the scattered neutron is not considered after this primary interaction. For fast neutrons, the first collision dose rate from neutrons of energy E is

$$\dot{D}_n(E) = \frac{\phi(E)E\sum_i\sigma_i f N_i}{1\text{J/kg/Gy}}, \quad (1)$$

where $\phi(E)$ is the flux of neutrons whose energy is E , in neutrons per cm^2 per second, σ_i is the scattering cross

section of the i th element for neutrons of energy E , in barns $\times 10^{-24} \text{ cm}^2$, f is the mean fractional energy transferred from neutron to scattered atom during collision with the neutron, and N_i is the number of atoms per kilogram of the i th element.

According to the neutron influence of the sample, the calculated absorbed doses of each group were 0.64 Gy, 0.95 Gy, 1.54 Gy, and 2.91 Gy, respectively (see more details in the Table S2).

$$\text{Total uncertainty} = \sqrt{\text{distance uncertainty}^2 + \text{distance uncertainty}^2 + \text{yield uncertainty}^2}. \quad (2)$$

2.3. Biometric Parameters Determination. Body weight of each mouse was measured every 3 days until they were sacrificed. The body weight curves were generated based on the average and standard error of mean (SEM) of each group. To calculate the spleen and testis indexes, both of the above were excised and weighted after the mice were killed. The following formula was adopted to get the final result:

$$\text{Organ index} = \frac{\text{organ weight(g)}}{\text{body weight (g)}} \times 1000\%. \quad (3)$$

2.4. Peripheral Complete Blood Count Analysis. Immediately after the mice were anesthetized by an anesthesia apparatus (Norvap, U.K.) with isoflurane, blood samples (0.7 ml) were obtained from the angular vein and collected into the ethylenediaminetetraacetic acid-coated anticoagulant tubes for the following analysis via an automatic blood cell analyzer (Mindray, Shenzhen, China) according to the manufacturer's instruction. Then, a comprehensive result involving WBCs, RBCs, PLTs, and their subsets was outputted and investigated.

2.5. Marrow Karyocyte Counting. Left femur of each sacrificed mouse was holed on both sides and washed repeatedly with 1 ml PBS for 3 times until the femur turned white. Then, the cell suspension was filtered through 100 μm cell strainer (BD FALCON, New Jersey USA) and centrifuged at 1500 rpm for 5 min. With the supernatant discarded, the pellet was lysed with 1 ml Red Blood Cell Lysis Buffer for 10 minutes to remove the erythrocytes, leaving the bone marrow nucleated cells which were washed and eventually resuspended with 1 ml PBS. Flow cytometry was then performed to enumerate the total nucleated cells of each femur within 1 min at the sample flow rate of 10 $\mu\text{l}/\text{min}$.

2.6. Splenocyte Apoptosis. The mouse spleen was isolated and ground with a metal bar on a 200-mesh metal net, and then, the single cell suspension was made. After being washed with 1 ml PBS twice, the cells were firstly incubated with FITC for 30 minutes and then stained with PI dye according to the manufacturer's operating manual (TransGen Biotech, Beijing, China). Flow cytometry was adopted to measure the

apoptotic performance of each group. At least 10,000 gated events were collected and analyzed for each sample.

2.7. Histopathology and Morphometry. Spleens and femurs were removed and fixed with 4% paraformaldehyde for at least 24 hours. Next, the samples were embedded in paraffin and cut into thin sections (4 μm thick) for the next staining analysis. We applied the hematoxylin and eosin staining (H&E) to conduct the regular histopathological microstructure discrimination. To determine the specific molecular alteration, we performed the immunohistochemistry analysis (IHC) using the according antibodies: anti-Heme oxygenase-1 (HO-1), 1:1000; anti-Kelch-like ECH-associated protein 1 (KEAP 1), 1:1500; and anti-sirtuin 1 (SIRT 1), 1:500. The H&E slides were investigated under a microscope (Nikon, T1-SAM, Japan) adapted with a CCD camera (Nikon, DS-Ri2, Japan) while the IHC slides were scanned using an automatic digital slide scanner (Panoramic MIDI, 3D HISTECH, Hungary). A quantitative analysis of the IHC pictures was performed using the IHC profiler plugin in the ImageJ software [16, 17].

2.8. Western Blot Assay. At the indicated time points, animals were sacrificed and the lung tissue was isolated and rapidly frozen in liquid nitrogen; then, they were stored at -80°C . The protein was extracted by using M-PER mammalian protein extraction reagent (Thermo Fisher Scientific) according to the manufacturer's instruction. After blocking for 1 hour at room temperature, the membranes were probed overnight at 4°C with the primary antibodies such as Bcl2 (Cell Signaling Technology, 1:1000) and Actin (Proteintech, 1:1000), and then the secondary antibody (Cell Signaling Technology, 1:5000).

2.9. Statistical Analysis. All data were presented as mean \pm SEM, and the statistical analysis was carried out using the SPSS 22.0 software (SPSS Inc., Chicago, USA). The GraphPad Prism 6 Software (GraphPad Software Inc., California, USA) was utilized to make the graphs. As for the survival rate comparison, the Kaplan-Meier method and the following log-rank test were performed to determine the significance. Besides, statistical significances between two groups were determined by Student's t -test. Differences

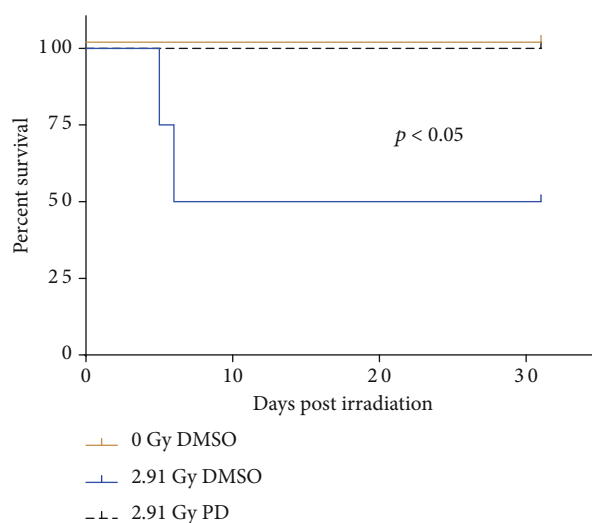


FIGURE 1: Survival curves of different treatment groups. $n = 10$; $p < 0.05$: 2.91 Gy DMSO vs. 2.91 Gy.

TABLE 1: List of the experimental animal groups with the according treatments.

Time post IR	Treatment	Explanation
D1	DMSO	Nonirradiated mice with DMSO administration for 1 day
	PD	Nonirradiated mice with PD administration for 1 day
	IR + DMSO	Irradiated (2.91 Gy) mice with DMSO administration for 1 day
	IR + PD	Irradiated (2.91 Gy) mice with PD administration for 1 day
D3	DMSO	Nonirradiated mice with DMSO administration for 3 days
	PD	Nonirradiated mice with PD administration for 3 days
	IR + DMSO	Irradiated (2.91 Gy) mice with DMSO administration for 3 days
	IR + PD	Irradiated (2.91 Gy) mice with PD administration for 3 days
D7	DMSO	Nonirradiated mice with DMSO administration for 7 days
	PD	Nonirradiated mice with PD administration for 7 days
	IR + DMSO	Irradiated (2.91 Gy) mice with DMSO administration for 7 days
	IR + PD	Irradiated (2.91 Gy) mice with PD administration for 7 days
D32	DMSO	Nonirradiated mice with DMSO administration for 32 days
	PD	Nonirradiated mice with PD administration for 32 days
	IR + DMSO	Irradiated (0.64 Gy, 0.95 Gy, 1.54 Gy, and 2.91 Gy as indicated, respectively) mice with DMSO administration for 32 days
	IR + PD	Irradiated (0.64 Gy, 0.95 Gy, 1.54 Gy, and 2.91 Gy as indicated, respectively) mice with PD administration for 32 days

were considered to be statistically significant when the p value was less than 0.05.

3. Results

3.1. Animal Survival. Twenty-four Balb/c mice were randomly assigned to different groups (8 mice for each) including 0 Gy DMSO group, 2.91 Gy DMSO group, and 2.91 Gy PD group. The animal performance was observed closely, and the survival curve was obtained. Although the upmost neutron radiation dose was adopted for this experiment, for which the animal tolerance to the circumstances was prudently considered, merely about half of the whole mice died until the end of one month after IR exposure (Figure 1). In

sharp contrast, none of the 2.91 Gy PD group mice died during the observation term just as the nonradiation group did.

3.2. Biometric Parameters. Biometric parameters of the experimental mice were measured 1 day, 3 days, 7 days, and 32 days after neutron irradiation. Mice, which were sacrificed on D32, received 0.64 Gy, 0.95 Gy, 1.54 Gy, and 0 Gy radiation dose while the other animals were only exposed to 2.91 Gy radiation (Table 1). Considering the IR caused potential deaths of the mice, we assigned another 10 mice into the 2.91 Gy IR DMSO group. The animal body weight from all D32 groups of Table 1 combined with the ones in the above survival analysis was all tracked, and the data were analysis integrated. Finally, at least 8 mice for each

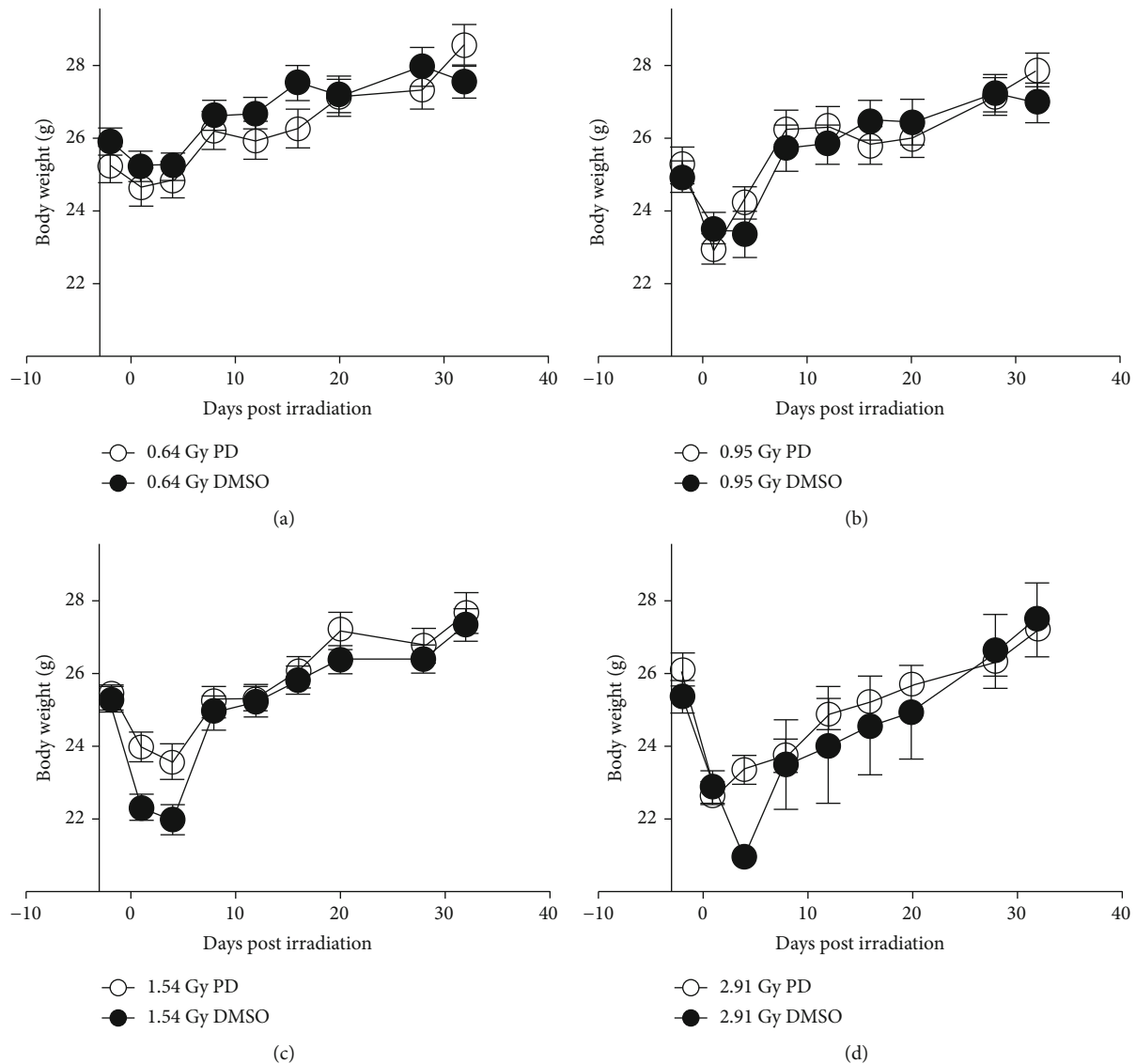


FIGURE 2: Acute mouse body weight loss due to 1.54/2.91 Gy HENR exposure was prevented greatly by PD. Body weight of every mouse was consistently measured ever few days till D32 post IR, and the alteration curves of each group was plotted here (a–d). $n = 8$, $*p < 0.05$, $**p < 0.01$, $***p < 0.001$.

group were enrolled into the body weight statistics. As depicted in the curves, no matter which of the IR dose was chosen, each of the experimental groups exhibited a first decrease and then increase tendency of body weight alteration (Figures 2(a)–2(d)). Particularly, when the doses rose up to 1.54 Gy or 2.91 Gy, a statistic significance with or without PD administration showed several days after IR (Figure 2(c): $p = 0.00782522$, $p = 0.0253507$; Figure 2(d): $p = 0.00115645$).

The irradiated groups including the 0.64 Gy, 0.95 Gy, and 1.54 Gy dose groups for D32 and the 2.91 Gy groups for D1, D3, and D7 were subjected to the organ index determination (Figure 3). In terms of the spleen, the organ index dropped sharply a relatively short period after IR (Figure 3(a), D1: $p = 0.00023741$, D3: $p = 0.000236877$, D7: $p = 0.000235673$). As compared to the IR + DMSO groups, this damaged parameter was turned by PD to be better

and better as time went by, with a significance showing on D7 ($p = 0.000113204$). On the 32th day post IR, the damaged splenic index caused by IR seemed to be restored to the normal level. Moreover, PD administration elevated this index markedly in the 0.95 Gy and 1.54 Gy groups comparing with their corresponding IR + DMSO treatment group (0.95 Gy, $p = 0.000115282$; 1.54 Gy, $p = 0.0138295$). As for the testis, the index was decreased by IR on D7, which was rectified by PD greatly ($p = 0.00348368$), while no significances were observed among the other comparisons (Figure 3(b)). However, a clear dose-dependent reduction showed up among the IR + DMSO groups 32 days post IR, with a slight elevation observed in the PD treated groups (Figure 3(d)).

3.3. Bone Marrow Nucleated Cells. Mice which were injected with 5% DMSO only or containing PD were exposed to 2.91 Gy neutron radiation or sham dose. Left femur of mice

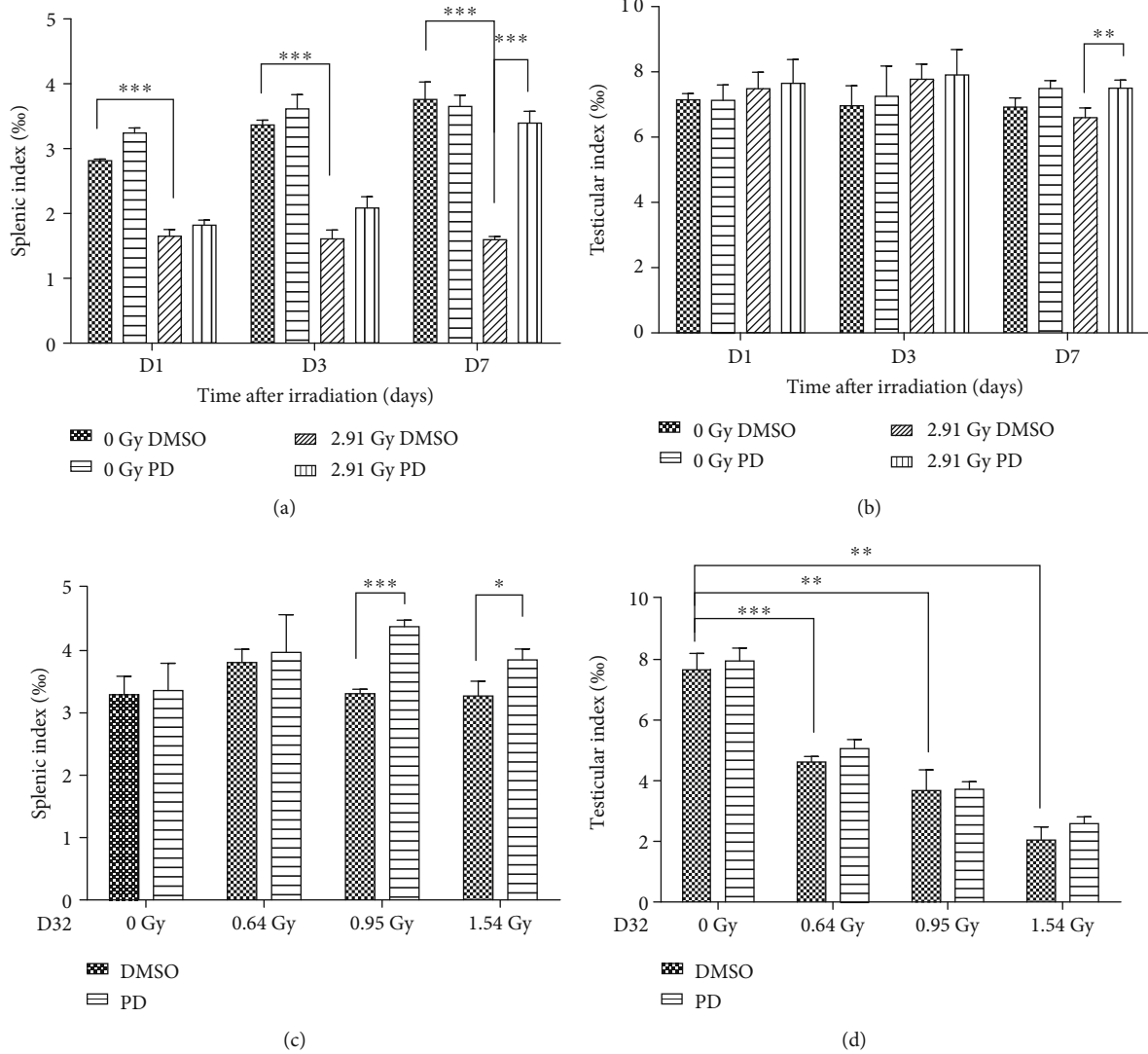


FIGURE 3: PD attenuated both the splenic and testicular index of the irradiated mice. (a, b) The splenic and testicular indexes were calculated at different time points (D1, D3, and D7) post 2.91 Gy neutron radiation. (c, d) On the 32th day after exposing to a variety of radiation doses (0.64 Gy, 0.95 Gy, 1.54 Gy, and 0 Gy as sham), the organ indexes of the above were analyzed again. * $p < 0.05$, ** $p < 0.01$, *** $p < 0.001$.

was isolated, and their bone marrow was flushed for BMNC assessment. Under IR exposure, the IR DMSO groups lost much of the BMNC compared with the DMSO groups at the corresponding time points (D1: $p = 0.0137359$; D3: $p = 0.000480536$; D7: $p = 0.00008394891$). Thanks to the PD administration, the IR-compromised BMNC of each IR DMSO group was greatly restored on D1 ($p = 0.026204$) and D3 ($p = 0.000321216$). Additionally, it seemed that the BMNC of nonradiated groups, including both the DMSO group and the PD group, began to decline on D7 as relative to the previous time points, which should be attributed to the hematopoietic toxicity of the solvent DMSO.

3.4. Peripheral Hematological Studies. To determine the ability of PD to ameliorate radiation-induced defects in hematopoiesis, the mouse peripheral complete blood count analysis (CBC) was carried out on D1, D3, and D7 post 2.91 Gy neutron radiation.

As seen in Figures 4(a)–4(d), the white blood cells (WBC), lymphocytes (Lymph), Monocytes (Mon), and the Granulocyte (Gran) shared a similar alteration style to IR injury, declining at all the three time points with the lowest count on D3. As for the WBC (Figure 4(a)), the differences were all considerable all through the time course ($p = 0.00343867$ for D1, $p = 0.00270821$ for D3, and $p = 0.00321815$ for D7), with an evident amelioration effect of PD treatment showing up simultaneously ($p = 0.00246184$ for D3 and $p = 0.0129618$ for D7). As the major component of WBC, lymph count also descended quickly and sharply after IR ($p = 0.0103933$ for D1, $p = 0.0111376$ for D3, and $p = 0.0050193$ for D7, compared to DMSO groups, respectively). PD rescued this defect as well, with a significance observed on D3 ($p = 0.00168689$ for D3, in comparison with the IR DMSO group). Moreover, PD seemed to improve the IR-suppressed Mon level on D1 and D7. However, the Mon

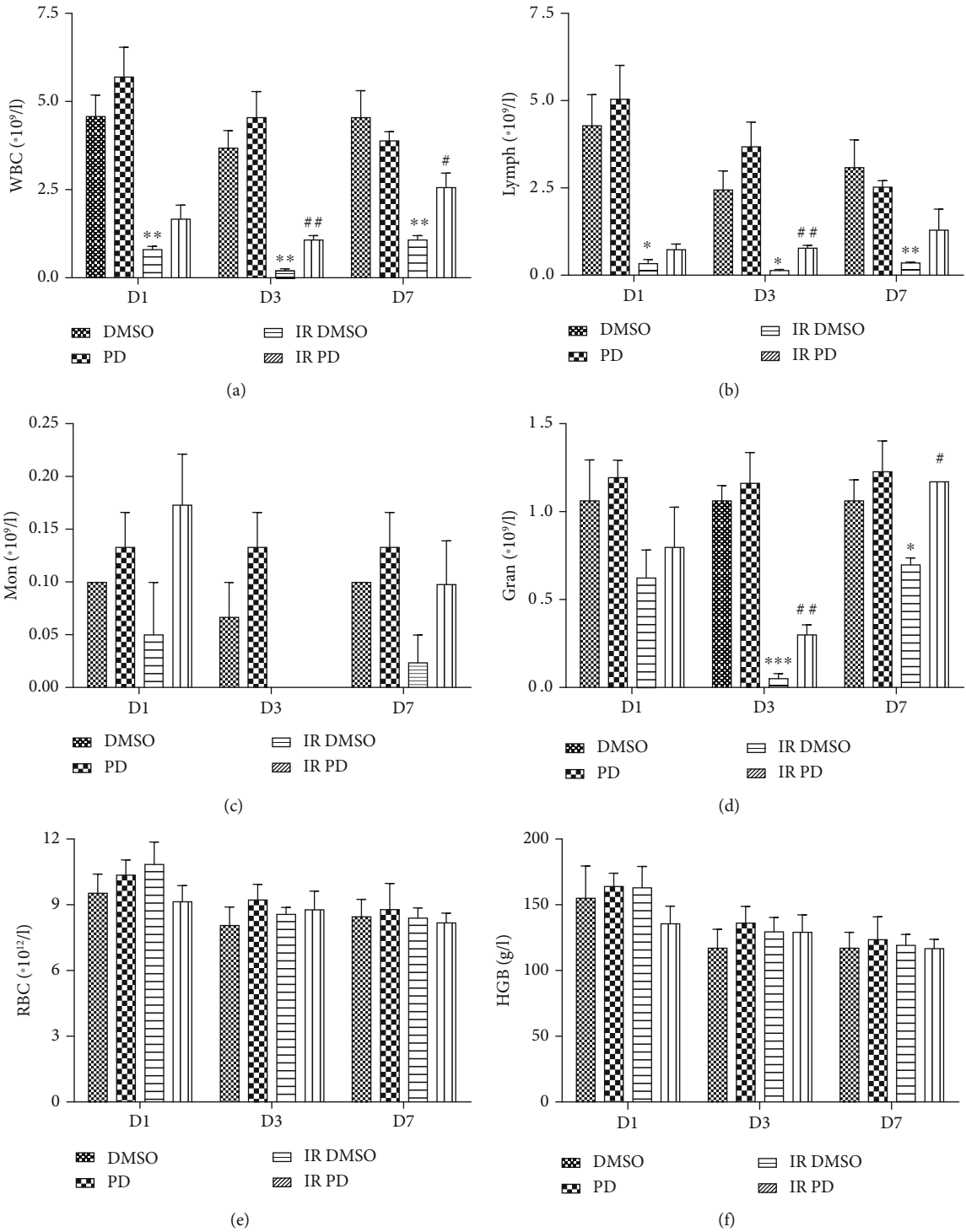


FIGURE 4: Continued.

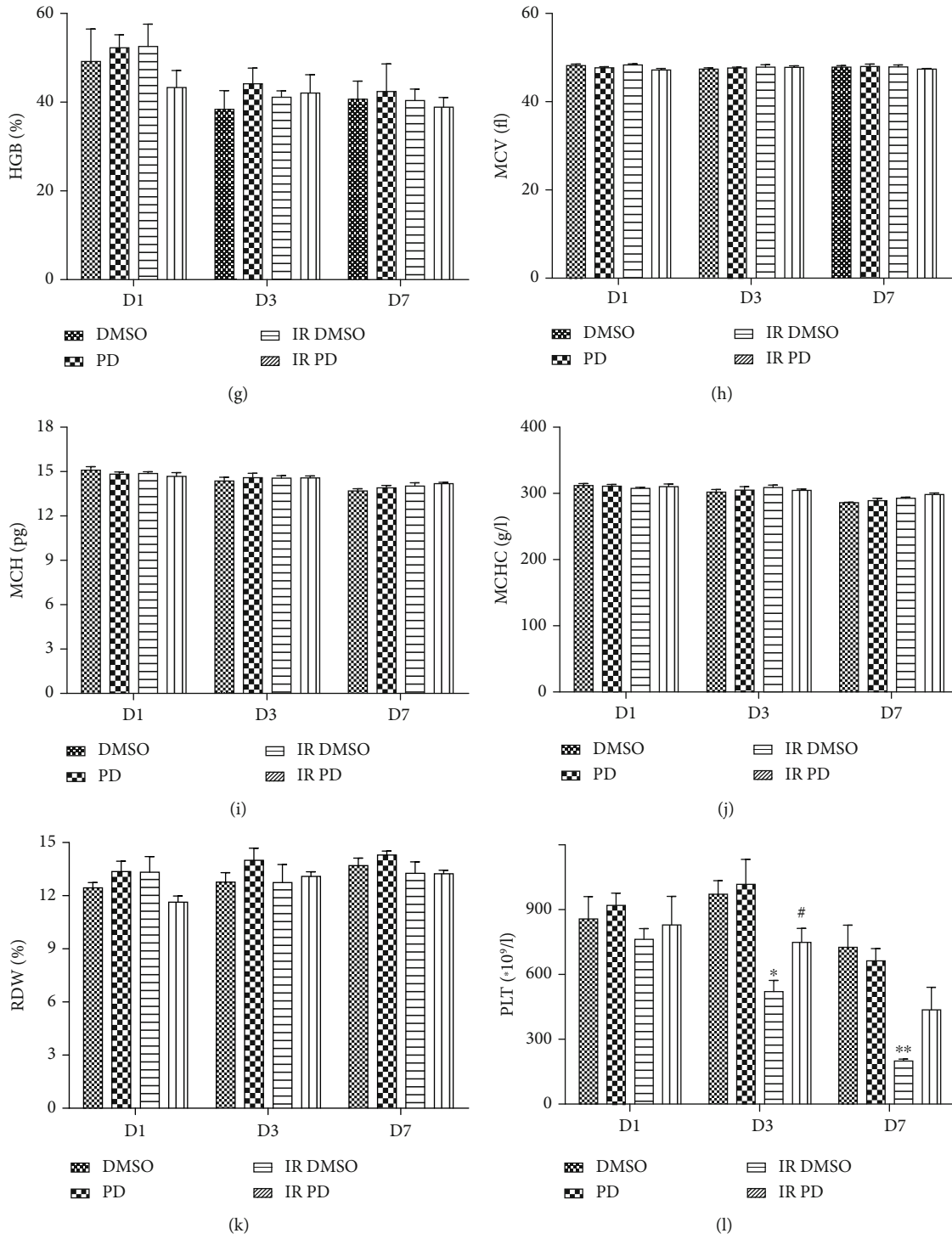


FIGURE 4: Continued.

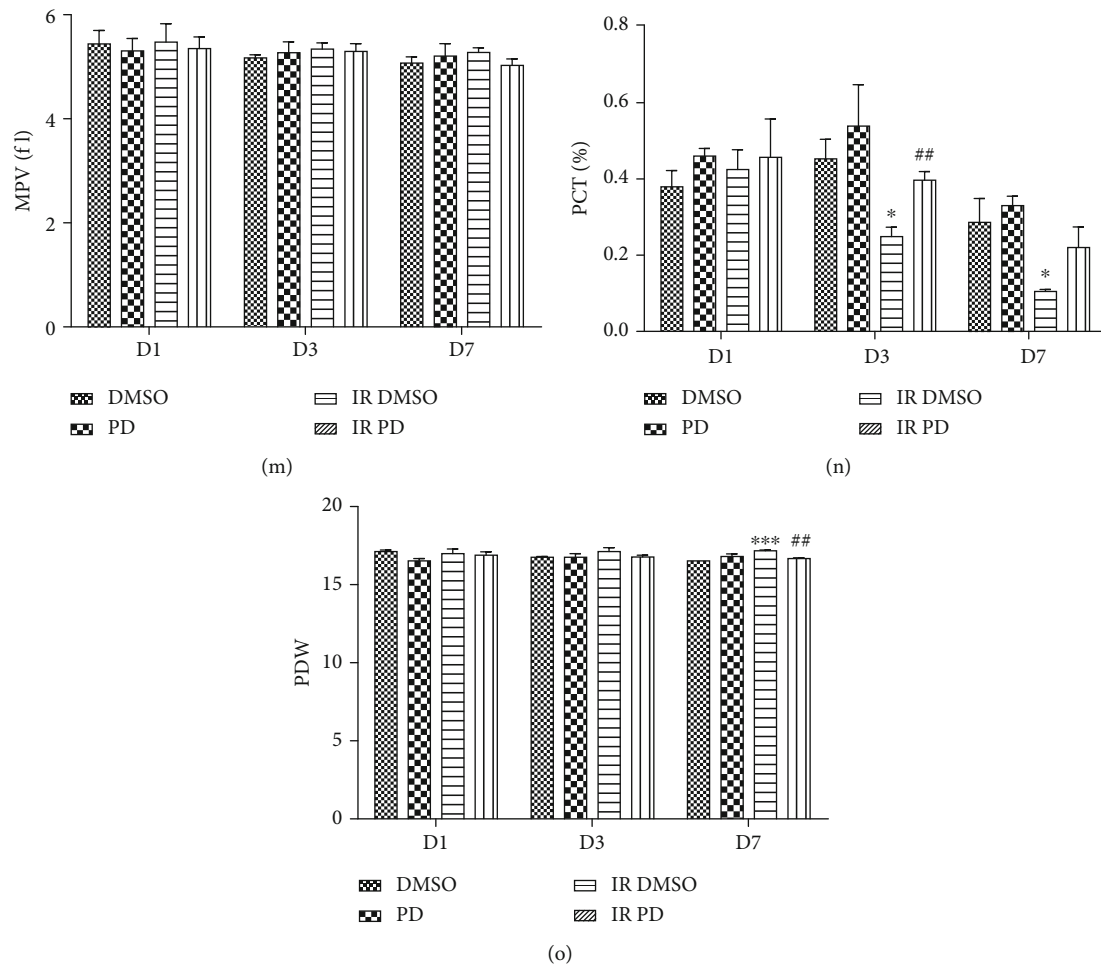


FIGURE 4: (a–d) Circulating WBC and its subsets of mice with/without PD administration in combination with IR or not. (a–d) WBC, Lymph, Mon, and Gran counts, respectively. Data are mean \pm SEM, $n = 8$. $*p < 0.05$, $**p < 0.01$, and $***p < 0.001$ vs. the DMSO group; $#p < 0.05$ and $##p < 0.01$ vs. the IR DMSO group. (e–k) Circulating RBC and the related parameters are shown here. (e–k) RBC, HGB concentration, HGB percentage, MCV, MCH, MCHC, and RDW, in sequence. Data are mean \pm SEM, $n = 8$. (l–o) The alterations of PLT and the relevant indicators in peripheral vessels of mice. (l–o) PLT, MPV, PCT percent, and PDW, sequentially. Data are mean \pm SEM, $n = 8$. $*p < 0.05$, $**p < 0.01$, and $***p < 0.001$ vs. the DMSO group; $##p < 0.01$ vs. the IR DMSO group.

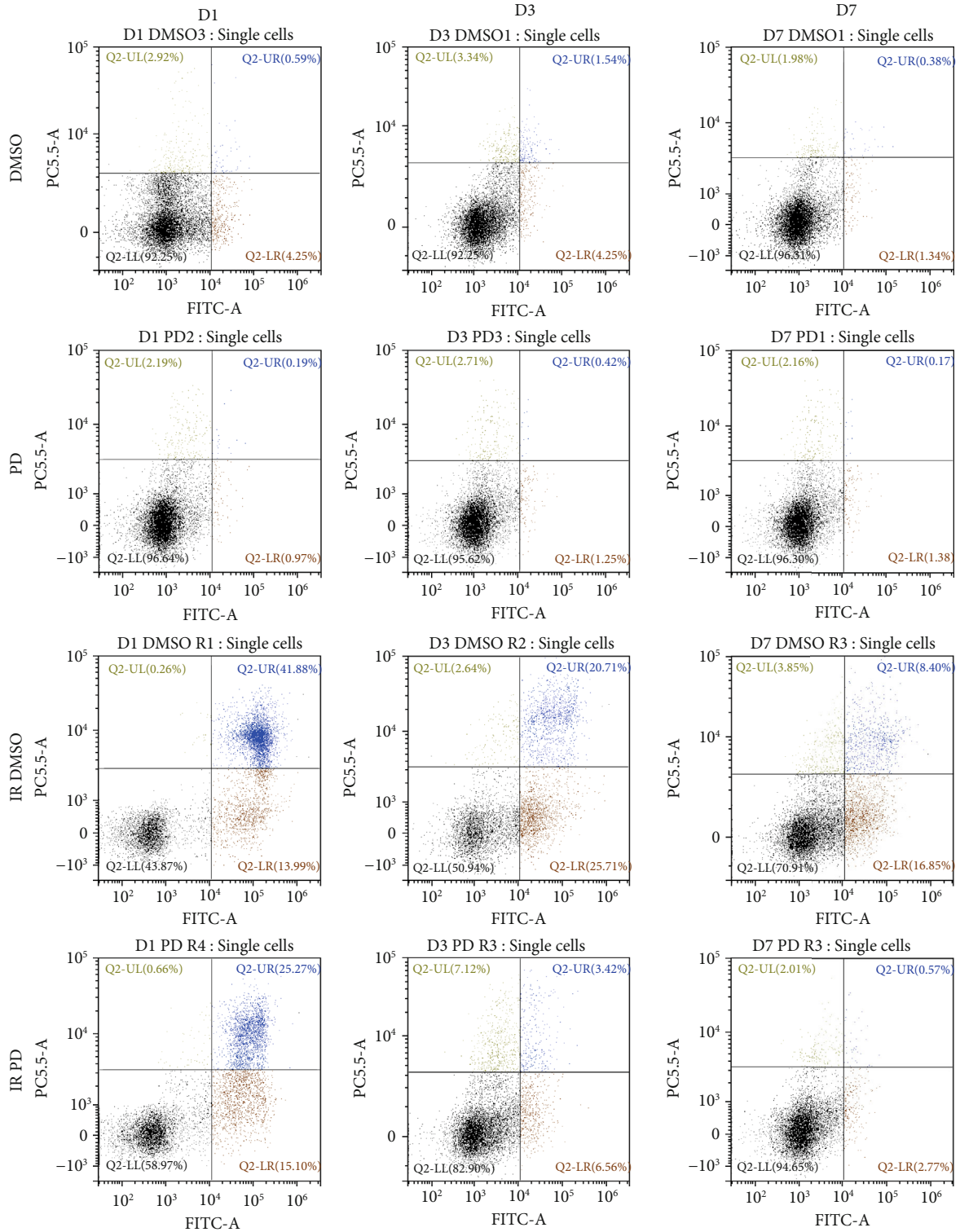
number was too few to be detected on D3 for both of the IR groups.

Figures 4(e)–4(k) depict the results of the red blood cells (RBC), the hemoglobin (HGB), the mean corpuscular volume (MCV), the mean corpuscular hemoglobin (MCH), the mean corpuscular hemoglobin concentration (MCHC), and the red blood cell distribution width (RDW) in mouse peripheral blood. Unlike the WBCs, no marked changes were found regarding this panel.

Three days after IR, the PLT value reduced significantly ($p = 0.0115232$) and continued to fall much lower level on D7 ($p = 0.00174034$). However, treatment with PD increased the PLT count in irradiated mice compared to irradiated mice ($p = 0.0479962$ for D3). Similar to this is the PCT performance, with a significant difference between IR DMSO and IR PD groups on D3 ($p = 0.00671847$). Though the MPV data told us the platelets of different groups should have similar individual volume (Figure 4(m)), the PDW level was apparently elevated by IR over time (D7, $p =$

0.000368411) which was attenuated again by PD treatment (D7, $p = 0.00154739$; Figure 4(o)).

3.5. Apoptosis. The spleen cells' apoptosis rate was evaluated by flow cytometry using an Annexin V/PI staining kit. The representative pictures of dot plot in Figure 5(a) were divided into four quadrants including the early apoptosis quadrant (LR) and the late apoptosis quadrant (UR), the sum of which indicated the total apoptosis rate. From the dot plots, we can achieve a direct assessment that at whichever time points, the combined dots of LR and UR quadrants turned to be much more as the individuals were irradiated, and this trend was partly prevented by the PD treatment (Figure 5(a)). Additionally, the summarized data of three independent repetitive experiments provides us with more specific statistics (Figure 5(b)). Under irradiation exposure, the percentage of apoptosis surged greatly in comparison with the corresponding DMSO groups (D1, $p = 0.000135389$; D3, $p = 0.0015616$; and D7, $p = 0.0081346$), while PD administration attenuated



(a)

FIGURE 5: Continued.

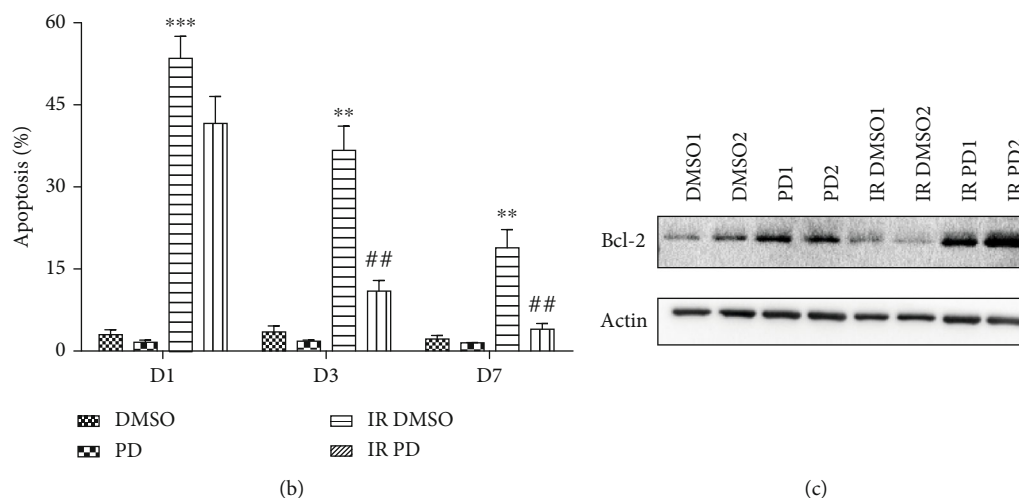


FIGURE 5: Mouse splenic and lung apoptosis changes after IR/sham combined with/without PD administration. (a) Representative dot plots chosen randomly from each treatment group. The X axis indicates FITC fluorescence intensity, and the Y axis represents PI fluorescence intensity (as the data were generated via the Beckman Coulter flow cytometry (CytoFLEX) and analyzed by the CytoExpert software, of which the channel of PC5.5 covers the wavelength of PI dye, and the channel name is PC5.5). The events of each quadrant were discriminated with different colors with the corresponding percentage showing in each corner. (b) The calculated statistical data from three independent identical experiments. Data are mean \pm SEM, $n = 8$. $**p < 0.01$ and $***p < 0.001$ vs. the DMSO group; $##p < 0.01$ vs. the IR DMSO group. (c) Immunodetection of mouse lung tissue from different treatment groups. Two samples were randomly selected from each group and underwent the WB analysis. For each well, 15 μ g protein were loaded here.

this disorder a lot thereafter (D3, $p = 0.00542718$; D7, $p = 0.00459456$). Moreover, it was suggested that the IR boosted splenic cell apoptosis rate reached the highest peak on D1, then descended gradually over time, showing the characteristic spleen cell apoptosis response style to neutron irradiation stress (Figure 5(b)).

To explore the apoptosis alteration more comprehensively, we applied the WB method to the mouse lung tissue to evaluate the antiapoptosis molecular Bcl-2 level. As depicted in Figure 5(c), IR deregulated the bcl-2 expression obviously. In contrast, PD administration reverted this change greatly, enhancing this key antiapoptosis regulator as much.

3.6. Histological Examination. The spleen and bone marrow from all the groups of mice were dissected and histopathologically examined at different time points along with the study. We conducted the microscopic examination at various magnification (Figures 6 and 7). As for the spleen, with the low-power objective, we found that the density of the white pulps of the spleen turned much lower after the IR exposure all through the experiment course. Furthermore, the white pulps lost the normal microstructure compared to the DMSO/PD groups which held much clearer border called the marginal zone. The high-power objective presented pictures with much more details showing that the overall cellular density of the radiated spleen was reduced greatly and most of the white pulps atrophied and became disorganized. Taking all the above observation outcomes into consideration to compare the IR groups on different days, we can see that the spleen got mostly damaged on D3 and recovered a little on D7. However, the histological investigation revealed that all the deleterious effects of neutron radiation on the spleen

microstructure were evidently relieved under the PD administration. With respect to the bone marrow, similar histological alterations were observed as that of the spleen (Figure 7). Neutrons seriously destroyed the microstructure of the bone marrow, causing vacuoles and disorganization, and greatly reduced the bone marrow cells, especially the series of the hematopoietic progenitor cells. In contrast, though the PD treated mice were also exposed to the same neutron radiation dose, their bone marrow specimen nearly looked the same as the sham-radiated groups, indicating that PD exerted strong hematopoietic process enhancement which helped the organism undergo the IR-induced crisis.

3.7. Immunohistochemistry Analysis. To explore the potential mechanism of the radioprotective effects of PD against neutron radiation detriments, we applied the IHC analysis for the detection of HO-1, KEAP 1, and SIRT 1. However, the splenic cellularity was so high that manual investigation and scoring of the IHC pictures would be more error prone due to the subjectivity of different pathologists. Hence, we conducted this part by the ImageJ software equipped with IHC profiler plugin. Although the representative images did not present a sharp visual contrast of positive staining occupation among different groups, significant differences were still observed after statistical calculation (Figure 8). For example, HO-1 expression was marked elevated by PD administration on D1 and D3 both pre ($p = 0.0453801$ for D1 and $p = 0.00783043$ for D7) and post IR ($p = 0.00432644$ for D1 and $p = 0.0142722$ for D7). As for both KEAP 1 and SIRT 1, there were no obvious changes between groups according to the statistical analysis. Though not significant, a slight increase of SIRT 1 expression after PD administration was still noticed here.

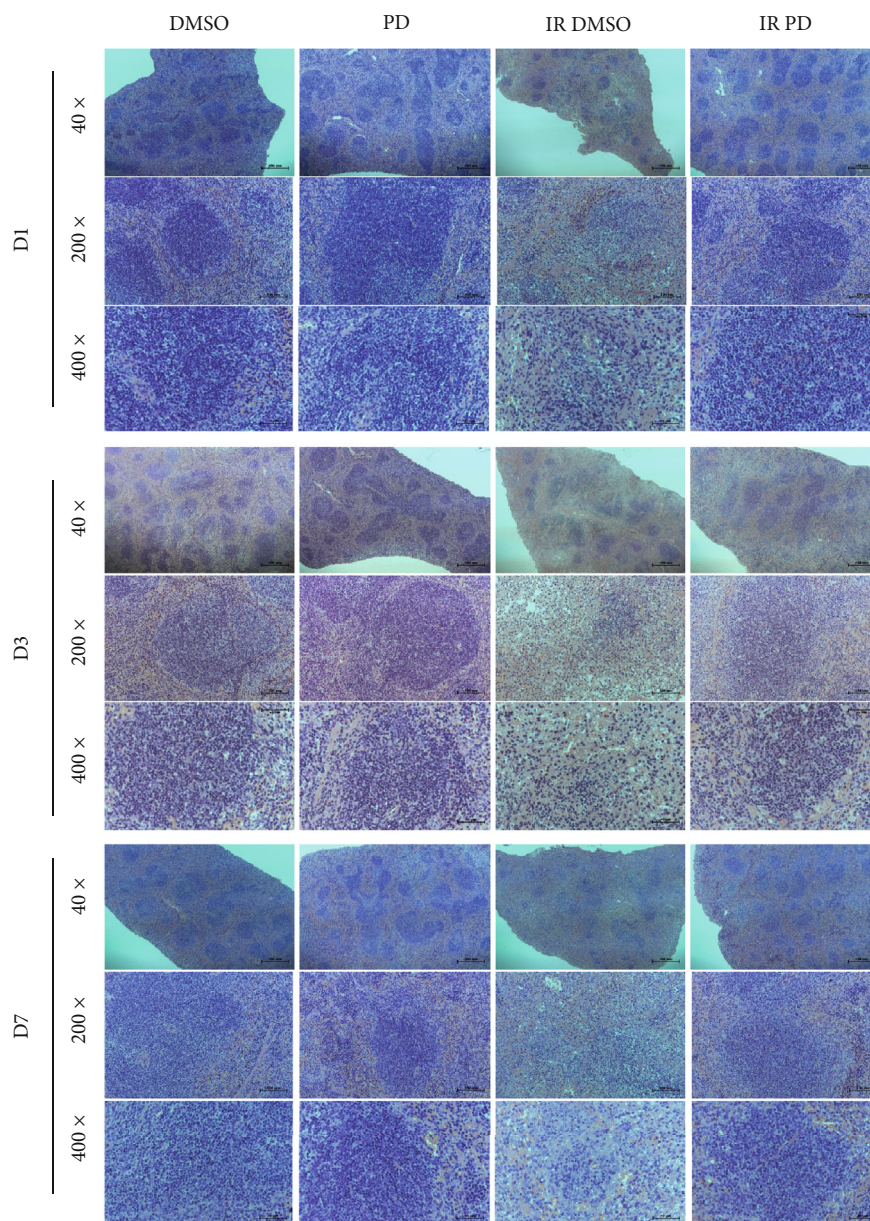


FIGURE 6: Histology analysis of mouse splenic tissue from different groups. The spleens from 3 mice every group were fixed in 4% formaldehyde and embedded in paraffin. Sections were stained with Hematoxylin-Eosin, and histological examination were applied.

4. Discussion

In this study, a neutron radiation-induced ARS mouse model was adopted to determine whether the potent natural antioxidant PD was able to prevent the severe injuries. The convincing data here positively favored this assumption, showing that the PD administration improved the survival rate after IR and ameliorated the IR-induced body weight loss and spleen and testis shrinking (Figures 1–3). In advance, obvious evidence indicated that PD could powerfully enhance both intra- and extramedullary hematopoiesis recovery against neutron detriments and present much better performance in the peripheral whole blood counting test (Figures 4 and 9), which was further ascertained by histological analysis of both the spleen and bone marrow (Figures 6

and 7). Additionally, it was suggested that the regulation of apoptosis and antioxidant signal pathway may play a vital role in PD's radioprotection in hematopoiesis (Figures 5 and 8).

Since the experimental discovery of neutron in 1932, its biological effects have attracted great interest, and there have been a mountain of related researches regarding neutron biology, among which the monoenergetic neutrons were paid more and more attention as it is more feasible and rational to explore the mechanism of the bioresponse to neutrons using single levels of energy instead of the sophisticated mixture [2]. Due to the limitation of the neutron flux of the previous irradiators, it was hard to make the high monoenergetic neutron-induced ARS animal model because of the conflict between the restrained duration for animal exposure and

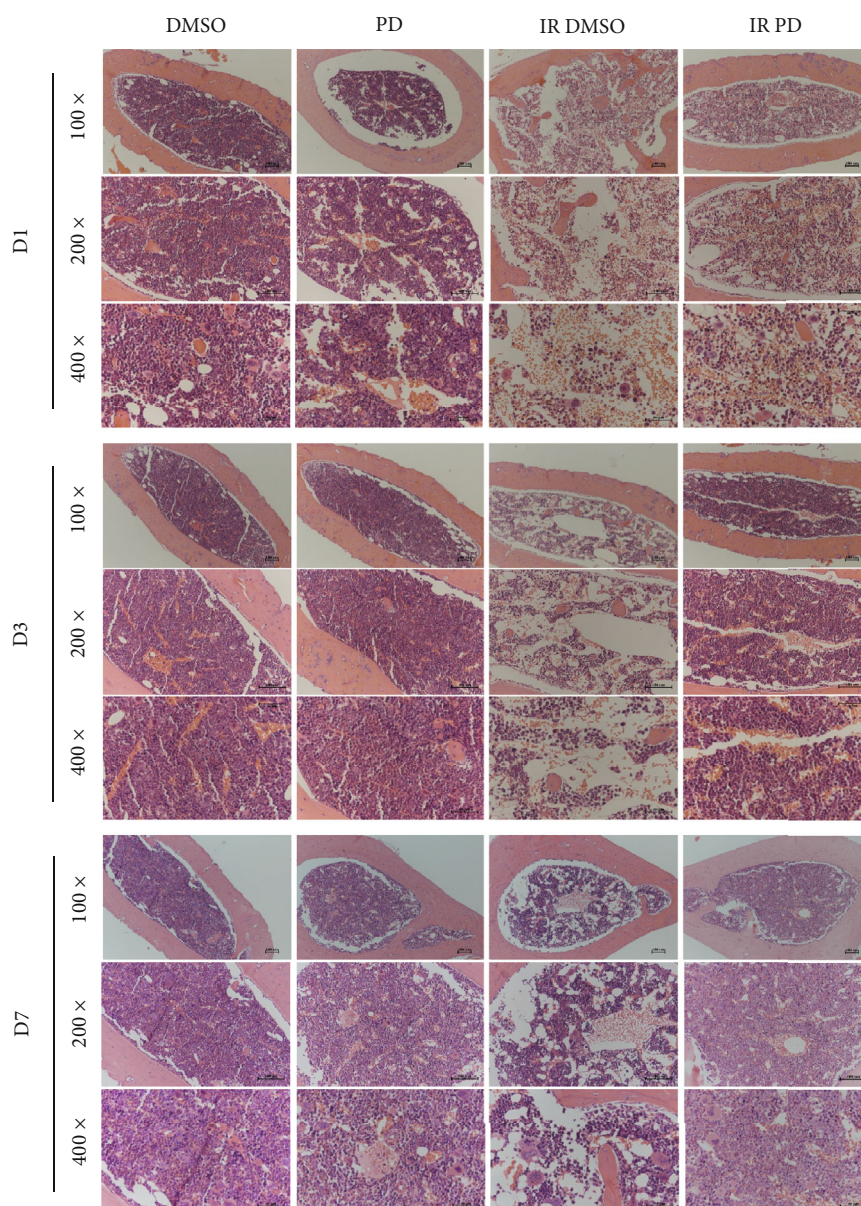


FIGURE 7: Histology analysis of mouse bone marrow from different groups. Femurs from at least 4 mice every group were isolated and fixed in 4% formaldehyde and embedded in paraffin. Sections were stained with Hematoxylin–Eosin, and histological examination was applied.

the insufficient dose rate. However, we adopted the HINEG system, which can present the high flux of 14.1 MeV neutrons as to generate the mouse ARS model utilized here, to conquer this obstacle. Compared with our previous studies about ionizing photons protection, similar phenomena such as survival rate decline, body weight loss, critical organ shrinking, and hematopoietic tissue cell loss were also obvious in the neutron ARS model here [18, 19]. The detriments by neutrons were much severer than that of photons, characterized by relatively low dose causing the similar outcomes and the advanced upcoming of injury peak, all of which promoted the insight of neutron biology at this condition.

In the current study, PD restored the survival rate from less than 50% up to 100%, showing its powerful protective

capacity against neutrons (Figure 1). Indeed, it would be more convincing if the neutron exposure could sacrifice most of the subjects. Therefore, we will increase the total dose by enhancing the neutron flux after the facility is upgraded in the near future. Body weight decreased obviously on the first few days after IR on a dose-dependent style, with the lowest average bodyweight value declining as the doses climbing (Figure 2). However, PD administration lessened the primary body weight loss significantly, reflecting its efficacy to helping getting through the critical early phase of ARS (Figure 2).

As is well known, injuries to the hematopoietic system is one of the major contributing factors for the ARS progression, resulting in the hematopoietic subsyndrome due to its profound detriments to the actively proliferating progenitor cells [20, 21]. For a long time, the main countermeasure

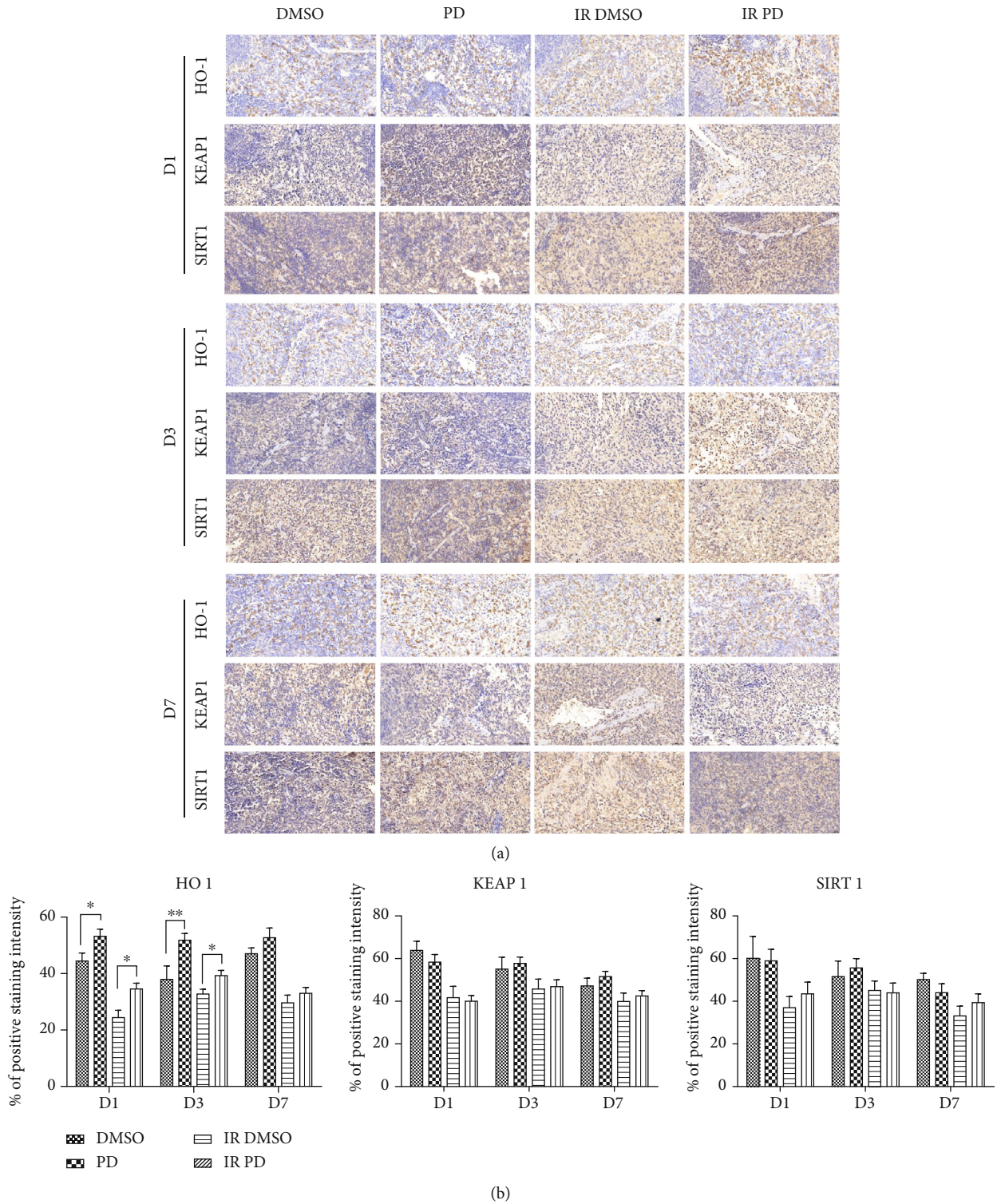


FIGURE 8: Immunohistochemistry analysis of HO-1, KEAP 1, and SIRT 1 using mouse spleen from different groups. The spleens from at least 4 mice each group were isolated and fixed in 4% formaldehyde and embedded in paraffin. Sections were stained with DAB and incubated with the corresponding antibodies. A whole slide scanning method was utilized to obtain the digital pictures which were then applied to calculate the IHC staining intensity score via the IHC profiler plugin in the ImageJ software. (a) Representative IHC images of each group; (b) quantified percentage score of IHC pictures from at least eight high-power fields ($\times 400$) every group was subjected to statistical analysis using a two-tailed unpaired t -test. The experiments were performed in triplicates, and data are presented here as mean \pm SEM. $*p < 0.05$, $**p < 0.01$.

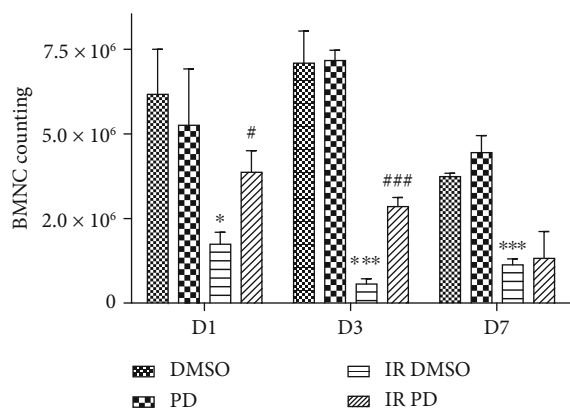


FIGURE 9: PD enhanced the IR-damaged BMNC. The IR dose with 2.91 Gy. DMSO with or without PD was administrated once a day until sacrifice. Data are mean \pm SEM, $n = 8$. * $p < 0.05$ and *** $p < 0.001$ vs. the DMSO group; # $p < 0.05$ and ### $p < 0.001$ vs. the IR DMSO group.

against IR was to seek protective strategies to preserve damaged hematopoietic precursor cells or restore their function [22]. Recently, the powerful effect of resveratrol to restore the pancytopenia induced by ionizing photons was observed [23]. As a precursor of resveratrol, PD exerts many similar biomedical properties such as antiplatelet aggregation, antioxidative action, cardioprotective activity, anti-inflammatory, and immune-regulating functions [24]. In the present study, PD elevated the IR-injured BMNCs (Figure 9) and mitigated the cellularity and microstructure of the bone marrow (Figure 7) which is the major source of blood cells and, as expected, alleviated the peripheral blood cell decline involving lymphocytes, granulocytes, WBCs, and PLTs (Figure 4). Additionally, identical tendency was found in the spleen specimen examination (Figure 6). Besides, all of the above indicators followed the same trend over time with the lowest value emerging on D3, except that PLT value entered into its bottom on D7 (Figure 4). This is probably due to the longer longevity and less radiosensitivity of PLTs compared to lymphocytes, causing the relatively delayed decline of PLTs in the peripheral blood.

Apoptosis surge is one the most important functioning manners of the IR cellular toxicity, so firstly, we conducted apoptosis detection for nucleated splenic cells to explore the potential mechanism. After IR, the apoptosis rate increased immediately and reached the top value on D1, followed by slightly continuous decreases on D3 and D7 (Figure 5). Collectively, the apoptotic nucleated splenic cells soared to the culmination immediately after IR and apparently responded quicker than the hematologic manifest. After all, it took some time from the onset of apoptosis to cell death, for which there existed the delay of the hematologic manifest. Nevertheless, PD alleviated the apoptosis greatly in spite of the time points with statistical differences on D3 and D7. What is more, WB data favored PD's antiapoptotic role in its radioprotection as well (Figure 5(c)). However, more extensive investigations such as detection of other apoptosis-relevant effectors should be considered to verify the antiapoptosis role of PD against HENR in the next study.

Previous studies indicated that PD could prevent neurons and hepatocytes by increasing the expression and activity of SIRT 1, which is very important for the function of hematopoietic stem cells [23, 25, 26]. As PD showed great performance in alleviating hematopoietic function injuries induced by HENR, we firstly hypothesized that SIRT 1 activation might improve hematopoiesis. However, from the IHC results, we found that PD merely elevated SIRT 1 positive staining slightly. Similarly, no significant alterations were observed in the KEAP 1 IHC analysis, which is an important inhibitor of the antioxidant gene Nrf 2. Taking the severe cell deaths caused by HENR into consideration, the IHC data reflected a comprehensive effect of the whole spleen cells, in which the former may play an even more important role resulting uniformly decline of positive staining after HENR regardless of protein targets. Even for the strong antioxidant enzyme, HO-1 were found decreased by HENR, but it was clearly raised by PD both pre- and post-HERN, suggesting a cytoprotective role of PD against various oxidative stress and inflammatory responses [27]. However, considering the confounding factors such as HENR-induced cell deaths mentioned above and the cellular heterogeneity of the in vivo studies, the more specific methods aiming directly at specific sorts of cells would be adopted in the future mechanism-exploration research.

In conclusion, the present study demonstrated that PD played a protective role against neutron IR injuries in mice by accelerating hematopoiesis, suppressing apoptosis of nucleated blood cells, and regulating the antioxidative function such as the HO-1 pathway. Our findings may throw light on some characterized bioeffects induced by the high flux of 14.1 MeV neutrons and propose that PD can powerfully mitigate these damages, indicating its potential role of new strategy for the prevention of high-energy neutron IR detriments.

Data Availability

All the data used to support the findings of this study were supplied by the Naval Medical University and Chinese Academy of Sciences in China under license and so cannot be made freely available. Requests for access to these data should be made to Dr. Guo via mailing to jiamingguonmu@smmu.edu.cn.

Conflicts of Interest

The authors declare no conflict of interest.

Authors' Contributions

Jiaming Guo, Tingting Liu, and Long Ma contributed equally to this work

Acknowledgments

This study was funded by the National Natural Science Foundation of China (31900890), Key Program of National

Natural Science Foundation of China (11635014), Shanghai Sailing Program (19YF1459000), and Naval Medical University Medical Protection Project (WL-MS-02).

Supplementary Materials

Figure S1: pictures of confined mice which were ready to receive HENR. Table S2: table of calculated dose values based on the straight-line distance to the radiation source. (*Supplementary Materials*)

References

- [1] C. N. Coleman, "Sixteenth Annual Warren K. Sinclair Keynote Address: frontiers in medical radiation science," *Health Physics*, vol. 118, no. 4, pp. 349–353, 2020.
- [2] D. T. Goodhead, "Neutrons are forever! Historical perspectives," *International Journal of Radiation Biology*, vol. 95, no. 7, pp. 957–984, 2019.
- [3] Y. Ishida, Y. Ohmachi, Y. Nakata et al., "Dose-response and large relative biological effectiveness of fast neutrons with regard to mouse fetal cerebral neuron apoptosis," *Journal of Radiation Research*, vol. 47, no. 1, pp. 41–47, 2006.
- [4] R. D. Stewart, S. W. Streitmatter, D. C. Argento et al., "Rapid MCNP simulation of DNA double strand break (DSB) relative biological effectiveness (RBE) for photons, neutrons, and light ions," *Physics in Medicine and Biology*, vol. 60, no. 21, pp. 8249–8274, 2015.
- [5] H. J. Lee, J. S. Kim, C. Moon, J. C. Kim, S. K. Jo, and S. H. Kim, "Relative biological effectiveness of fast neutrons in a multiorgan assay for apoptosis in mouse," *Environmental Toxicology*, vol. 23, no. 2, pp. 233–239, 2008.
- [6] K. Tanaka, N. Gajendiran, S. Endo, K. Komatsu, M. Hoshi, and N. Kamada, "Neutron energy-dependent initial DNA damage and chromosomal exchange," *Journal of Radiation Research*, vol. 40, pp. 36–44, 1999.
- [7] S. Nambiar and J. T. Yeow, "Polymer-composite materials for radiation protection," *ACS Applied Materials & Interfaces*, vol. 4, no. 11, pp. 5717–5726, 2012.
- [8] C. G. Broustas, Y. Xu, A. D. Harken, G. Garty, and S. A. Amundson, "Comparison of gene expression response to neutron and x-ray irradiation using mouse blood," *BMC Genomics*, vol. 18, no. 1, p. 2, 2017.
- [9] L. Yang, R. Wang, Y. Gao et al., "The protective role of interleukin-11 against neutron radiation injury in mouse intestines via MEK/ERK and PI3K/Akt dependent pathways," *Digestive Diseases and Sciences*, vol. 59, no. 7, pp. 1406–1414, 2014.
- [10] Z. Y. Yu, M. Li, A. R. N. Han et al., "RhG-CSF improves radiation-induced myelosuppression and survival in the canine exposed to fission neutron irradiation," *Journal of Radiation Research*, vol. 52, no. 4, pp. 472–480, 2011.
- [11] Y. C. Wu, "Development of high intensity D-T fusion neutron generator HINEG," *International Journal of Energy Research*, vol. 42, no. 1, pp. 68–72, 2018.
- [12] B. Pan, Y. Ren, and L. Liu, "Uncovering the action mechanism of polydatin via network pharmacological target prediction," *RSC Advances*, vol. 8, no. 34, pp. 18851–18858, 2018.
- [13] J. Kim, J. Oh, J. N. Averilla, H. J. Kim, J. S. Kim, and J. S. Kim, "Grape peel extract and resveratrol inhibit wrinkle formation in mice model through activation of Nrf2/HO-1 signaling pathway," *Journal of Food Science*, vol. 84, no. 6, pp. 1600–1608, 2019.
- [14] L. Li, K. Zhang, J. Zhang et al., "Protective effect of polydatin on radiation-induced injury of intestinal epithelial and endothelial cells," *Bioscience Reports*, vol. 38, no. 6, 2018.
- [15] Y. Ma and X. Jia, "Polydatin alleviates radiation-induced testes injury by scavenging ROS and inhibiting apoptosis pathways," *Medical Science Monitor*, vol. 24, pp. 8993–9000, 2018.
- [16] F. Varghese, A. B. Bukhari, R. Malhotra, and A. de, "IHC profiler: an open source plugin for the quantitative evaluation and automated scoring of immunohistochemistry images of human tissue samples," *PLoS One*, vol. 9, no. 5, article e96801, 2014.
- [17] S. Sawant, H. Dongre, A. K. Singh et al., "Establishment of 3D co-culture models from different stages of human tongue tumorigenesis: utility in understanding neoplastic progression," *PLoS One*, vol. 11, no. 8, article e0160615, 2016.
- [18] J. Guo, Z. Liu, D. Zhang et al., "TLR4 agonist monophosphoryl lipid A alleviated radiation-induced intestinal injury," *Journal of Immunology Research*, vol. 2019, Article ID 2121095, 10 pages, 2019.
- [19] K. Cao, X. Lei, H. Liu et al., "Polydatin alleviated radiation-induced lung injury through activation of Sirt3 and inhibition of epithelial-mesenchymal transition," *Journal of Cellular and Molecular Medicine*, vol. 21, no. 12, pp. 3264–3276, 2017.
- [20] S. Charrier, A. Michaud, S. Badaoui et al., "Inhibition of angiotensin I-converting enzyme induces radioprotection by preserving murine hematopoietic short-term reconstituting cells," *Blood*, vol. 104, no. 4, pp. 978–985, 2004.
- [21] J. K. Waselenko, T. MacVittie, W. F. Blakely et al., "Medical management of the acute radiation syndrome: recommendations of the Strategic National Stockpile Radiation Working Group," *Annals of Internal Medicine*, vol. 140, no. 12, pp. 1037–1051, 2004.
- [22] V. K. Singh, V. L. Newman, A. N. Berg, and T. J. MacVittie, "Animal models for acute radiation syndrome drug discovery," *Expert Opinion on Drug Discovery*, vol. 10, no. 5, pp. 497–517, 2015.
- [23] X. R. Song, Y. Q. Cheng, D. F. Su, and A. J. Liu, "The Sirt1 activator resveratrol improved hematopoiesis in pancytopenia mice induced by irradiation," *Journal of Pharmacological Sciences*, vol. 140, no. 1, pp. 79–85, 2019.
- [24] Q. H. Du, C. Peng, and H. Zhang, "Polydatin: a review of pharmacology and pharmacokinetics," *Pharmaceutical Biology*, vol. 51, no. 11, pp. 1347–1354, 2013.
- [25] H. Bai, Y. Ding, X. Li et al., "Polydatin protects SH-SY5Y in models of Parkinson's disease by promoting Atg5-mediated but parkin-independent autophagy," *Neurochemistry International*, vol. 134, p. 104671, 2020.
- [26] Z. Zeng, Y. Yang, X. Dai et al., "Polydatin ameliorates injury to the small intestine induced by hemorrhagic shock via SIRT3 activation-mediated mitochondrial protection," *Expert Opinion on Therapeutic Targets*, vol. 20, no. 6, pp. 645–652, 2016.
- [27] J.-S. Deng, W. P. Jiang, C. C. Chen et al., "Cordyceps cicadae-Mycelia ameliorate cisplatin-induced acute kidney injury by suppressing the TLR4/NF- κ B/MAPK and activating the HO-1/Nrf2 and Sirt-1/AMPK pathways in mice," *Oxidative Medicine and Cellular Longevity*, vol. 2020, Article ID 7912763, 17 pages, 2020.

Review Article

Hematopoietic Stem Cells and Mesenchymal Stromal Cells in Acute Radiation Syndrome

Liren Qian  and Jian Cen

Department of Hematology, The Sixth Medical Center, Chinese PLA General Hospital, Fucheng Road #6, Beijing 100048, China

Correspondence should be addressed to Liren Qian; qlr2007@126.com

Received 10 April 2020; Revised 2 July 2020; Accepted 24 July 2020; Published 13 August 2020

Academic Editor: Ilaria Peluso

Copyright © 2020 Liren Qian and Jian Cen. This is an open access article distributed under the Creative Commons Attribution License, which permits unrestricted use, distribution, and reproduction in any medium, provided the original work is properly cited.

With the extensive utilization of radioactive materials for medical, industrial, agricultural, military, and research purposes, medical researchers are trying to identify new methods to treat acute radiation syndrome (ARS). Radiation may cause injury to different tissues and organs, but no single drug has been proven to be effective in all circumstances. Radioprotective agents are always effective if given before irradiation, but many nuclear accidents are unpredictable. Medical countermeasures that can be beneficial to different organ and tissue injuries caused by radiation are urgently needed. Cellular therapy, especially stem cell therapy, has been a promising approach in ARS. Hematopoietic stem cells (HSCs) and mesenchymal stromal cells (MSCs) are the two main kinds of stem cells which show good efficacy in ARS and have attracted great attention from researchers. There are also some limitations that need to be investigated in future studies. In recent years, there are also some novel methods of stem cells that could possibly be applied on ARS, like “drug” stem cell banks obtained from clinical grade human induced pluripotent stem cells (hiPSCs), MSC-derived products, and infusion of HSCs without preconditioning treatment, which make us confident in the future treatment of ARS. This review focuses on major scientific and clinical advances of hematopoietic stem cells and mesenchymal stromal cells on ARS.

1. Introduction

Nuclear technology has been widely used in different fields, like medicine, industry, agriculture, military, and medicine. Exposure to radiation or nuclear leakage is sometimes unavoidable and potentially catastrophic. More than 400 radiological accidents have happened since the middle of the 20th century [1], and thousands of persons have been injured by irradiation. It is reported that over 600 of the 10 million sealed radioactive materials used worldwide have been lost or stolen [2, 3]. It can be inferred that there may still be parts of the lost radioactive materials that are undocumented. With the increasing number of conflicts between countries and terrorist threats, and with the increasing application of radiotherapy in clinics, radiotherapy accidents like radiation overdose and nuclear leakage caused by machine malfunction are also not rare [4]; thus, there is an unprecedented urgency to develop new methods to treat acute radiation syndrome (ARS). In recent years, many new radio-

protectants like antioxidants and toll-like receptor 5 agonist have been found to be effective against radiation [5–15]. Radioprotectants are supposed to exert their efficacy if present before irradiation. However, nuclear leakage accidents are always unpredictable. Accidents from medical nuclear devices, the collapse of nuclear power plants caused by natural calamities, and the explosion of nuclear weapons may cause a huge loss of life and a considerable number of injuries. Developing new therapeutic methods to treat the injuries caused by irradiation is quite essential. Stagnation in supportive therapy on ARS is the major current situation [16]. Through in vivo studies, it has been found that cytokines like granulocyte colony-stimulating factor (G-CSF), granulocyte-monocyte colony-stimulating factor (GM-CSF), pegylated G-CSF (pegfilgrastim), interleukin-11, interleukin-3, and erythropoietin can either reduce the duration of pancytopenia or improve outcomes [16–21]. Other supportive treatments include blood product transfusion, anti-infective therapy, and antiemetic drugs. These treatments

are mostly symptomatic approaches. However, etiological treatments are usually not easy to implement, and studies of etiological treatments of ARS lag further behind. A manual entitled “Medical Management of Radiation Accidents: Manual on the Acute Radiation Syndrome” provide recommendations for the medical management of radiation accident victims [22] based on clinical archives and preclinical experiments. The role of hematopoietic stem cells (HSCs) has attracted researchers’ attention since 1951 when Lorenz et al. found that infusion of bone marrow cells could prolong the survival time of irradiated mice [23, 24], while the role of mesenchymal stromal cells (MSCs) in ARS has just been found in recent decades in mice, for their power to migrate to the site of injury [25–27]. MSCs home in to injured tissues when coinjected with HSCs to treat a radiation-induced multiorgan failure syndrome [28]. The objective of this review was to offer an overview of the major scientific and clinical advances of HSCs and MSCs as therapeutic countermeasures against irradiation.

2. Acute Radiation Syndrome

ARS can be clinically manifested as a continuous progression, according to the radiation dose, from nausea and vomiting in the prodromal stage to a hematopoietic, gastrointestinal tract, cutaneous, or neurovascular syndrome [29, 30]. ARS has four different phases: the prodromal phase, the latent phase, the illness phase, and one phase of recovery or death. Time to death is very often dictated by type of organ injury. When an individual is exposed to a dose of 10-20 Gy or higher, prodromal symptoms will appear within 1 to 72 hours, including fever, loss of appetite, nausea and vomiting, electrolyte disturbances, and even hypotension, loss of consciousness, and finally death in a few days. A severe rapid prodromal stage suggests a higher absorbed dose and predicts poor clinical prognosis. Target organ damage occurs subsequently after the prodromal period. The severity of radiation injuries depends on the radiation dose incurred, the dose rate, the radiosensitivity of affected tissues and organs, and the area and extent to which the body has been exposed [31]. METREPOL clinically divides hematopoietic ARS into four grades (H1-H4) based on patients’ peripheral blood cells over 60 days after irradiation [32]. H1 represents mild damage which need no specific therapy, and H2-H4 represents moderate, severe, and irreversible damage, respectively [32, 33]. The accident at the Chernobyl Nuclear Power Plant on 26 April 1986 resulted in the hospitalization of 237 patients identified as severely overexposed persons. ARS was diagnosed in 134 persons admitted to the specialized hospitals in Moscow and Kyiv. Among them, 28 died within three months of ARS associated with extensive local radiation burns combined with thermal burns. ARS was not confirmed in another 103 hospitalized patients [34].

The effects of ionizing radiation on biomolecules can be divided into direct and indirect effects (Figure 1) [35]. Direct effect means the energy of radiation rays may transfer to biomolecules directly causing ionization and excitation. Radiation rays can also act on water molecules, causing activation of water molecules and formation of free radicals.

These activated products then act on other biomolecules. The effects produced in this way are called indirect effects. Because the body and cells contain a large amount of water, most of the radiant energy is absorbed by water resulting in decomposition of water molecules to generate a large number of free radicals [5]. They can damage various biological macromolecules in the body. This indirect effect causes damage to the body accounting for about 80% of the radiation damage [9, 36]. DNA can be damaged by irradiation through either direct or indirect action [37]. During the repair process of DNA post irradiation, some DNA injuries can completely recover by complex metabolic and immunological mechanisms, while some DNA injuries can recover but with mistakes in DNA repair like nonclonal genetic deletion and genetic insertion [38]. Accumulated gene mutation or instabilities may lead to malignant diseases several years later. Stem cell therapy has been proven effective in genetic diseases, like sickle cell disease, thalassemia, and immunodeficiency diseases [39–41]. Oxidative stress caused by free radicals generated from radiation plays a major role in radiation-induced injury. Besides, the reactive oxygen/nitrogen species that results from irradiation of normal tissues can be used as intracellular and intercellular signals to change cell and tissue functions. The increase of free radicals can lead to changes in molecular pathways. These signaling pathways play an important role in the pathogenesis of many pathological states, including inflammation, cancer, and diseases of some organs, and can promote the process of aging [42].

HSCs and MSCs are two types of cells much more successful in clinical applications that have also been proven to be effective in treating ARS either in preclinical models or in clinical case studies [30, 43].

3. Hematopoietic Stem Cell Transplantation in ARS

HSCs are multipotential stem cells with the ability to differentiate and self-renew. Because radiation may cause bone marrow failure, the question of whether infusion of bone marrow cells can be engrafted and have the ability to self-renew and differentiate to peripheral blood cells has aroused the thinking of early scientists.

As early as 1951, Lorenz et al. have found that infusion of bone marrow cells has a therapeutic effect on lethal doses of radiation [23]. They found that infusion of bone marrow cells from homologous animals 10 to 15 minutes after a lethal dose of radiation can reduce the mortality of mice to less than 30% and the mortality of guinea pigs to less than 50%. Infusion of bone marrow cells from heterologous animals also has a therapeutic effect, which can reduce the mortality to about 60% [24]. The cause of higher mortality with a heterologous transplant of bone marrow is probably caused by graft-versus-host disease (GVHD) after transplantation, when there was still no clear concept of GVHD. Since then, with the development of HSCT, the role of HSC in radiation became an interesting area for scientific researchers. In the following years, many preclinical studies have repeatedly confirmed the role of HSC in radiation and tried to explain its mechanism [44, 45]. Although HSCT has shown exciting

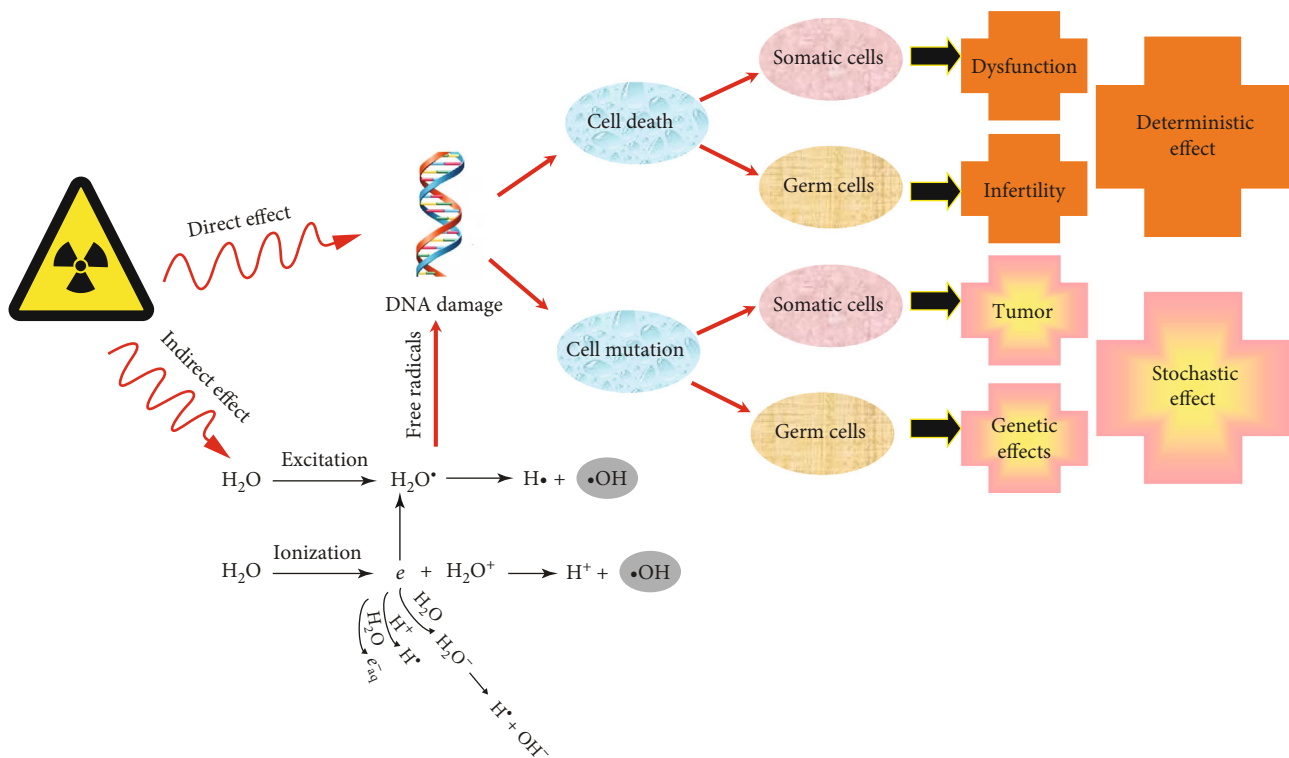


FIGURE 1: Biological effects of radiation.

therapeutic effects in preclinical animal experiments with acute radiation injury, its effects are still controversial in clinical applications. The earliest HSCT in clinical patients dates back to the middle of the last century. Bone marrow cells were transfused into 4 patients in one nuclear accident in 1958 [46]. In the Yugoslavian accident, 6 persons were exposed to radiation; 1 died, and 4 of the recovered victims received total allogeneic bone marrow injections. The victims presented not only hematopoietic syndrome but also gastrointestinal tract syndrome and neurovascular syndrome. Although the patients who have been infused with bone marrow cells have had a transient graft, the implantation has not significantly restored peripheral blood cells. The author thought it might be due to the late timing of infusion [46]. Temporary implantation may indicate that bone marrow cell infusion may have potential therapeutic effects on acute radiation injury. To date, about 50 patients with acute radiation sickness have been treated with allogeneic hematopoietic stem cell transplants [38]. However, the median survival time of these patients has not yet exceeded one month [1, 47]. In addition, patients who have had a longer or even more than one-year survival period have shown autologous hematopoietic recovery, which has led researchers to question the role of HCT in acute radiation injury.

Radiation can also cause severe damage to multiple systems and organs throughout the body, such as damage to the heart and nervous system. Radiation can cause damage to heart pump function and myocardium. The most serious type of radiation-induced heart disease (RIHD) seems to be a type of myocardial degeneration, i.e., perivascular and

interstitial fibrosis 6-10 weeks after radiation [9]. For example, in patients with clinical chest tumors undergoing radiation therapy, radiation can affect the heart, blood vessels, lungs, and spinal cord, resulting in the remodeling of related tissue cells and adverse side effects. This complex process is mediated by the complex biological effects of radiation. Radiation can cause inflammation, endothelial cell dysfunction, and thrombosis and eventually lead to organ dysfunction and heart failure in the form of pathological entities of RIHD [42]. Radiation may also induce spinal cord damage which is relatively rare and usually called radiation myelopathy (RM) due to radiation-induced cell apoptosis, like oligodendrocytes and endothelial cells [48]. Interestingly, HSCs have also been reported to regenerate nonhematopoietic tissues in recent decades, like myocardium and nerves [49–51]. To date, 29 clinical trials can be found for stem cell transplantation and myocardial infarction, including 5 closed. Orlic et al. found that 68% of newly formed myocardial tissue formed in the infarcted myocardial area 9 days after transplantation of bone marrow cells from transgenic mice [52]. Following the study, some clinical trials have been initiated using stem cell transplantation to treat myocardial infarction [50, 51]. However, this opinion was opposed by Balsam et al. [49]. Their findings were inconsistent with Orlic et al. They used a fluorescent labeling method to track the differentiation of HSCs from transgenic mice in ischemic myocardium. They found that the cells that differentiated from the transplanted HSCs in the myocardium did not express the cardiomyocyte markers, but instead appeared as the hematopoietic marker CD45 and the myeloid marker Gr-1, a protein also known

as Ly-6G/Ly-6C. They explained that the differences between their study and Orlic et al.'s study may be due to an "anaesthetic and/or surgical technique." They also pointed out that Orlic et al. did not stain the transplanted cells for additional hematopoietic markers, like CD45 or Gr-1, which may lead to a different conclusion. They also called for caution in the use of HSCs in the treatment of myocardial infarction in clinical trials, otherwise it is easy to delay the best time for patients.

Besides cardiomyocytes, many studies have confirmed that HSCs can differentiate into nerve cells [53–56]. Sigurjonsson et al. found that 4 to 9 days after CD34+ HSCs were implanted into lesions of the developing spinal cord, some of the implanted cells began to differentiate into neural cells expressing NeuN and MAP2. While HSCs differentiate into neural tissue cells, their CD34+ expression gradually disappeared [57]. They also found that the spinal microenvironment and cell differentiation efficiency are closely related. Although there are still debates as to whether HSCs can be regenerated into nonhematopoietic cells, no matter from the basic experiments or clinical trials, this has made us look forward to this application. This cannot help, but let us consider whether the use of hematopoietic stem cell transplantation for ARS is not only for the reconstruction of the hematopoietic system and the immune system but also for the regeneration of other organ cells.

There are also some limitations for using HSCT to treat ARS. Because patients often cannot be expected to be irradiated before accepting a nuclear accident, few patients have stored their own HSCs, which makes the application of autologous stem cell transplantation in ARS almost impossible. Engraftment syndrome (ES) after allogeneic HSCT is increasingly diagnosed [58], occurring independently of GVHD in 79% of the patients [59], which is manifested as fever, pulmonary vascular leak, rash, and organ dysfunction. Allogeneic HSCT also has some intractable limitations: (1) lack of donor sources for HLA-matched sibling HSCs; (2) the preconditioning before hematopoietic stem cell transplantation will cause a secondary blow to the body and can cause serious infections, bleeding, organ failure, and other complications; (3) immunosuppressants used to prevent graft-versus-host diseases (GVHD) after allogeneic HSCT can cause serious infections and even threaten life; (4) GVHD can cause damage to multiple organs and tissues throughout the body, which can make a third blow to the body; and (5) radiation often causes damage to multiple organs throughout the body, not only the hematopoietic system and the immune system. The above factors combined with the current small number of patients with ARS, lack of clinical experiences, and other factors have led to the limitation of the application of HSCT in ARS, and to the current insufficient success rate. The above problems are also the next steps for radiation specialists and hematologists. I believe that if the above problems are solved well, HSCT will greatly improve the survival time and life quality of patients with ARS. The emergency treatment of populations requires the availability of ready-to-use frozen products to treat a group of individuals. "Drug" stem cell banks obtained from clinical grade human induced pluripotent stem cells (hiPSCs)

will make it possible to produce stem cells of different types to treat the population [60]. hiPSCs from these "universal" donors are already available (<http://www.gait.global/>).

4. Mesenchymal Stromal Cells in ARS

The mesenchymal "stem" cell, which was first reported by Friedenstein et al. in 1968 [61], has the ability to self-renew and differentiate into three kinds of cells, including osteoblasts, chondrocytes, and adipocytes. It is a kind of spindle-shaped plastic adherent cell, which is isolated from bone marrow or other sources [62]. Heterogeneous procedures for isolating and cultivating mesenchymal "stem" cells among laboratories have prompted the International Society for Cellular Therapy (ISCT) to issue criteria for identifying unique populations of these cells. Consequently, the isolation of mesenchymal "stem" cells according to ISCT criteria has produced heterogeneous, nonclonal cultures of stromal cells containing stem cells with different multipotent properties, committed progenitors, and differentiated cells [63]. This group of cells separated by plastic adherence does not have the homogeneity of stem cells, and the true stemness of stem cells should be more complicated. The current recognized function of this group of cells does not meet the criteria for stem cells. Therefore, it was recommended to use the term *mesenchymal stromal cell* which should be more suitable for this group of heterogeneous cells instead of the term *mesenchymal stem cell* [62].

Although there are not many studies and reports on the application of MSCs in ARS, some of the biological functions recognized so far can support its efficacy in ARS. Firstly, MSCs can directly and indirectly secrete many cytokines, such as interleukin- (IL-) 6, IL-7, IL-8, IL-11, IL-12, IL-14, IL-15, macrophage colony-stimulating factor (M-CSF), stem cell factor (SCF), granulocyte colony-stimulating factor (G-CSF), and granulocyte-macrophage colony-stimulating factor (GM-CSF). These cytokines play a key role in promoting hematopoiesis, tissue repair, and maintaining homeostasis [64]. Secondly, after infusion of MSCs, they can migrate to the injury site under chemotactic factors while maintaining their original functions to play a mediating role [25, 65]. They can also differentiate into injured tissue cells or promote the repair of tissues at the injury site, like the heart, nervous system, skin, bone, fat, cartilage, muscle, and intestine [43, 65–67]. Thirdly, MSCs have immunomodulatory, anti-inflammatory properties [68]. MSCs have been proven to exert therapeutic effects in graft-versus-host disease after allogeneic HSCT due to its immune modulation properties [69]. MSCs' role in ARS has attracted the attention of researchers, and its efficacy has also been confirmed in different organs [43]. In 2013, MSC therapy of refractory irradiation-induced colitis was safe and effective on pain, diarrhea, hemorrhage, inflammation, and fistulization accompanied by modulation of the lymphocyte subsets toward an increase in T regulatory cells and a decrease in activated effector T cells. Mesenchymal stem cells represent a safe therapy for patients with refractory inflammatory bowel diseases [70]. And MSC treatment induces stimulation of endogenous host progenitor cells to improve the

regenerative process and constitutes an initial approach to arguing in favor of the use of MSCs to limit/reduce colorectal damage induced by radiation [71]. Furthermore, allogeneic MSCs can be used in irradiated patients without rejection, making them quicker and easier to use to treat a group of people immediately after an accident if ready-to-use cell banks are available.

5. MSCs in Hematopoietic ARS

In 2005, Mourcin et al. demonstrated that *in vitro* experiments, the coculture of MSCs and irradiated CD34+ cells can significantly increase the expansion of CD34+ cells. The number of CD34+ cells in the MSC group is 4.9 times that of the non-MSC group. From this article, it can be inferred that the infusion of MSCs after receiving radiation irradiation may promote the expansion of patients' own HSCs and promote the recovery of their hematopoietic function [72]. MSCs can restore the bone marrow microenvironment in order to sustain hematopoiesis as demonstrated by Fouillard et al. in a phase 1 clinical trial [73]. In 2010, Hu et al. reported that infusion of MSCs 4 h after irradiation can significantly accelerate the recovery of peripheral blood cells. On the 26th day, the white blood cell counts of mice in the MSC group could recover to 90% compared to that before irradiation, but the white blood cell counts can only be restored to 80% in the non-MSC group, and MSCs could significantly reduce the apoptosis of bone marrow cells. They also found that the survival rate of the 5×10^7 /kg MSC group was significantly higher than that of the 2.5×10^7 /kg and 1.5×10^8 /kg groups [66]. Their research also demonstrated the therapeutic effects of MSCs on acute radiation injury on the hematopoietic system and confirmed that the number of cells returned to MSCs should have a certain upper limit value. If the upper limit value is exceeded, the effect will have more disadvantages than benefits. Cell stimulating factors have been routinely used in ARS. In 2013, Shim et al. reported a study that compared human umbilical cord blood-derived MSCs (hUCB-MSCs) and granulocyte colony-stimulating factor (G-CSF) in bone marrow ARS. They found that hUCB-MSC-treated mice had significantly better peripheral blood leukocyte recovery than the G-CSF-treated mice post irradiation [74]. This paper suggests to us that MSCs can be used as an ideal method for complementary or combined cytokine therapy on ARS. There are other sources of MSCs used for bone marrow ARS. A recent research applied Wharton's jelly MSCs (WJ-MSCs) from human umbilical cord to the treatment of ARS and found that WJ-MSCs can significantly enhance spleen and bone marrow cell capacity [75]. The volume of bone marrow cells in mice of the combined WJ-MSCs and antibiotic group was more than twice the volume of bone marrow cells of mice in the simple irradiation group at 60 days after infusion. A comprehensive treatment combination of radioprotective agents before radiation and MSCs after radiation was also proven to have a good therapeutic effect on acute radiation injury on the hematopoietic system [76]. In 2019, Mahmoud et al. demonstrated that delivering silymarin to rats 3 days before

radiation and MSCs 24 hours after radiation can significantly reduce the radiation injury on the hematopoietic system [76].

6. MSCs in Gastrointestinal ARS

In addition to its good therapeutic effects on radiation-induced bone marrow failure, MSCs also have potential efficacy on gastrointestinal ARS. Several teams have demonstrated that bone marrow-derived adherent stromal cells (BMASCs) can alleviate acute gastrointestinal radiation syndrome [77–79]. Saha et al. found that compared with the control group, the ability of the crypt epithelial cells in the BMASC group to synthesize DNA can be increased by nearly 2 times, and the number of Lgr5-positive crypt base columnar cells can be increased to 10 times that of the control group at 3.5 days post irradiation [77]. WJ-MSCs can also significantly protect the intestines of irradiated mice. In a research in 2020, Bandekar et al. found that the length of mice jejunum villi of the WJ-MSC and antibiotic group was significantly longer than that of the radiation-only group [75]. In the group that received WJ-MSCs at 24 h after irradiation, the length of the jejunum recovered almost back to its normal length. With the delay in WJ-MSC infusion time, the therapeutic effects gradually decreased [75].

7. MSCs in Cutaneous ARS

Radiation can also cause severe acute damage to the skin, often manifested as erythema, edema, ulcers, necrosis, and so on. Severe burns can occur, and high exposition can lead to amputation [80]. In 2007, Francois et al. reported that infusion of MSCs 24 h after irradiation can significantly reduce skin phenotypic score and wound size from one to eight weeks post irradiation [81]. Horton et al. also reported that MSCs can significantly reduce skin lesions caused by radiation. They found that the level of interleukin-10 (IL-10) in the skin tissue could be significantly increased, and the level of interleukin 1 β (IL-1 β) was significantly reduced 14 days after infusion of MSCs. They demonstrated that MSCs play a therapeutic role through tumor necrosis factor receptor 2 (TNF-R2) mediating the production of IL-10 [82].

Besides the organs above, MSCs have also been shown to have therapeutic effects in radiation damage to other organs, such as the lungs, nervous system, and glands [83–90]. Although the role of MSCs in acute radiation injury is clear, the mechanism is still not very clear. MSCs may provide protection against some radiation-induced organ injuries, like liver injury by an antioxidative process, vasculature protection, hepatocyte differentiation, and trophic effects [91]. Francois et al. found that infusion of BM-MSCs can reduce the mir-27b level of NOD/SCID mice liver exposed to radiation and increase the level of SDF1 α , which can also reduce oxidative stress post irradiation and increase the level of Nfr2 and SOD genes by the ROS-Nfr2 pathway. The pathway reduces the production of ROS, thereby reducing the damage to the liver caused by irradiation [91]. The "niche" or micro-environment where stem cells are located has been identified as a key element driving MSC differentiation, migration, and proliferation [92].

Research by Yang et al. found that MSCs aggregated in the lungs 4 hours after infusion of MSCs, while they were not distributed to other tissues or organs, including bone marrow, and mostly cleared up 24 hours after infusion. The authors speculated that MSCs may have a therapeutic effect on ARS, not directly but through soluble factors [93]. However, the lung was found to promote platelet production, and it was found to produce hematopoietic progenitor cells in recent years [94]. Opposite to these findings, the other team has demonstrated that MSCs migrate to irradiated tissues and stay there until 15 days [95]. Whether MSCs promote the differentiation of hematopoietic progenitor cells into peripheral blood cells through the produced cytokines or directly act on hematopoietic progenitor cells in the lungs still needs further investigation. Saha et al. suggested that BMASC can activate the Wnt β -catenin signaling pathway exerting a therapeutic effect on ARS [77]. And in the research by Bandekar et al., they found that the therapeutic effect of WJ-MSCs on ARS was significantly weakened by knocking out Nrf-2 and knocking down G-CSF and IL-6. From this article, it can also be speculated that MSCs may treat ARS through secreting cytokines and signal regulation [75]. During the last 2 decades, many preclinical animal studies have shown that MSCs mainly accelerate angiogenesis and reepithelialization through the secretory activity of extracellular vesicles (EVs), control inflammation and antiapoptosis, protect vessels, and promote tissue regeneration, thereby repairing radiation-induced injury [96, 97]. The emergency treatment of populations exposed to radiation requires that the treatment measures are ready, and it would be wise to suggest keeping MSC-derived extracellular vesicles available [97].

MSC-derived products also have shown their efficacy in tissue repair, which may be used in radiation induce injury. The MSC-derived extracellular matrix (ECM) has been shown to have the ability to promote cell proliferation while retaining stem cell properties. ECM produced by young cells can rejuvenate senescent cells by increasing their proliferation rate and differentiation potential [98]. Besides MSC-derived ECM, MSC-derived trophic factors (TFs) can also stimulate cell regeneration, promote tissue recovery, and protect cells from further injury [99].

Gene therapy of MSCs also showed promise in radiation-induced injury. In 2012, Drouet et al. used Amara technology to nucleofect adipocyte-derived multipotent MSCs with mock and Sonic hedgehog (Shh) pIRES2 plasmids [100]. When the monkeys were exposed to radiation for 48 hours, they were treated with manipulated MSCs, showing good tolerance. Shh-MSCs show good effects on reducing the duration of radiation-induced pancytopenia and increasing the slope of recovery of polymorphonuclear cells and platelets. Riccobono et al. also reported the therapeutic potential of transfected adipocyte-derived stem cells (ADSCs) to cure cutaneous ARS in a minipig model. ADSCs were transiently transfected by electroporation with a plasmid coding for Sonic hedgehog, which showed that injection of low-dose transfected cells can repair skin injury caused by radiation, avoiding necrosis and uncontrollable pain [101].

8. Conclusion

Although the therapeutic effects of HSCs and MSCs have been proven in both basic and clinical studies, there are still many unresolved problems as mentioned above. If these problems are solved well, it is believed that the survival time and quality of life of ARS patients will be further improved. With the development of cell-based therapies, it can make up for many of the drawbacks of cell replacement therapy, and the coordinated development of the two may benefit radiation-injured patients. For example, in recent years, HSC- and MSC-derived products have opened the door to develop new and innovative methods to reverse tissue damage caused by radiation as an alternative to cell transplants [99, 102]. Moreover, with the further understanding of human tissues and organs, it is believed that the role of HSCs and MSCs in ARS will be further optimized in the future. For example, studies have also found that the niches of the human hematopoietic system are not saturated [103–107], and that the allogeneic HSCs infused can be implanted well. Then, the question is whether we can increase the infused cell number to increase its efficacy especially when the human body is not treated in time after receiving radiation. In addition, a series of issues needs to be further discussed, such as how effective is the combined infusion of HSCs and MSCs in patients; what are the order, time, and dose of the two kinds of infused cells; and what can be done with graft rejection [108]. In conclusion, no matter how many are the unknown factors, HSCs and MSCs are two important treatments for ARS. With the advancement of research, the expectations they bring to the treatment of ARS patients are still worth looking forward to.

Conflicts of Interest

The authors declare no competing interest.

Authors' Contributions

Liren Qian and Jian Cen contributed equally to this work.

Acknowledgments

This work was supported by a grant from the National Natural Science Foundation of China (Grant No. 81800180) and the National Young Elite Scientists Sponsorship Program by the China Association for Science and Technology (Grant No. 17-JCJQ-QT-032).

References

- [1] N. Dainiak and R. C. Ricks, "The evolving role of haematopoietic cell transplantation in radiation injury: potentials and limitations," *The British Journal of Radiology*, vol. 78, pp. 169–174, 2005.
- [2] United States, General Accounting Office, MARCIVE - York University, *Nuclear nonproliferation. DOE action needed to ensure continued recovery of unwanted sealed radioactive sources*, U.S. General Accounting Office, 1999, <http://purl.access.gpo.gov/GPO/LPS32097>.

- [3] G. D. Kutz, G. Aloise, J. W. Cooney, and MARCIVE - York University, United States Congress Senate, Committee on Homeland Security and Governmental Affairs, Permanent Subcommittee on Investigations, United States, Government Accountability Office, *Nuclear security. Actions taken by NRC to strengthen its licensing process for sealed radioactive sources are not effective: testimony before the Permanent Subcommittee on Investigations, Committee on Homeland Security and Governmental Affairs, U.S. Senate*, Testimony GAO-07-1038 T. U.S. Govt. Accountability Office, 1999, <http://purl.access.gpo.gov/GPO/LPS85762>.
- [4] M. Benderitter, F. Caviggioli, A. Chapel et al., “Stem cell therapies for the treatment of radiation-induced normal tissue side effects,” *Antioxidants & Redox Signaling*, vol. 21, no. 2, pp. 338–355, 2014.
- [5] L. Qian, J. Shen, Y. Chuai, and J. Cai, “Hydrogen as a new class of radioprotective agent,” *International Journal of Biological Sciences*, vol. 9, no. 9, pp. 887–894, 2013.
- [6] L. G. Burdelya, V. I. Krivokrysenko, T. C. Tallant et al., “An agonist of toll-like receptor 5 has radioprotective activity in mouse and primate models,” *Science*, vol. 320, no. 5873, pp. 226–230, 2008.
- [7] K. Mei, S. Zhao, L. Qian, B. Li, J. Ni, and J. Cai, “Hydrogen protects rats from dermatitis caused by local radiation,” *The Journal of Dermatological Treatment*, vol. 25, pp. 182–188, 2014.
- [8] L. Qian, F. Cao, J. Cui et al., “Radioprotective effect of hydrogen in cultured cells and mice,” *Free Radical Research*, vol. 44, no. 3, pp. 275–282, 2010.
- [9] L. Qian, F. Cao, J. Cui et al., “The potential cardioprotective effects of hydrogen in irradiated mice,” *Journal of Radiation Research*, vol. 51, no. 6, pp. 741–747, 2010.
- [10] Y. Chuai, L. Qian, X. Sun, and J. Cai, “Molecular hydrogen and radiation protection,” *Free Radical Research*, vol. 46, no. 9, pp. 1061–1067, 2012.
- [11] Y. Chuai, F. Gao, B. Li et al., “Hydrogen-rich saline attenuates radiation-induced male germ cell loss in mice through reducing hydroxyl radicals,” *The Biochemical Journal*, vol. 442, no. 1, pp. 49–56, 2012.
- [12] J. Li, L. Feng, Y. Xing et al., “Radioprotective and antioxidant effect of resveratrol in hippocampus by activating Sirt1,” *International Journal of Molecular Sciences*, vol. 15, no. 4, pp. 5928–5939, 2014.
- [13] M. Laube, T. Kniess, and J. Pietzsch, “Development of antioxidant COX-2 inhibitors as radioprotective agents for radiation therapy—a hypothesis-driven review,” *Antioxidants*, vol. 5, no. 2, p. 14, 2016.
- [14] E. K. Fetisova, M. M. Antoschina, V. D. Cherepanynets et al., “Radioprotective effects of mitochondria-targeted antioxidant SkQR1,” *Radiation Research*, vol. 183, no. 1, pp. 64–71, 2015.
- [15] M. Satyamitra, L. Cary, D. Dunn, G. P. Holmes-Hampton, L. J. Thomas, and S. P. Ghosh, “CDX-301: a novel medical countermeasure for hematopoietic acute radiation syndrome in mice,” *Scientific Reports*, vol. 10, no. 1, p. 1757, 2020.
- [16] L. Stenke, K. Lindberg, M. Lagergren Lindberg et al., “Coordination of management of the acute radiation syndrome,” *Radiation Protection Dosimetry*, vol. 182, no. 1, pp. 80–84, 2018.
- [17] A. M. Farese, M. V. Cohen, R. B. Stead, W. Jackson 3rd, and T. J. Macvittie, “Pegfilgrastim administered in an abbreviated schedule, significantly improved neutrophil recovery after high-dose radiation-induced myelosuppression in rhesus macaques,” *Radiation Research*, vol. 178, no. 5, pp. 403–413, 2012.
- [18] T. J. MacVittie, A. M. Farese, W. G. Smith, C. M. Baum, E. Burton, and J. P. McKearn, “Myelopoiectin, an engineered chimeric IL-3 and G-CSF receptor agonist, stimulates multilineage hematopoietic recovery in a nonhuman primate model of radiation-induced myelosuppression,” *Blood*, vol. 95, no. 3, pp. 837–845, 2000.
- [19] A. B. Agarwal and A. McBride, “Understanding the biosimilar approval and extrapolation process—a case study of an epoetin biosimilar,” *Critical Reviews in Oncology/Hematology*, vol. 104, pp. 98–107, 2016.
- [20] A. F. Burnett, P. G. Biju, H. Lui, and M. Hauer-Jensen, “Oral interleukin 11 as a countermeasure to lethal total-body irradiation in a murine model,” *Radiation Research*, vol. 180, no. 6, pp. 595–602, 2013.
- [21] J. G. Kiang, M. Zhai, D. L. Bolduc et al., “Combined therapy of pegylated G-CSF and Alxn4100TPO improves survival and mitigates acute radiation syndrome after whole-body ionizing irradiation alone and followed by wound trauma,” *Radiation Research*, vol. 188, no. 5, pp. 476–490, 2017.
- [22] I. Friesecke, K. Beyrer, and T. M. Fliedner, “How to cope with radiation accidents: the medical management,” *The British Journal of Radiology*, vol. 74, no. 878, pp. 121–122, 2001.
- [23] E. Lorenz, D. Uphoff, T. R. Reid, and E. Shelton, “Modification of irradiation injury in mice and guinea pigs by bone marrow injections,” *Journal of the National Cancer Institute*, vol. 12, no. 1, pp. 197–201, 1951.
- [24] E. Lorenz, C. Congdon, and D. Uphoff, “Modification of acute irradiation injury in mice and guinea-pigs by bone marrow injections,” *Radiology*, vol. 58, no. 6, pp. 863–877, 1952.
- [25] S. François, M. Bensidhoum, M. Mouiseddine et al., “Local irradiation not only induces homing of human mesenchymal stem cells at exposed sites but promotes their widespread engraftment to multiple organs: a study of their quantitative distribution after irradiation damage,” *Stem Cells*, vol. 24, no. 4, pp. 1020–1029, 2006.
- [26] E. B. Eaton Jr. and T. R. Varney, “Mesenchymal stem cell therapy for acute radiation syndrome: innovative medical approaches in military medicine,” *Military Medical Research*, vol. 2, no. 1, p. 2, 2015.
- [27] L. V. Kursova, A. G. Konoplyannikov, V. V. Pasov, I. N. Ivanova, M. V. Poluektova, and O. A. Konoplyannikova, “Possibilities for the use of autologous mesenchymal stem cells in the therapy of radiation-induced lung injuries,” *Bulletin of Experimental Biology and Medicine*, vol. 147, no. 4, pp. 542–546, 2009.
- [28] A. Chapel, J. M. Bertho, M. Bensidhoum et al., “Mesenchymal stem cells home to injured tissues when co-infused with hematopoietic cells to treat a radiation-induced multi-organ failure syndrome,” *The Journal of Gene Medicine*, vol. 5, no. 12, pp. 1028–1038, 2003.
- [29] V. Nair, D. N. Karan, and C. S. Makhani, “Guidelines for medical management of nuclear/radiation emergencies,” *Medical journal, Armed Forces India*, vol. 73, no. 4, pp. 388–393, 2017.
- [30] E. H. Donnelly, J. B. Nemhauser, J. M. Smith et al., “Acute radiation syndrome: assessment and management,” *Southern Medical Journal*, vol. 103, no. 6, pp. 541–546, 2010.

- [31] I. Turai, K. Veress, B. Gunalp, and G. Souchkevitch, "Medical response to radiation incidents and radionuclear threats," *BMJ*, vol. 328, no. 7439, pp. 568–572, 2004.
- [32] M. Port, B. Pieper, H. D. Dorr, A. Hubsch, M. Majewski, and M. Abend, "Correlation of radiation dose estimates by DIC with the METREPOL hematological classes of disease severity," *Radiation Research*, vol. 189, no. 5, pp. 449–455, 2018.
- [33] M. Lopez and M. Martin, "Medical management of the acute radiation syndrome," *Reports of Practical Oncology and Radiotherapy*, vol. 16, no. 4, pp. 138–146, 2011.
- [34] L. A. Il'in, *Chernobyl: Myth and Reality*, Megapolis, Moscow, 1995.
- [35] D. Schulte-Frohlinde, "Comparison of mechanisms for DNA strand break formation by the direct and indirect effect of radiation," *Basic Life Sciences*, vol. 38, pp. 19–27, 1986.
- [36] J. F. Ward, "DNA damage produced by ionizing radiation in mammalian cells: identities, mechanisms of formation, and reparability," *Progress in Nucleic Acid Research and Molecular Biology*, vol. 35, pp. 95–125, 1988.
- [37] E. S. Kempner, "Damage to proteins due to the direct action of ionizing radiation," *Quarterly Reviews of Biophysics*, vol. 26, no. 1, pp. 27–48, 1993.
- [38] S. Asano, "Current status of hematopoietic stem cell transplantation for acute radiation syndromes," *International Journal of Hematology*, vol. 95, no. 3, pp. 227–231, 2012.
- [39] A. Leonard, J. Tisdale, and A. Abraham, "Curative options for sickle cell disease: haploidentical stem cell transplantation or gene therapy?," *British Journal of Haematology*, vol. 189, no. 3, pp. 408–423, 2020.
- [40] U. Anurathapan, S. Hongeng, S. Pakakasama et al., "Hematopoietic stem cell transplantation for severe thalassemia patients from haploidentical donors using a novel conditioning regimen," *Biology of Blood and Marrow Transplantation*, vol. 26, no. 6, pp. 1106–1112, 2020.
- [41] D. Dimitrova, J. Gea-Banacloche, S. M. Steinberg et al., "Prospective study of a novel, radiation-free, reduced-intensity bone marrow transplantation platform for primary immunodeficiency diseases," *Biology of Blood and Marrow Transplantation*, vol. 26, no. 1, pp. 94–106, 2020.
- [42] J. Slezak, B. Kura, P. Babal et al., "Potential markers and metabolic processes involved in the mechanism of radiation-induced heart injury," *Canadian Journal of Physiology and Pharmacology*, vol. 95, no. 10, pp. 1190–1203, 2017.
- [43] R. Fukumoto, "Mesenchymal stem cell therapy for acute radiation syndrome," *Military Medical Research*, vol. 3, no. 1, p. 17, 2016.
- [44] J. M. Main and R. T. Prehn, "Successful skin homografts after the administration of high dosage X radiation and homologous bone marrow," *Journal of the National Cancer Institute*, vol. 15, no. 4, pp. 1023–1029, 1955.
- [45] C. E. Ford, J. L. Hamerton, D. W. Barnes, and J. F. Loutit, "Cytological identification of radiation-chimaeras," *Nature*, vol. 177, no. 4506, pp. 452–454, 1956.
- [46] G. A. Andrews, "Criticality accidents in Vinca, Yugoslavia, and Oak Ridge, Tennessee. Comparison of radiation injuries and results of therapy," *Journal of the American Medical Association*, vol. 179, no. 3, pp. 191–197, 1962.
- [47] S. Taniguchi, "The role of hematopoietic stem cell transplantation in the treatment of acute radiation injury," *Nihon rinsho Japanese Journal of Clinical Medicine*, vol. 70, no. 3, pp. 503–507, 2012.
- [48] S. Akyurek, "The effect of erythropoietin in the prevention of radiation-induced spinal cord damage," *Medical Hypotheses*, vol. 68, no. 1, pp. 238–239, 2007.
- [49] L. B. Balsam, A. J. Wagers, J. L. Christensen, T. Kofidis, I. L. Weissman, and R. C. Robbins, "Haematopoietic stem cells adopt mature haematopoietic fates in ischaemic myocardium," *Nature*, vol. 428, no. 6983, pp. 668–673, 2004.
- [50] H. F. Tse, Y. L. Kwong, J. K. Chan, G. Lo, C. L. Ho, and C. P. Lau, "Angiogenesis in ischaemic myocardium by intramyocardial autologous bone marrow mononuclear cell implantation," *The Lancet*, vol. 361, no. 9351, pp. 47–49, 2003.
- [51] C. Stamm, B. Westphal, H. D. Kleine et al., "Autologous bone-marrow stem-cell transplantation for myocardial regeneration," *The Lancet*, vol. 361, no. 9351, pp. 45–46, 2003.
- [52] D. Orlic, J. Kajstura, S. Chimenti et al., "Bone marrow cells regenerate infarcted myocardium," *Nature*, vol. 410, no. 6829, pp. 701–705, 2001.
- [53] A. J. Wagers, R. I. Sherwood, J. L. Christensen, and I. L. Weissman, "Little evidence for developmental plasticity of adult hematopoietic stem cells," *Science*, vol. 297, no. 5590, pp. 2256–2259, 2002.
- [54] T. R. Brazelton, F. M. Rossi, G. I. Keshet, and H. M. Blau, "From marrow to brain: expression of neuronal phenotypes in adult mice," *Science*, vol. 290, no. 5497, pp. 1775–1779, 2000.
- [55] C. M. Morshead, P. Benveniste, N. N. Iscove, and D. van der Kooy, "Hematopoietic competence is a rare property of neural stem cells that may depend on genetic and epigenetic alterations," *Nature Medicine*, vol. 8, no. 3, pp. 268–273, 2002.
- [56] C. R. Cogle, A. T. Yachnis, E. D. Laywell et al., "Bone marrow transdifferentiation in brain after transplantation: a retrospective study," *The Lancet*, vol. 363, no. 9419, pp. 1432–1437, 2004.
- [57] O. E. Sigurjonsson, M. C. Perreault, T. Egeland, and J. C. Glover, "Adult human hematopoietic stem cells produce neurons efficiently in the regenerating chicken embryo spinal cord," *Proceedings of the National Academy of Sciences of the United States of America*, vol. 102, no. 14, pp. 5227–5232, 2005.
- [58] T. R. Spitzer, "Engraftment syndrome: double-edged sword of hematopoietic cell transplants," *Bone Marrow Transplantation*, vol. 50, no. 4, pp. 469–475, 2015.
- [59] A. K. Omer, H. T. Kim, B. Yalamarti et al., "Engraftment syndrome after allogeneic hematopoietic cell transplantation in adults," *American Journal of Hematology*, vol. 89, no. 7, pp. 698–705, 2014.
- [60] L. Guyonneau-Harmand, B. L'Homme, B. Birebent et al., "Transgene-free hematopoietic stem and progenitor cells from human induced pluripotent stem cells," *BioRxiv Preprint*, Article ID 177691, 2017.
- [61] A. J. Friedenstein, K. V. Petrakova, A. I. Kurolesova, and G. P. Frolova, "Heterotopic of bone marrow. Analysis of precursor cells for osteogenic and hematopoietic tissues," *Transplantation*, vol. 6, no. 2, pp. 230–247, 1968.
- [62] E. M. Horwitz, K. le Blanc, M. Dominici et al., "Clarification of the nomenclature for MSC: the International Society for Cellular Therapy position statement," *Cytotherapy*, vol. 7, no. 5, pp. 393–395, 2005.
- [63] M. Dominici, K. le Blanc, I. Mueller et al., "Minimal criteria for defining multipotent mesenchymal stromal cells. The

- International Society for Cellular Therapy position statement," *Cytotherapy*, vol. 8, no. 4, pp. 315–317, 2006.
- [64] R. J. Deans and A. B. Moseley, "Mesenchymal stem cells: biology and potential clinical uses," *Experimental Hematology*, vol. 28, no. 8, pp. 875–884, 2000.
- [65] L. Wang, Y. Li, X. Chen et al., "MCP-1, MIP-1, IL-8 and ischemic cerebral tissue enhance human bone marrow stromal cell migration in interface culture," *Hematology*, vol. 7, pp. 113–117, 2002.
- [66] K. X. Hu, Q. Y. Sun, M. Guo, and H. S. Ai, "The radiation protection and therapy effects of mesenchymal stem cells in mice with acute radiation injury," *The British Journal of Radiology*, vol. 83, no. 985, pp. 52–58, 2010.
- [67] M. F. Pittenger and B. J. Martin, "Mesenchymal stem cells and their potential as cardiac therapeutics," *Circulation Research*, vol. 95, no. 1, pp. 9–20, 2004.
- [68] K. Le Blanc and D. Mougiakakos, "Multipotent mesenchymal stromal cells and the innate immune system," *Nature Reviews Immunology*, vol. 12, no. 5, pp. 383–396, 2012.
- [69] J. Kurtzberg, H. Abdel-Azim, P. Carpenter et al., "A phase 3, single-arm, prospective study of remestemcel-L, ex vivo culture-expanded adult human mesenchymal stromal cells for the treatment of pediatric patients who failed to respond to steroid treatment for acute graft-versus-host disease," *Biology of Blood and Marrow Transplantation*, vol. 26, no. 5, pp. 845–854, 2020.
- [70] J. Voswinkel, S. Francois, N. C. Gorin, and A. Chapel, "Gastro-intestinal autoimmunity: preclinical experiences and successful therapy of fistulizing bowel diseases and gut graft versus host disease by mesenchymal stromal cells," *Immunologic Research*, vol. 56, no. 2–3, pp. 241–248, 2013.
- [71] A. Semont, C. Demarquay, R. Bessout, C. Durand, M. Benderitter, and N. Mathieu, "Mesenchymal stem cell therapy stimulates endogenous host progenitor cells to improve colonic epithelial regeneration," *PLoS One*, vol. 8, no. 7, article e70170, 2013.
- [72] F. Mourcin, N. Grenier, J. F. Mayol et al., "Mesenchymal stem cells support expansion of *in vitro* irradiated CD34 cells in the presence of SCF, FLT3 ligand, TPO and IL3: potential application to autologous cell therapy in accidentally irradiated victims," *Radiation Research*, vol. 164, no. 1, pp. 1–9, 2005.
- [73] L. Fouillard, S. Francois, S. Bouchet, M. Bensidhoum, A. Elm'selmi, and A. Chapel, "Innovative cell therapy in the treatment of serious adverse events related to both chemoradiotherapy protocol and acute myeloid leukemia syndrome: the infusion of mesenchymal stem cells post-treatment reduces hematopoietic toxicity and promotes hematopoietic reconstitution," *Current Pharmaceutical Biotechnology*, vol. 14, no. 9, pp. 842–848, 2013.
- [74] S. Shim, S. B. Lee, J. G. Lee et al., "Mitigating effects of hUCB-MSCs on the hematopoietic syndrome resulting from total body irradiation," *Experimental Hematology*, vol. 41, no. 4, pp. 346–353.e2, 2013, e2.
- [75] M. Bandekar, D. K. Maurya, D. Sharma et al., "Xenogeneic transplantation of human WJ-MSCs rescues mice from acute radiation syndrome via Nrf-2-dependent regeneration of damaged tissues," *American Journal of Transplantation*, vol. 20, no. 8, pp. 2044–2057, 2020.
- [76] A. Z. Mahmoud, H. A. Ibrahim, M. R. El-Sawi, and M. N. Habza, "Effects of silymarin and mesenchymal stem cells on hematological and some biochemical changes induced by gamma radiation in albino rats," *International Journal of Radiation Biology*, vol. 96, no. 2, pp. 220–227, 2020.
- [77] S. Saha, P. Bhanja, R. Kabarriti, L. Liu, A. A. Alfieri, and C. Guha, "Bone marrow stromal cell transplantation mitigates radiation-induced gastrointestinal syndrome in mice," *PLoS One*, vol. 6, no. 9, article e24072, 2011.
- [78] A. Sémont, M. Mouiseddine, A. François et al., "Mesenchymal stem cells improve small intestinal integrity through regulation of endogenous epithelial cell homeostasis," *Cell Death & Differentiation*, vol. 17, no. 6, pp. 952–961, 2010.
- [79] C. Linard, E. Busson, V. Holler et al., "Repeated autologous bone marrow-derived mesenchymal stem cell injections improve radiation-induced proctitis in pigs," *Stem Cells Translational Medicine*, vol. 2, no. 11, pp. 916–927, 2013.
- [80] J. J. Lataillade, C. Doucet, E. Bey et al., "New approach to radiation burn treatment by dosimetry-guided surgery combined with autologous mesenchymal stem cell therapy," *Regenerative Medicine*, vol. 2, no. 5, pp. 785–794, 2007.
- [81] S. François, M. Mouiseddine, N. Mathieu et al., "Human mesenchymal stem cells favour healing of the cutaneous radiation syndrome in a xenogenic transplant model," *Annals of Hematology*, vol. 86, no. 1, pp. 1–8, 2006.
- [82] J. A. Horton, K. E. Hudak, E. J. Chung et al., "Mesenchymal stem cells inhibit cutaneous radiation-induced fibrosis by suppressing chronic inflammation," *Stem Cells*, vol. 31, no. 10, pp. 2231–2241, 2013.
- [83] Y. Yao, Z. Zheng, and Q. Song, "Mesenchymal stem cells: a double-edged sword in radiation-induced lung injury," *Thoracic Cancer*, vol. 9, no. 2, pp. 208–217, 2018.
- [84] J. Y. Lim, J. C. Ra, I. S. Shin et al., "Systemic transplantation of human adipose tissue-derived mesenchymal stem cells for the regeneration of irradiation-induced salivary gland damage," *PLoS One*, vol. 8, no. 8, article e71167, 2013.
- [85] H. Liao, H. Wang, X. Rong, E. Li, R. H. Xu, and Y. Peng, "Mesenchymal stem cells attenuate radiation-induced brain injury by inhibiting microglia pyroptosis," *BioMed Research International*, vol. 2017, Article ID 1948985, 11 pages, 2017.
- [86] T. Xu, Y. Zhang, P. Chang, S. Gong, L. Shao, and L. Dong, "Mesenchymal stem cell-based therapy for radiation-induced lung injury," *Stem Cell Research & Therapy*, vol. 9, no. 1, p. 18, 2018.
- [87] A. Fujishiro, Y. Miura, M. Iwasa et al., "Effects of acute exposure to low-dose radiation on the characteristics of human bone marrow mesenchymal stromal/stem cells," *Inflammation and Regeneration*, vol. 37, no. 1, p. 19, 2017.
- [88] D. Klein, A. Schmetter, R. Imsak et al., "Therapy with multipotent mesenchymal stromal cells protects lungs from radiation-induced injury and reduces the risk of lung metastasis," *Antioxidants & Redox Signaling*, vol. 24, no. 2, pp. 53–69, 2016.
- [89] G. H. Wang, Y. Liu, X. B. Wu et al., "Neuroprotective effects of human umbilical cord-derived mesenchymal stromal cells combined with nimodipine against radiation-induced brain injury through inhibition of apoptosis," *Cytotherapy*, vol. 18, no. 1, pp. 53–64, 2016.
- [90] X. Jiang, X. Jiang, C. Qu et al., "Intravenous delivery of adipose-derived mesenchymal stromal cells attenuates acute radiation-induced lung injury in rats," *Cytotherapy*, vol. 17, no. 5, pp. 560–570, 2015.
- [91] S. Francois, M. Mouiseddine, B. Allenet-Lepage et al., "Human mesenchymal stem cells provide protection against

- radiation-induced liver injury by antioxidative process, vasculature protection, hepatocyte differentiation, and trophic effects," *BioMed Research International*, vol. 2013, Article ID 151679, 14 pages, 2013.
- [92] R. Zamilpa, M. M. Navarro, I. Flores, and S. Griffey, "Stem cell mechanisms during left ventricular remodeling post-myocardial infarction: repair and regeneration," *World Journal of Cardiology*, vol. 6, no. 7, pp. 610–620, 2014.
- [93] X. Yang, I. Balakrishnan, B. Torok-Storb, and M. M. Pillai, "Marrow stromal cell infusion rescues hematopoiesis in lethally irradiated mice despite rapid clearance after infusion," *Advances in Hematology*, vol. 2012, Article ID 142530, 5 pages, 2012.
- [94] E. Lefrancais, G. Ortiz-Muñoz, A. Caudrillier et al., "The lung is a site of platelet biogenesis and a reservoir for haematopoietic progenitors," *Nature*, vol. 544, no. 7648, pp. 105–109, 2017.
- [95] L. Moussa, B. Usunier, C. Demarquay et al., "Bowel radiation injury: complexity of the pathophysiology and promises of cell and tissue engineering," *Cell Transplantation*, vol. 25, no. 10, pp. 1723–1746, 2016.
- [96] S. Wen, M. Dooner, Y. Cheng et al., "Mesenchymal stromal cell-derived extracellular vesicles rescue radiation damage to murine marrow hematopoietic cells," *Leukemia*, vol. 30, no. 11, pp. 2221–2231, 2016.
- [97] J. S. Schoefinius, B. Brunswig-Spickenheier, T. Speiseder, S. Krebs, U. Just, and C. Lange, "Mesenchymal stromal cell-derived extracellular vesicles provide long-term survival after total body irradiation without additional hematopoietic stem cell support," *Stem Cells*, vol. 35, no. 12, pp. 2379–2389, 2017.
- [98] Y. Sun, W. Li, Z. Lu et al., "Rescuing replication and osteogenesis of aged mesenchymal stem cells by exposure to a young extracellular matrix," *FASEB Journal*, vol. 25, no. 5, pp. 1474–1485, 2011.
- [99] A. Kumar, H. K. Mishra, P. Dwivedi, and J. R. Subramaniam, "Secreted trophic factors of human umbilical cord stromal cells induce differentiation and neurite extension through PI3K and independent of cAMP pathway," *Annals of Neurosciences*, vol. 22, no. 2, pp. 97–106, 2015.
- [100] M. Drouet, D. Agay, P. Garrigou, A. Peinnequin, and F. Herodin, "Gene therapy to mitigate radiation-induced bone marrow aplasia: preliminary study in highly irradiated monkeys," *Health Physics*, vol. 103, no. 2, pp. 138–142, 2012.
- [101] D. Riccobono, F. Forcheron, D. Agay, H. Scherthan, V. Meineke, and M. Drouet, "Transient gene therapy to treat cutaneous radiation syndrome: development in a minipig model," *Health Physics*, vol. 106, no. 6, pp. 713–719, 2014.
- [102] A. Saudemont and J. A. Madrigal, "Immunotherapy after hematopoietic stem cell transplantation using umbilical cord blood-derived products," *Cancer Immunology, Immunotherapy*, vol. 66, no. 2, pp. 215–221, 2017.
- [103] M. Shimoto, T. Sugiyama, and T. Nagasawa, "Numerous niches for hematopoietic stem cells remain empty during homeostasis," *Blood*, vol. 129, no. 15, pp. 2124–2131, 2017.
- [104] G. Brecher, J. D. Ansell, H. S. Micklem, J. H. Tjio, and E. P. Cronkite, "Special proliferative sites are not needed for seeding and proliferation of transfused bone marrow cells in normal syngeneic mice," *Proceedings of the National Academy of Sciences of the United States of America*, vol. 79, no. 16, pp. 5085–5087, 1982.
- [105] F. M. Stewart, R. B. Crittenden, P. A. Lowry, S. Pearson-White, and P. J. Quesenberry, "Long-term engraftment of normal and post-5-fluorouracil murine marrow into normal nonmyeloablated mice," *Blood*, vol. 81, no. 10, pp. 2566–2571, 1993.
- [106] P. J. Quesenberry, M. F. Stewart, S. Peters et al., "Engraftment of hematopoietic stem cells in nonmyeloablated and myeloablated hosts," *Stem Cells*, vol. 15, no. S2, pp. 167–170, 1997.
- [107] A. C. Wilkinson, R. Ishida, M. Kikuchi et al., "Long-term ex vivo haematopoietic-stem-cell expansion allows nonconditioned transplantation," *Nature*, vol. 571, no. 7763, pp. 117–121, 2019.
- [108] N. Frickhofen, M. Korbling, and T. M. Fliedner, "Is blood a better source of allogeneic hematopoietic stem cells for use after radiation accidents?," *Bone Marrow Transplantation*, vol. 17, pp. 131–135, 1996.